CONTROL STRATEGY OF WIND ENERGY CONVERSION SYSTEM FOR GRID CONNECTION

2023
PhD THESIS
ELECTRICAL-ELECTRONICS ENGINEERING

Fathi Abdulmajeed M. ALREMALI

Thesis Advisor
Prof. Dr. İhsan ULUER

CONTROL STRATEGY OF WIND ENERGY CONVERSION SYSTEM FOR GRID CONNECTION

Fathi Abdulmajeed M. ALREMALI

Thesis Advisor
Prof. Dr. İhsan ULUER

T.C.
Karabuk University
Institute of Graduate Programs
Department of Electrical-Electronics Engineering
Prepared as PhD Thesis

KARABUK
January 2023

I certify that in my opinion the thesis submitted by Fathi Abdulmajeed M. ALREMALI titled "CONTROL STRATEGY OF WIND ENERGY CONVERSION SYSTEM FOR GRID CONNECTION" is fully adequate in scope and in quality as a thesis for the degree of PhD.

Prof. Dr. İhsan ULUER .....
Thesis Advisor, Department of Electrical-Electronics Engineering

This thesis is accepted by the examining committee with a unanimous vote in the Department of Electrical-Electronics Engineering as a PhD thesis. January 16, 2023

Examining Committee Members (Institutions)	Signature
Chairman : Prof. Dr. Şerafettin EREL (AYBU)	.....
Member : Prof. Dr. İhsan ULUER (OSTİMTech Univ.)	.....
Member : Assist. Prof. Dr. Ersagun Kürşat YAYLACI (KBU)	.....
Member : Assoc. Prof. Dr. Muhammet Tahir GÜNEŞER (KBU)	.....
Member : Assist. Prof. Dr. Cihat ŞEKER (KBU)	.....

The degree of PhD by the thesis submitted is approved by the Administrative Board of the Institute of Graduate Programs, Karabuk University.

Prof. Dr. Müslüm KUZU .....
Director of the Institute of Graduate Programs

I declare that all the information within this thesis has been gathered and presented in accordance with academic regulations and ethical principles, and I have according to the requirements of these regulations and principles cited all those which do not originate in this work as well."

Fathi Abdulmajeed M. ALREMALI

ABSTRACT

Ph.D. Thesis

CONTROL STRATEGY OF WIND ENERGY CONVERSION SYSTEM FOR GRID CONNECTION

Fathi Abdulmajeed M. ALREMALI

Karabük University
Institute of Graduate Programs
The Department of Electrical-Electronics Engineering

Thesis Advisor:
Prof. Dr. İhsan ULUER
January 2023, 108 pages

This work presents a combination of artificial neural network (ANN) with the grey wolf optimization algorithm (GWO) to improve the power quality of a grid-connected distributed power generation system (DPGS). The GWO is a meta-heuristic optimization method inspired by the hunting behavior of grey wolfs. To assess the effectiveness of the proposed algorithm, a grid-tied of small-scale wind energy conversion system (WECS) is selected. The power quality issues refer to the output voltage and frequency fluctuation and harmonics arising because of the intermittent nature of wind speed and power converters. Power quality improvement is achieved through the cascaded control system's optimal tuning of three proportional-integral (PI) controllers of the grid-side inverter (GSI). However, because the DPGS model is computationally costly, it is approximated using ANN to serve as a surrogate model of DPGS, which is considered a salient feature of this research. The input-output datasets were obtained by repeatedly simulating the proposed power system and were

used to test and train the ANN model. Furthermore, the GWO is combined with an ANN model to improve optimization precision and shorten GWO execution time. According to the ANN model's performance evaluation, the correlation coefficient (R) is close to one, while the mean squared error (MSE) is near zero. These findings demonstrate the ANN model's great accuracy in approximating the DPGS model. Using MATLAB/Simulink, the system's performance is evaluated using the optimum values obtained using GWO-ANN for various wind speed profiles. It showed the suggested power quality method's improved stability, convergence behavior, the control mechanism's effectiveness, and the proposed topology's robustness.

Key Words : Artificial Neural Network, Grey Wolf Optimizer, PI controller, Grid Connection, Power Quality, Wind Energy.

Science Code : 90544

ÖZET

Doktora Tezi

ŞEBEKE BAĞLANTISI İÇİN RÜZGAR ENERJİSİ DÖNÜŞÜM SİSTEMİNİN KONTROL STRATEJİSİ

Fathi Abdulmajeed M. ALREMALI

Karabük Üniversitesi
Lisansüstü Eğitim Enstitüsü
Elektrik-Elektronik Mühendisliği Anabilim Dalı

Tez Danışmanı:
Prof. Dr. İhsan ULUER
Ocak 2023, 108 sayfa

Bu çalışma, şebekeye bağlı dağıtılmış güç üretim sisteminin (DPGS) güç kalitesini iyileştirmek için gri kurt optimizasyon algoritması (GWO) ile yapay sinir ağının (YSA) bir kombinasyonunu sunar. GWO, gri kurtların avlanma davranışından ilham alan bir meta-sezgisel optimizasyon yöntemidir. Önerilen algoritmanın etkinliğini değerlendirmek için, şebekeye bağlı küçük ölçekli rüzgar enerjisi dönüşüm sistemi (WECS) seçilmiştir. Güç kalitesi sorunları, çıkış voltajı ve frekans dalgalanması ile rüzgar hızının ve güç dönüştürücülerinin kesintili doğası nedeniyle ortaya çıkan harmonikleri ifade eder. Güç kalitesi iyileştirmesi, kademeli kontrol sisteminin şebeke tarafı invertörün (GSI) üç oransal-tümleşik (PI) kontrolörünün optimal ayarıyla elde edilir. Ancak, DPGS modeli hesaplama açısından maliyetli olduğu için, bu araştırmanın göze çarpan bir özelliği olarak kabul edilen DPGS'nin bir vekil modeli olarak hizmet etmek için YSA kullanılarak yaklaşık olarak tahmin edilmiştir. Dikkate alınan güç sistemi, YSA modelini doğrulayan ve eğiten girdi-çıktı veri kümelerini elde

etmek için tekrar tekrar simüle edildi. Ayrıca, ANN modeli, optimizasyon kesinliğini artırmak ve GWO'nun yürütme süresini en aza indirmek için GWO ile birlikte kullanılır. YSA modelinin performans değerlendirmesine göre korelasyon katsayısı (R) bire yakınken, ortalama karesel hata (MSE) sıfıra yakındır. Bu bulgular, YSA modelinin DPGS modeline yaklaşmadaki büyük doğruluğunu göstermektedir. MATLAB/Simulink kullanılarak, çeşitli rüzgar hızı profilleri için GWO-ANN kullanılarak elde edilen optimum değerler kullanılarak sistemin performansı değerlendirilir. Önerilen güç kalitesi yönteminin gelişmiş kararlılığını, yakınsama davranışını, kontrol mekanizmasının etkinliğini ve önerilen topolojinin sağlamlığını gösterdi.

Anahtar Kelimeler : Yapay sinir ağı, gri kurt optimize edici, PI denetleyici, şebeke bağlantısı, güç kalitesi, rüzgar enerjisi.

Bilim Kodu **:** 90544

ACKNOWLEDGMENT

First, I would like to thank Almighty Allah for enabling me to complete my Ph.D. research. I would like to express my sincere gratitude and appreciation to my primary supervisor Prof. Dr. İhsan ULUER, and to thank my Doctoral Committee members, Dr. Ersagun Kürşat YAYLACI and Prof. Dr. Şerafettin EREL for their professional supervision, notes, and many beneficial propositions during my research work. I would also like to thank the Academic Attaché at the Libyan Embassy in the Republic of Turkey for their unlimited support throughout the study period. And I don't forget to thank my family for their prayer, encouragement, and support.

CONTENTS

Page

Page

Page

LIST OF FIGURES

Page

Page

LIST OF TABLES

Page

SYMBOLS AND ABBREVITIONS INDEX

SYMBOLS

α : Alpha

β : Beta

δ : Delta

ω : Omega

ABBREVITIONS

ABC : Artificial Bee Colony

AC : Alternating Current

ACO : Ant Colony Optimization

AI : Artificial Intelligence

ANN : Artificial Neural Network

BA : Bee Algorithm

BC : Boost Converter

BTB : Back-to-Back

CPP : Conventional Power Plants

CRO : Chemical Reaction Optimization

CSA : Cuckoo Search Algorithm

CSI : Current Source Inverter

DC : Direct Current

DD : Direct Driven

DE : Differential Evolution

DER : Distributed Energy Resource

DFIG : Double-Fed Induction Generator

DG : Distributed Generation

DOE : Design of Experiments

DPC : Direct Power Control

DPGS : Distributed Power Generation System

DTC : Direct Torque Control

EMC : Electromagnetic Compatibility

FOC : Field Oriented Control

FRT : Fault Ride Through

GA : Genetic Algorithm

GC : Grid Code

GCI : Grid Connected Inverter

GSC : Grid Side Converter

GSI : Grid Side Inverter

GWO : Grey Wolf Optimizer

HS : Harmony Search

IEC : International Electrotechnical Commission

IEEE : Institute of Electrical Engineers

IGBT : Insulated Gate Bipolar Transistor

LQR : Linear Quadratic Regulator

LVRT : Low Voltage Ride Through

MG : Micro Grid

MPC : Model Predictive Control

MPPT : Maximum Power Tracking Point

MSC : Machine Side Converter

MSE : Mean Square Error

NPC : Neutral Point diode

PCC : Point of Common Coupling

PI : Proportional Integral

PID : Proportional Integral Derivative

PLL : Phase Locked Loop

PMSG : Permanent magnet Synchronous Generator

PO : Perturb Observe

PQ : Power Quality

PSO : Particle Swarm Optimization

PV : Photo Voltaic

PWM : Pulse Width Modulation

RES : Renewable Energy Sources

SG : Synchronous Generator

SMC : Sliding Mode Control

SPWM : Sinusoidal Pulse Width Modulation

SCIG : Total Harmonic Distortion

THD : Total Harmonic Distortion

TSO : Transmission System Operator

TSR : Tip Speed Ratio

VC : Vector Control

VSC : Voltage Source Converter

VSI : Voltage Source Inverter

VSWT : Variable Sped Wind turbine

WECS : Wind Energy Conversion System

WRIG : Wound Rotor Induction Generator

WRSG : Wound Rotor Synchronous Generator

WT : Wind Turbine

PART 1

INTRODUCTION

There is an ever-increasing demand for electric energy due to the exponential growth of economic development and industrialization [1]. The fastest demand growth since 2010 saw +5.4% in 2021 [2]; therefore, countries should boost electrical energy production to keep up with the increase in demand. Nuclear energy, renewable energy, and fossil fuels can all be utilized to generate electricity [3]. But nuclear energy creates hazardous compounds that endanger human health and the environment as well as the potential challenges associated with the disposal of nuclear waste, whereas fossil fuels have a limited supply, fluctuate in price, and release emissions that contribute to global warming and climate change [4]. Utilizing renewable energy sources is mostly driven by this issue (RESs). RESs are characterized as clean energy sources that limit negative environmental effects, produce little to no secondary waste, and are sustainable in light of a country's energy, economic, and social needs [5]. The RES actually stands out for its variety of energy supply options, decreased reliance on fossil fuels, increase in net employment, development of export markets, decrease in greenhouse gas emissions, production of little to no secondary waste, and sustainability based on the energy and economic factors [6]. Marine, biomass, geothermal, wind, and solar energy are a few examples of RES sources. The capacity of renewable energy sources increased globally in 2021, adding more than 314 GW, according to the Renewable Energy Policy Network report (REN21). The total installed capacity of renewable energy increased by 11% globally to around 3,146 GW. In 2021, renewable energy accounted for 28.3% of the world's electricity mix [7]. Figure 1.1 depicts the increase in renewable energy capacity (2011 – 2021). The most extensively used RES sources are solar and wind energy, which are also predicted to grow more than any other energy source by the middle of this century and play a significant role in the 21st Century [8,9]. With an increase from 9.3% in 2020 to 10.3% in 2021, wind and solar power generated twice as much electricity as they did in 2015 (4.6%), the year the Paris

Climate Agreement was signed [2]. Given this, the global weighted average cost of solar photovoltaics, decreased by 13% in 2021, while onshore and offshore wind decreased by 15% and 13%, respectively, compared to 2020 [10].

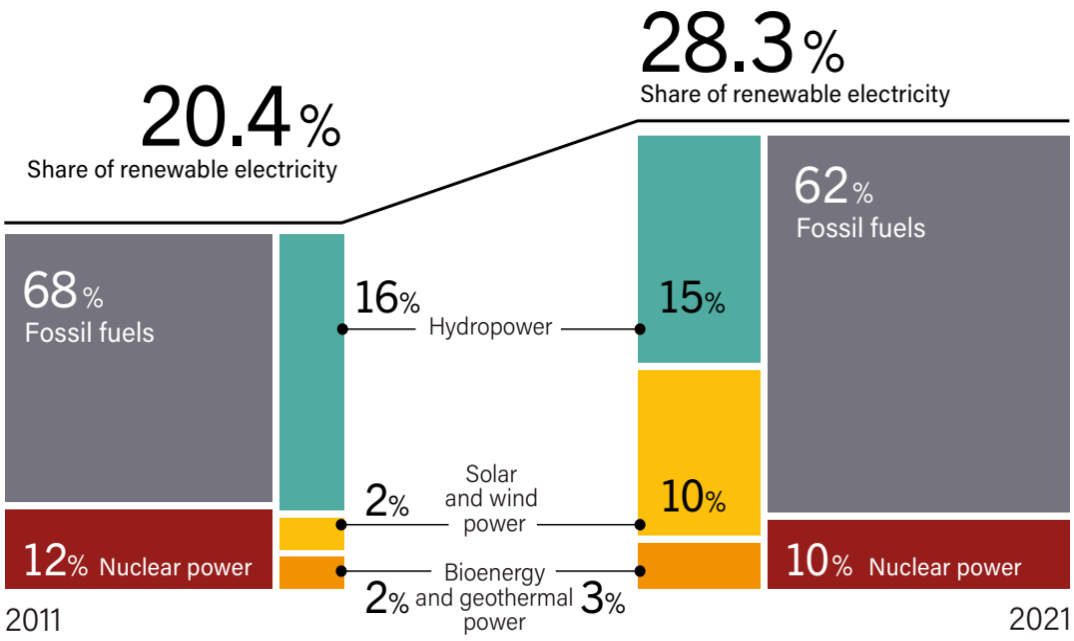

Figure 1.1. Renewable power capacity growth [7].

Wind power has the quickest growth, which makes it the second-largest renewable resource [8]. The 837 GW total global wind generating capacity increased by 93.6 GW after new installations in 2021, representing a 12% year-over-year increase [11] despite the COVID-19 pandemic entering its second year. This is a glaring indication of the world's wind industry's extraordinary resilience and growing trend. The future of wind energy globally predicts an average annual growth rate of 6.6%. The Global Wind Energy Council (GWEC) estimates that 557 GW of additional capacity will be added during the following five years, or more than 110 GW of new installations each year until 2026 [11]. On the other hand, grid-connected wind energy is expanding more quickly than any other renewable electricity generation resource achieving global annual growth rates of 20–30 % [12]. Wind power, the second-largest renewable resource after hydropower, is one of the energy sources with the fastest expansion. The main advantages of employing wind as a power source are the quick installation, scalability, and minimal carbon effect of the associated infrastructure throughout the project's life cycle [13]. In addition, more energy may be produced close to load centers

because of the increased accessibility of RESs, which lowers the cost of long-distance power transmission. Figure 1.2 depicts the increasing global wind-power generating capacity from 2001 to 2021.

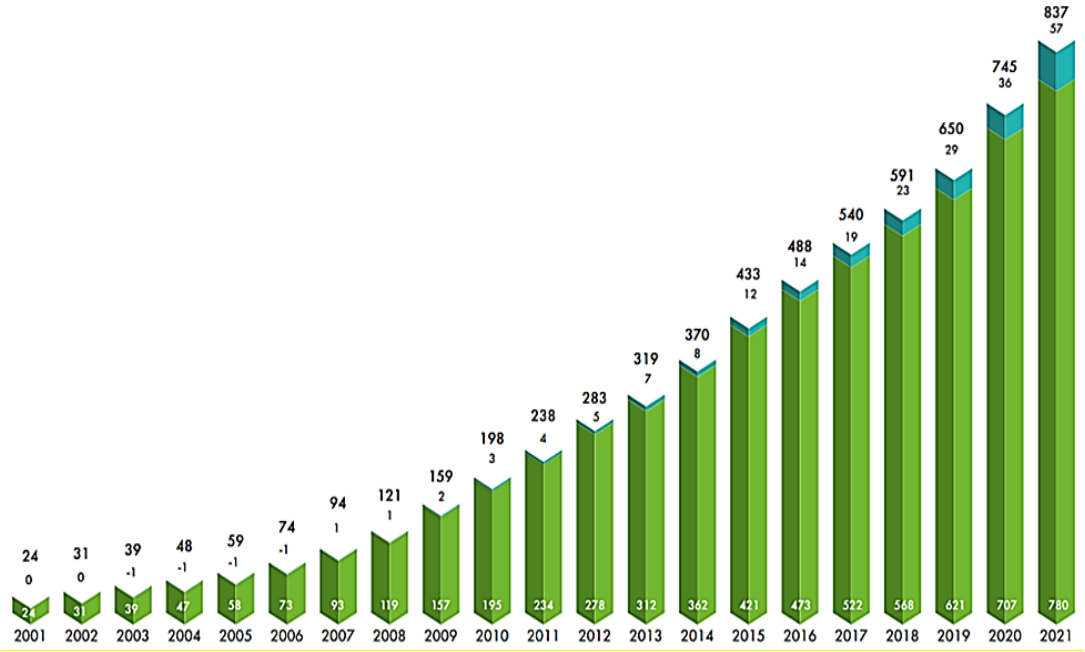

Figure 1.2. Historic development of complete installations [11].

The wind is more affordable for producing electricity than conventional energy sources [14,15]. However, finding the ideal site to generate electricity from renewable sources is challenging. Thus, employing a wind turbine (WT) to transform wind energy into electrical energy mechanically is valuable. Over the past two decades, several WT concepts have contributed to rapid wind power generation advancements and enormous power generation capacity expansion [16].

1.1. DISTRIBUTED WTS AND INTEGRATION ISSUES

Because of the technology development and environmental protection, low-power WTs can be used in grid-connected distributed power generated systems (DPGs) to meet the growing electricity demand and reduce electricity consumption from the utility grid. Without using any energy storage, the excess power generated by the WT that is more than the household or community needs is pumped into the utility [17,18]. On the other hand, power is removed to compensate for the shortfall when the

generator cannot provide enough power to support the demand. The use of distributed power generation (DPG) units has increased significantly. This approach offers lower transmission losses and generation redundancy as a way to decentralize the production and transmission of power, among other advantages. On the other side, it might introduce inherent difficulties in system operations and reliability [19].

Additionally, using individual distributed generators can result in various issues, including islanding, local voltage rise, the ability to exceed the thermal limits of specific lines and transformers, and high capital costs [20,21]. The output power of generation units and the accompanying loads have been treated as main grid subsystems, known as microgrids (MG), to overcome grid connection concerns [22]. These microgrids typically include a distribution-level grid with distributed energy resources (DER) like micro-turbines, PV panels, fuel cells, small hydropower, mini-wind turbines, and small diesel generators operating in a controllable system, and capable of supplying reliable energy to a local area [23]. The advantage of the microgrid over the conventional power plant is: It provides electricity more sustainably by cutting down on transmission power losses and network congestion. If suitable control techniques are used, the micro-grid systems also offer the opportunity to integrate diverse locally accessible renewable resources to construct relatively bigger power generation capacity systems and improve power system reliability [24,25]. Power electronic converters flexibly manage reactive power output, the voltage output of generation, and active power, so they are used to interface a majority of DERs in a microgrid, increasing the resilience of the power grid [26]. MG was connected to the distribution network through a voltage range of 0.4 kV to 33 kV [27]. Figure 1.3 clarify the general configuration of grid connected-MG.

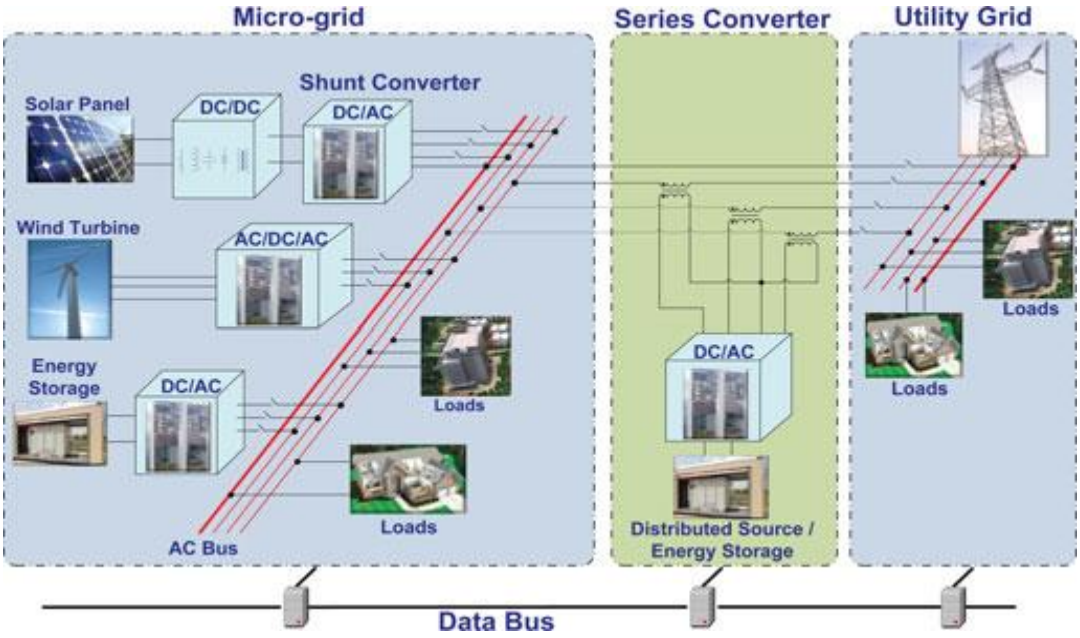

Figure 1.3. The architecture of Grid-connected DPGS [28].

A microgrid is often connected to a grid that can connect to and disconnect from the grid for it to operate in islanded mode and supply local loads in both ways. [29]. The primary challenge faced by grid-connected DPGSs compared to traditional power plants is the variable and unpredictable nature of wind speed (CPPs). Any slight variation in wind speed significantly impacts the quantity of power generated on the grid because a wind turbine's output power is inversely proportional to the cube of the wind speed. These variations have an impact on the grid's losses and electricity quality. Any voltage or current issue resulting in frequency variations, equipment failure, or improper operation is referred to as a power quality issue. Different difficulties are acknowledged in real-world situations where wind power penetration is high. In order to help the restoration of grid stability, WTs must connect to the grid for a predetermined period of time at low voltage, known as low voltage ride through (LVRT) capabilities. To guarantee the stability and dependability of the power system, transmission system operators (TSO) set operational regulations (grid codes) that regulate the behaviors of CPPs. Grid codes are the guidelines established by the government for connecting to the network and operating in accordance with the standards by all of its stakeholders, including customers and power generating stations [30]. The stability and dependability of the overall power system have recently been impacted by the rising penetration level of DPGs, necessitating the management of

DPG behavior in the same way that CPP behavior is regulated. Under normal circumstances, DPGs should contribute to frequency and voltage regulation, LVRT capabilities, and reactive current delivery during voltage sags [31].

1.2. PROBLEM STATEMENT

Unlike classical sources of electric power, wind energy is fluctuating source and non-controllable by nature. Therefore, it has a distinct function in the existing power system. The main problem handled by this research is the quality of the injected power into the grid.

Given the recent increase in wind energy penetration into the grid or transmission systems, additional grid constraints are added to protect stable electric network operations. Technical issues such as fault ride-through capabilities, power quality, and active and reactive power regulation must be considered while integrating wind energy with the electrical network [32]. Thus, the WECS operating parameters should be comparable to the utility grid parameters to guarantee the energy supply's stability, dependability, and availability. Additionally, the injected power should maintain magnitude and frequency in the sinusoidal voltage under usual conditions. Additionally, it's important to stay within the permitted limitations for harmonic and flicker emissions [33]. Poor supply quality will result from the DPG system's incompatibility with the utility grid's power quality specifications [34]. Another challenge is that the DPGS is computationally complex, which is unavoidably a disadvantage when applying optimization techniques directly to the power system, especially when the grey wolf optimizer (GWO) algorithm is subjected to many iterations.

1.3. RESEARCH MOTIVATION

The accessibility of electrical energy is indispensable for the functioning of modern society, which comprises a wide range of industrial activities, transportation, lighting, food processing, storage, information, and communication technology. According to studies, there is a strong correlation between socioeconomic development and energy

use [35]. Thus, one of the main drivers of the current energy research trends is the rising need for electricity. Because of RES, wind energy is today regarded as the foundation of renewable power generation and the energy source with the fastest growth rate worldwide because of its advantages of being one of the most abundant and clean renewable forms of energy in nature [36–39]. Furthermore, onshore and offshore wind saw a 15% and 13% leveled cost of power drop [10]. The main factors behind the widespread global interest in wind-powered electrical systems are the benefits it offers in terms of both the economy and the environment. Its costs are also continually falling due to technological advancements, making it competitive with other energy sources [40].

1.4. LITERATURE REVIEW

A power electronic converter, consisting of a machine-side converter (MSC) and a grid-side inverter (GSI) with a DC capacitor, connects the DPGS, which is DD-PMSG-VSWT, to the grid. The MSC and GSI can be controlled using a variety of control strategies, including feedback linearization [41,42], sliding mode control [43], feedback linearization [44,45], etc. This research focuses on GSI controllers related to the grid-connected DD-PMSG-VSWT. Numerous control methods have been created in order for the inverter to output the current regulation that is supplied to utility grids. These techniques gave rise to controllers, such as the predictive controller, linear proportional-integral (PI) controller, and hysteresis controller [46]. Due to their adaptability, capability, and long-term stability margins, popular controllers are still used as PI regulators in the industry [46]. However, configuring the PI controller's settings can be challenging, particularly in industrial systems with high order, delay time, and nonlinearities [47]. As a result, the gains must be appropriately calibrated. The Cohen-Coon-PID [48], Taguchi technique [49], Trial and Error method [50,51], Artificial Neural Network (ANN) [52], Ziegler-Nichols method [53], and Affine projection algorithm [54], etc.] have been used for fine-tuning PI regulators in the literature.

The aforementioned tuning strategies, however, are dependent on the beginning values and are, therefore, unable to modify higher-order, more complex processes [47,55].

Then, the PI controller parameters can also be fine-tuned using meta-heuristic algorithms, such as Differential Evolution Algorithm (DE) [56], Particle Swarm Optimization (PSO) [57], Whale Optimization Algorithm (WOA) [58], Genetic Algorithm (GA) [59], etc. can serve as effective methods for adjusting the PI controller's parameters. This study employs the GWO meta-heuristic technique to identify the best parameters for cascaded PI controllers in GSI control of the grid-connected DPGS.

In this research, an extensive literature review is conducted on using the traditional and metaheuristic algorithms for optimum tuning of PI controller gains as well as approximating the heavy systems to the ANN model. The GWO and other metaheuristic algorithms used for optimizing the PI gains are stated as follows.

In a study [60], the optimal PID control parameters are determined using Chien-Hrones-Reswick tuning, Cohen-Coon tuning, and Ziegler-Nichols step response methods. The Cohen-Coon tuning methodology was the most successful control tuning technique.

The DC circuit voltage control system performs for the PI, PI-PSO, and FO-PI-PSO controllers have been compared in a study [61] between the primary grid and a PV array. Numerical simulations confirmed the FOPI-PSO voltage controller's superiority to a benchmark system.

An active structural control using three separated metaheuristics tuned PID type controllers is presented in the study [62]. The applied algorithms are Flower Pollination Algorithm, Teaching Learning Based Optimization (TLBO), and Jaya algorithm. The three algorithms discovered various PID control parameters during the optimization process. The most effective algorithm among these three was TLBO.

A PID controller design for DC motor speed control is provided in [63]. The metaheuristic algorithms, Genetic GA, PSO, Simulated Annealing (SA), and Nelder-Mead (NM) are thoroughly compared to traditional approaches like the Zeigler-

Nichols and Cohen-Coon methods. It concluded that better outcomes were achieved with the aid of metaheuristic algorithms.

A comparison study between the traditional pole approach and those based on metaheuristic optimization to fine-tune the PI controller is presented in [64]. It is found that meta-metaheuristic algorithms, as opposed to conventional ones, are very effective at enhancing dynamic performance.

Response Surface Methodology (RSM) and Genetic Algorithms (GAs) were used in [65] to propose the best design process for the cascaded PI controller that is used in the frequency converter of the DD-PMSG-VSWT. It is discovered that the characteristics of the DD-PMSG-VSWT's frequency converter, which was derived from GAs-RSM, can be significantly improved in terms of fault-ride-through.

An application of a Whale Optimization Algorithm (WOA) has been proposed in [66] for finding the optimal parameters of the conventional PI controllers for the PMSG-based WECS on machine side converter. The optimal dynamic performance of PMSG under grid fault can be easily achieved.

According to another study [67], Artificial Bee Colony (ABC) -based optimization for PID controller tuning was one of the finest new tuning techniques compared to other meta-heuristic algorithms.

The Chemical Reaction Optimization technique (CRO) was first used in a study [68] to find the best PI controller parameters for a double-fed induction generator model. According to the simulation results, utilizing CRO for PI tuning has advantages over using the traditional method in terms of performance index and setting time.

Ant Colony Optimization (ACO) and Differential Evolution (DE), two metaheuristic algorithms, are used in a study [69] to optimize the PI controllers in three-phase induction motor control loops. In all tests, the acquired findings demonstrated good performance of the system structure using optimized PI controllers, with DE optimization performing slightly better than ACO.

Among all the meta-heuristic techniques, the GWO proposed by [70] is one of the most potent meta-heuristic. As a recently created algorithm, it has the potential to compete with existing algorithms in terms of solution correctness, minimal computational effort, and avoidance of premature convergence, including PSO, GA, and many other algorithms [71]. Outstanding research applications from numerous important research disciplines have been assessed as a result of the GWO's exceptional benefits. These applications include machine learning, the electrical grid, the communication network, engineering, wireless sensor networks, environmental modeling, health and bioinformatics, image processing, and other areas [72–75]. According to the side of engineering applications, GWO has been adapted to numerous engineering applications, which include designing and tuning controllers, power dispatch issues, robotics and path planning, and many others, as listed below, are thoroughly and in-depth explored in this section. Furthermore, more articles in the field of control engineering look into using GWO to fine-tune the parameters of controllers like integral (I), proportional-integral (PI), and proportional-integral-derivative (PID) [76]. In this regard, the following extensive revision is offered.

GWO is used to optimize the parameters of the PI controllers of closed-loop condensing pressure control systems [77]. The experimental findings demonstrated GWO's superiority over other optimizers like GA and PSO.

Based on determining the ideal size of the microgrid sources, a GWO and an intelligent energy-management technique are proposed in [71] to address the load dispatch issues. The GWO algorithm has been proven to be superior to other algorithms, including GA, BA, PSO, and the improved bat algorithm.

A new variant of GWO is proposed in [78] for fine-tuning the parameters of the proportional-integral controllers for the wind turbine with the doubly fed induction generator. By comparing the proposed approach with that of other heuristic algorithms, it is verified that a better global convergence, more accurate power tracking, and improved fault ride-through capability.

The wind turbine's pitch angle control was altered utilizing the PI controller's best gains in [79], which were discovered with GWO to deal with the delayed convergence into local optimum associated with the PSO and GA tuning approaches. This was done to improve the fixed-speed wind turbine integrated into the distribution system's efficiency and reduce output variance.

PID controller tuning for water treatment plants was proposed in work [80] utilizing the GWO algorithm and other cutting-edge optimization methods. The proposed method might result in good transient responses for flux and conductivity while reducing mistakes. Comparative simulations showed that the GWO approach is more efficient and suitable for optimizing the controller parameters than other techniques.

The GWO is used by the authors of [81] to determine the ideal PI controller parameters by minimizing the proposed objective function for managing the charge and discharge operation of the superconducting magnetic energy storage (SMES) unit. The simulation findings showed that under actual wind speed data with significant range variation, the best-managed SMES smoothed down the output wind power and reduced its overall harmonic distortion.

A new GWO algorithm for tuning the parameters of Takagi-Sugeno proportional-integral-fuzzy controllers PI-FCs has been proposed in [82] for a class of nonlinear servo systems. The three Takagi-Sugeno PI-FC parameters are acquired using a novel, cost-effective tuning method. Furthermore, the tuning strategy is validated by experimental data of the angular position control of a laboratory servo system.

The GWO method and a novel hybrid cuckoo search algorithm are utilized in [83] to build and adjust the PI controller parameters. Such carefully thought-out PI controller performance is shown in both transient and dynamic conditions. The suggested algorithm's realistic stability was tested in particular during symmetrical and unsymmetrical faults. The collected results demonstrated its superiority to other conventional algorithms, such as the Genetic Algorithm.

A PI controller for a wind turbine with a fixed speed was tuned using the GWO in [84]. Compared to PSO and GA tuning techniques, the GWO tuning method produced better results. In comparison to the other two approaches, it displayed quicker convergence and better time response specification.

Researchers have used the GWO method effectively [85] to optimize the gains of two PID controllers for a quadruped robot to ensure single footstep control in the desired trajectory. The proposed technique has been compared with GA and PSO algorithms and proved that the GWO algorithm is the best for the PSO algorithm and GA.

A fixed-speed wind turbine's pitch angle control system has been successfully tuned with the help of GWO and the PI controller [79]. The same distribution system also employed the Ziegler Nichols (ZN) tuned PI controller, PI-fuzzy logic, and fuzzy logic controllers. With PI-GWO, the tuned controllers improved efficiency and smoothed down the output power.

The findings of a thorough review of 83 previously published articles from investigations relating to GWO in diverse applications from the years 2014 to 2017 are presented in the literature [86]. An overview of the research trend for the GWO optimization technique is given, along with a description of the characteristics of the GWO algorithm and how it reduces the various difficulties in the various applications. It was found that GWO's excellent local search criteria work remarkably well for a variety of issues and solutions and enable it to solve single and multi-objective problems effectively.

GWO is used to tune PI controllers in [87] DC/DC and DC/AC converters for performance enhancement of grid-connected photovoltaic systems. The GWO's effectiveness was compared to the WOA, Grasshopper Optimization, and Salp Swarm algorithms were tried under changing irradiance conditions. The transient performance obtained demonstrated the practicality and feasibility of the chosen GWO technique.
In [88], the GWO algorithm was recommended for fine-tuning the PID controller parameters for a DC-DC boost converter. The performance of the suggested GWO, PSO, and GA algorithms under variable load conditions was examined, along with the

Root Mean Squared Error (RMSE) between the output voltage and reference. The GWO method, as opposed to PSO and GA, has a reduced RMSE, according to the results.

The GWO is utilized in [89] to find the proper gain factors of eight PI regulators of MSC and GSI control schemes to improve the low voltage ride-through capability, MPPT, and the steady-state operation of grid-connected DD-PMSG-VSWT. The GWO algorithm offered the best convergence and superior response of the MPPT and the LVRT capability during symmetrical and asymmetrical faults than the GA and simplex techniques.

On the other hand, the computational complexity of the DPGS system is undoubtedly a drawback when applying optimization methods directly to the power system, especially when the GWO algorithm is subjected to a lot of iterations. For this reason, several efforts have been made to create a novel model that can be used as a substitute for complex simulation models such as the considered DPGS [90]. Different objectives for using these novel models include sensitivity analysis, uncertainty quantification, risk analysis, and optimization [91]. These cutting-edge models often referred to as proxies, surrogate models, or metamodels in engineering, are frequently used for design optimization in order to cut down on the amount of computationally demanding simulations. The objective of using surrogate models is that it is helpful to assist the design optimization process in which they aim to produce the output in a concise amount of time [92].

In the study [91], different classes of proxy models are reviewed and discussed, and a new classification based on the development strategy is proposed. In this overview, many proxy modeling construction steps are thoroughly covered.

A proxy ANN model to track reservoir temperature and pressure using wellhead data has been created [93]. An ANN model is trained using an extensive set of wellhead data in a calibrated wellbore simulator. For a variety of production situations in a liquid phase reservoir, it is observed that the ANN model can accurately estimate reservoir pressure and temperature.

For groundwater remedial design, the GWO are integrated with the ANN model (ANN-GWO) in [94]. The ANN model is used for approximating the flow and transport mechanisms of two unconfined aquifer case studies. The outcomes demonstrated the excellent level of accuracy of the ANN model. The recommended methd showed improved stability and convergence behavior when compared to the findings of the ANN-Differential Evolution and ANN-PSO models.

In [92], a surrogate fluid flow model is developed using artificial intelligence and machine learning techniques. It is approved that the model can generate the results of a complex numerical simulation model at the grid block level with reasonable accuracy in a concise time with significantly less computational cost.

A performance evaluation of artificial neural networks-imperialist competitive algorithm (ANN-ICA) and artificial neural networks-gray wolf optimizer (ANN-GWO) models was presented [95] for crop yield prediction. According to the results, ANN-GWO proved a better performance in crop yield prediction compared to the ANN-ICA model.

An optimization process based on the ANN-wake-power model and the Genetic Algorithm is established in [96] to find a set of yaw angles of wind turbines that can maximize the power generation of a cluster of wind turbines. The ANN-wake-power model performed fast simulation for the total power generation of wind turbines with high accuracy.

A surrogate model has been constructed in [97] for predicting the power and fatigue loads of turbines in a wind farm wherein three regression methods, namely, Linear Regression, Artificial Neural Network, and Gaussian Process Regression, have been addressed. The model trained by Gaussian Process Regression has achieved superior accuracy.

In [98], ANN is used in conjunction with two metaheuristic approaches, GA and harmony search (HS), to forecast the weather in six Turkish cities. The performance measurements and graphical analysis showed that forecasting average temperatures

have improved. However, although the proposed hybrid GA-ANN and HS-ANN methods ensured remarkable results, it has some limitations.

An ANN model was trained in [99] in an oil reservoir under gas injection using a combination of simulation runs known as the design of experiments (DOE). The results' accuracy indicated that ANN as a proxy model with DOE is a fast and reliable tool that can replace the simulator.

Based on the cuckoo search algorithm (CSA), the study [100] demonstrated the best tuning method for five PI controller settings for grid-tied photovoltaic systems. An ANN is used to create the mathematical model of the PV system to reduce the design effort. Furthermore, the system stability of the ANN-based CSA is validated in case of any transient situations.

A proxy model has been created in [92] based on machine learning and artificial intelligence to roughly represent the resolution of a difficult reservoir simulation model. It was determined that the established proxy model could produce results from a sophisticated numerical simulation model with a respectable level of accuracy in a concise amount of time at a much lower cost.

1.5. METHOD AND OBJECTIVES

The primary aim of this work is to improve the output power quality of DGS injected into the grid under various wind speeds. This research concerns the grid-side controller, which focuses on the quality of voltage and current waveforms injected into the grid. The controller tasks include: improving the DPG system’s output power quality, regulating the power exchange between the DPG plant and grid, performing reactive power compensation, achieve a high output power factor. The term power quality here refers to voltage regulation, constant frequency, less total harmonic distortion in voltage and current waveforms, along with DC link voltage stability and grid synchronization. This is achieved by finding optimum gains of three cascaded PI controllers in the grid side inverter by combining the grey wolf optimizer (GWO) and

artificial neural network (ANN). The above objectives are accomplished by applying the following steps:

- To design and develop a grid integration-based DPG system. The system is small-scale wind energy. Wherein DD-PMSG-VSWT is considered.
- Comprehensively review control methods used in grid interfaced DPG grid side
- inverter control and design a control method-based PI controller to improve power quality with grid code compliance.
- To deal with computational complexity and reduce computational time, which is undoubtedly a disadvantage when applying optimization techniques directly to the DPGS, an alternative ANN model of the DPGS should be designed. Additionally, GWO's optimization accuracy has improved.
- To design GWO code by MATLAB to obtain the best proportional and integral gains for each PI controller. That means six optimum gains are required.
- Using the MATLAB/Simulink program for performance assessment of the system utilizing the best GWO-ANN results at different wind speeds.

1.6. THESIS ORGANIZATION

Part one contains the general concept of renewable energy resources; grid integration-based distributed generation systems, state of the arts related to the topic of the thesis, objectives of the work, and the objective and methodology.

Part two deals with configurations and topologies of grid integration-based WECS. Further, contains grid integration requirements and grid code.

Part three presents a detailed control strategy for grid integration based-WECS. Also, the techniques for tuning of PI Controller are presented.

Part four includes the following methodology, which consists of the detailed steps for GWO, building an approximate model for DPGS, and then implementing the

conjunction of ANN-GWO to optimize the cascaded PI controllers. Also, the obtained results and discussion are presented in this part.

Part five summarizes the research outcomes and significant research contributions. Additionally, it suggests certain areas for further study.

An index of pertinent references is provided after the conclusion of the thesis.

PART 2

SYSTEM MODELING

2.1. WIND ENERGY CONVERSION SYSTEM (WECS)

In WECS, a wind turbine and an electric generator are used to produce electrical energy from the wind. The prime mover and the wind turbine can be connected directly or through a gearbox configuration. The generator's rotor's shaft is where the prime mover is connected, and the stator is connected to either freestanding loads or the utility grid via an appropriate power electronic interface [101]. Figure 2.1 depicts the block diagram of a typical grid-connected WECS.

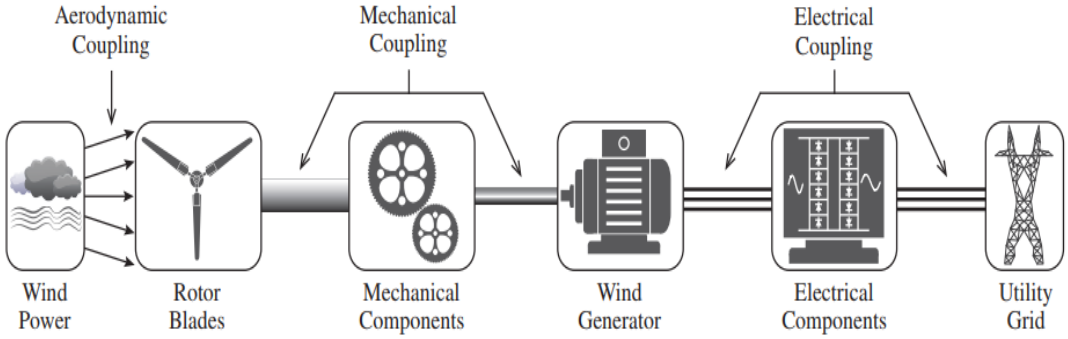

Figure 2.1. Typical grid-connected WECS

The kinetic wind power P_w flowing out of an area A at speed v_ω is [102]:

$$P_w = 0.5\ \rho A v_\omega^3, \qquad A = \pi r^2 \tag{2.1}$$

where ρ is air density (kg/m^3), v_ω is the wind speed (m/s). A is the rotor swept area (m^2), and r is the blade radius (m). Air density depends on temperature, humidity, and altitude. The Air has a typical density of 1.225 kg/m^3 of 15◦C at sea

level. Aerodynamic conversion losses are significant during the transformation of mechanical energy into practical electricity. However, in practice, factors like a hub and tip effects, wake effects, and aerofoil blade roughness restrict the typical maximum efficiency of a wind rotor to around 30%, as shown in Figure 2.2 [103,104].

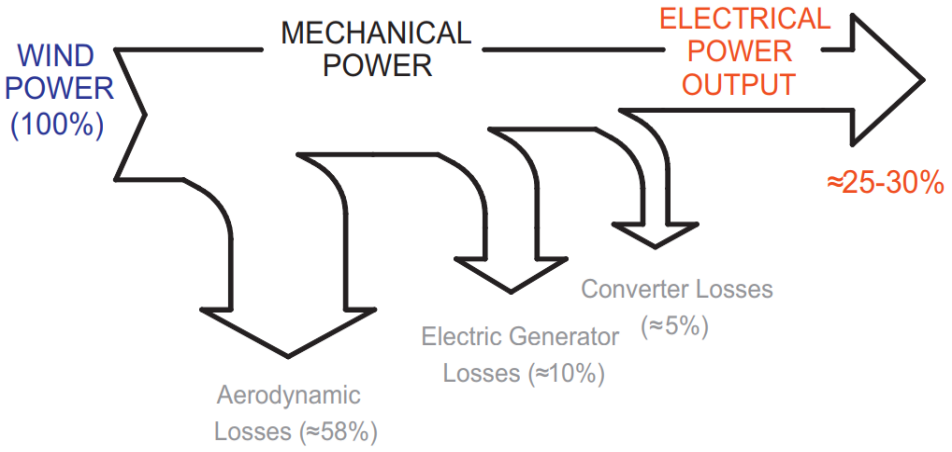

Figure 2.2. Power stages of wind energy conversion system [103,104].

The Betz limit is the theoretical upper energy limit that can be extracted with c_P = 16/27 = 0.593 [105]. The mechanical power P_m that can be obtained from the kinetic wind power P_w is thus given by:

$$P_t = P_w \times c_p = 0.5\ \rho A\ v_\omega^3\ c_P \quad , \quad c_P = f(\lambda, \beta) \tag{2.2}$$

where; P_t is the turbine's mechanical power which, absorbed by the wind turbine, v_ω shows wind velocity (m/s), ρ represents the air density (Kg/m^3), P_t is the turbine's mechanical power absorbed by the wind turbine, A shows the turbine's swept area by the blades (m^2), λ shows the tip speed ratio (TSR), β is the blade pitch angle (C), and c_p shows the performance coefficient. The TSR is described as follows:

$$\lambda = r\,\omega / v_\omega \tag{2.3}$$

Here ω implies the blades' rotational speed (rad/s) and r represents the blade radius (m). The c_p parameter can be given as follows.

$$c_p(\lambda,\beta) = c_1\left(\frac{c_2}{\lambda_i} - c_3\,\beta - c_4\right)\exp\left(\frac{-c_5}{\lambda_i}\right) + c_6\,\lambda \tag{2.4}$$

$$\frac{1}{\lambda_i} = \left(\frac{1}{\lambda + 0.08\beta} - \frac{0.035}{\beta^3 + 1}\right) \tag{2.5}$$

The output power is optimized by the performance coefficient c_p, which is based on the turbine's tip speed ratio λ and the pitch angle β of the blades. The turbine's mechanical design affects its TSR. As a result, many investigations have been carried out to enhance the TSR value with the structure of the desired blades [106].

Variable-speed wind turbines (VSWT) need a full or partial-order power converter to control power flow, MPPT, and supply high-quality electricity, in contrast to fixed-speed wind turbines (FSWT) [107,108]. Since these turbines can vary their rotating speed to correspond to the instantaneous variations in wind speed, they are able to maintain a constant rotational speed-to-wind speed ratio, or ideal tip speed ratio (TSR) [14]. Typically, wind turbines are constructed in fixed-speed or variable-speed varieties WECS. A fixed-speed WECS does not need power converter hardware because it is directly attached to the electrical system. For various factors, including decreased mechanical stress, increased power collection, better controllability, and power quality—all of which are crucial for grid integration—variable speed operation is preferable to fixed speed systems [102].

On the other hand, a variable-speed WECS communicates with the power grid through power electronic converters to enable variable-speed operation. Synchronous Generators (SGs), which are used by direct-drive wind turbines and must be connected to the grid by a full-capacity power converter, are used [109]. Indirect-drive wind turbines utilize a Doubly-Fed Induction Generator (DFIG), or a Wound-Rotor Induction Generator (WRIG), using controlled rotor resistance. A DFIG is connected to the grid through partial capacity converters. Subsequently, A broad WECS

configuration range can be achieved by utilizing various designs and combinations with some or all of these electrical and mechanical components, including the following four types:

Type 1: Fixed-speed WECS with SCIG.
Type 2: Semi-variable-speed WECS with WRIG.
Type 3: Semi-variable-speed WECS with DFIG.
Type 4: Full-variable-speed WECS with PMSG, WRSG, and SCIG.

The four configurations mentioned above are thoroughly explained in this section. Each WECS configuration's key mechanical and electrical parts, working theory, benefits, and drawbacks are explained.

2.1.1. Type 1 WECS

The most common wind turbine systems of this type, based on squirrel cage induction generators (SCIG).and utilizing WECS with no power converter interface, are shown in Figure 2.3.

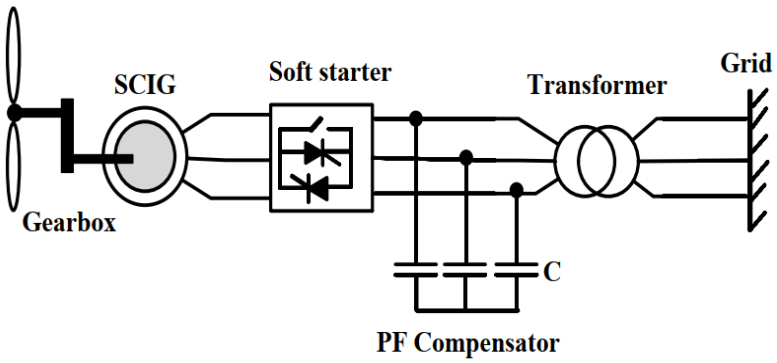

Figure 2.3. Squirrel-Cage Induction Generator-equipped WECS.

The generator, connected to the primary grid by a soft starter and step-up transformer, was frequently utilized during the early stages of wind turbine installation [104]. A three-phase soft starter is employed to reduce the SCIG's undesired inrush current and facilitate a smooth start-up. In order to match their respective speeds, a three-stage gearbox frequently connects the turbine rotor and wind generator [110]. Induction

generators will maintain a speed that varies by only 1% to 2% [6]. Fixed-speed WECSs experience severe mechanical strains during wind gusts as well [111].

2.1.2. Type 2 WECS Configuration

The system is built up similarly to a Type 1 turbine, except that a Wound-Rotor Induction Generator (WRIG) with coupled rotor windings acts as the external resistor in place of a SCIG. The power converter comprises an insulated gate bipolar transistor (IGBT) and a three-phase diode-bridge rectifier. A semi-variable-speed WECS configuration using a half-rated (10%) power converter and WRIG, as Figure 2.4 shows.

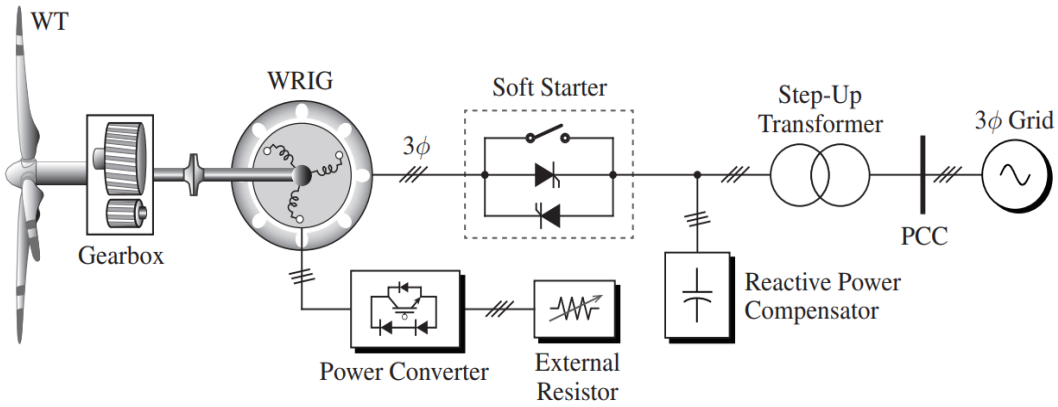

Figure 2.4. Type 2 Wound-Rotor Induction Generator-equipped WECS.

Moreover, using this control approach, the operation speed can be altered by up to 5% [112]. WECS can capture more wind power with less strain on the mechanical parts and semi-variable-speed operations, but energy losses occur because of rotor resistance. Similar to a Type 1 turbine, this system requires a soft starter, reactive power correction, and a gearbox. Because of operating at a semi-variable speed, this arrangement has fewer adverse effects on grid frequency and has greater energy conversion efficiency than Type 1 turbines. Cons include higher maintenance costs because of the WRIG's slide rings and brushes, higher starting costs because of the power converter, and decreased dependability because of system losses and the external resistor

2.1.3. Type 3 WECS Configuration

Soft starters and grid-side reactive power compensators are dropped in favor of Type 3, which also increased the speed range at which WTs could operate. In this setup, a power converter takes the role of the Type 2 turbine's converter-controlled external resistor. The coupling transformer connects the DFIG windings to the grid directly, as opposed to the rotor windings of the DFIG, which are connected to the grid via an AC-DC-AC Voltage Source Converter (VSC). The rotor circuit converter only controls slip power, and only 30% of the generator's power should be made accessible to it [113]. The DFIG-based WECS needs gearboxes because multipole low-speed DFIGs are impossible. Figure 2.5 shows a typical configuration for the DFIG-based WECS.

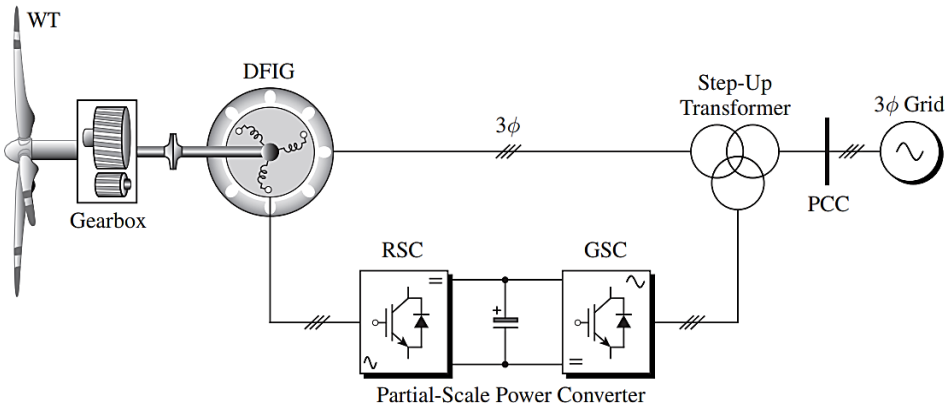

Figure 2.5. Type 3 with variable-speed DFIG - equipped WECS [17].

The Type 3 WECS' main features include challenging fault ride through (FRT) compliance, a bi-directional power flow in the rotor circuit, grid-side reactive power compensation, a smooth grid connection, robustness against power disturbances, and improved dynamic performance compared to Type 1 and 2, and lack of fit for offshore wind farms due to the requirement for regular maintenance [114].

2.1.4. Type 4 WECS Configuration

Type 4 turbines use a power converter to move all the produced electricity between the utility grid and the wind generator stator terminals, unlike Type 3 turbines. The full-scale power converter's variable speed range is 0% to 100%. As a result, the power

converter's capacity rises from 30% to 100%. This arrangement has been utilized by the SCIG, Wound Rotor Synchronous Generator (WRSG), and PMSG [115]. Because of its benefits over other wind generator classes, PMSG is the most common type of wind generator in Type 4 WECS [116]. Using a multi-pole number SG and running the power converters at medium voltage makes it possible to do away with both the step-up transformer and the gearbox. Compared to Type 1, 2, and 3 turbines, this arrangement is more robust to power system problems [117]. The most promising system currently is the direct-drive WECS with PMSG since it does not require external excitation or slip rings compared to the WRSG, leading to the great efficiency and reliability [107]. Figure 2.6 depicts a typical setup for a variable-speed wind turbine with a wind generator and a full-scale power converter made up of a DC-link capacitor, a machine-side converter (MSC), and a grid-side inverter (GSI).

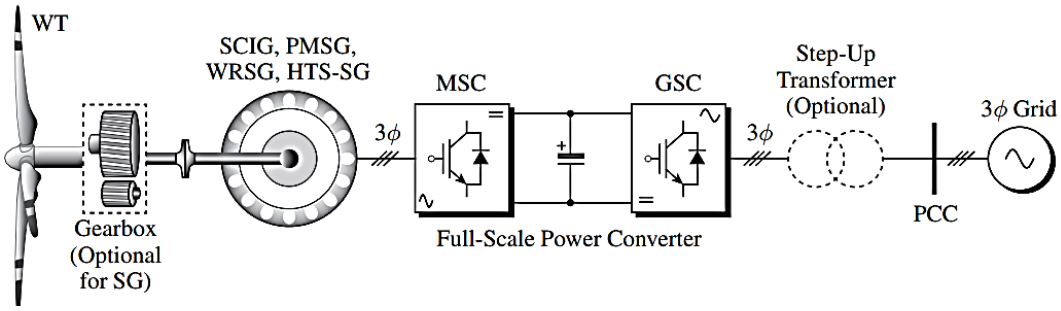

Figure 2.6. Type 4 WECS with complete variable speed [17].

The key advantages of this configuration: The generator is completely cut off from the grid and produces a lot of energy without putting any strain on its mechanical parts. Controlling active and reactive power independently helps to ensure good FRT compliance. Further, a full-scale power converter has a smooth grid connection in contrast to the variable speed method with a partial-scale power converter over the entire speed range. Because of all this, the power converter is more expensive, resulting in more power losses [115,118]. Additionally, the price of Permanent Magnet materials may also be subject to some uncertainty.

In order to install a wind energy system, numerous structures outfitted with various types of induction generators have been created. The problem with these machines is that they need both an excitation and a multistage gearbox. However, because of its

improved efficiency and durability, superior performance, and capacity to work at low speed, which eliminates the need for a gearbox, PMSG has attracted researchers' attention in recent years [119,120]. Additionally, this way of control is appropriate for minimal maintenance usage. Therefore, the grid-connected of DD-PMSG-VSWT-based WECS is the subject of this research.

2.2. MPPT CONCEPT

Eq. (2.2) shows that the power produced by a turbine P_m at a given wind speed v_ω relies on the value of c_p the air density ρ, the turbine's design parameters, and other variables [14]. Hence, with a fixed blade pitch angle turbine, the output power mostly depends on the value of c_p and that value depends on the wind turbine's rotor speed. As a result, when c_p is maximal, the output power of a wind turbine is at its highest. This ideal value c_p occurs at various values λ as specified in Eq (2.4). There is only one optimum rotor speed for a specific wind speed, which c_p is the greatest $c_{p\_\max}$ and optimum λ_{opt} for maximizing the extracted power, as illustrated in Figure 2.7.

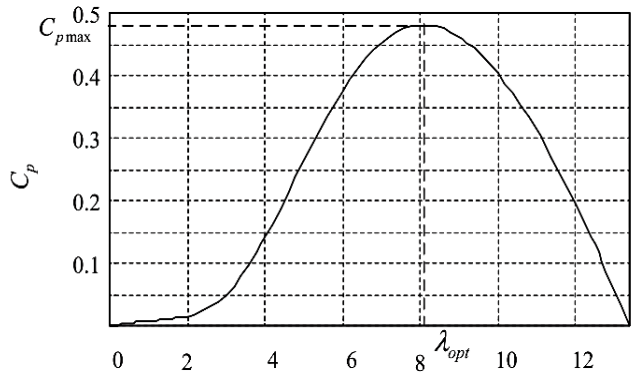

Figure 2.7. The curve of power coefficient c_p versus tip speed ratio λ.

To operate the system at MPP in all operating conditions, it is essential to vary the rotational speed due to the instantaneous variations in wind speed. The nonlinear power-speed characteristic curve of a turbine depicted in Figure 2.8 [14] illustrates how the output power capacity of a wind turbine can be adjusted by modifying rotor speed and keeping operational points on $c_{p\_\max}$. Although the form of the curve is the

same, its magnitude varies depending on the wind speed [121,122]. Each curve in this diagram has a distinct rotor speed $\omega_{m\ opt}$ that corresponds to the wind velocity's maximum power point (MPP) [108]. This effectively means that maximum power may be collected from the wind for a given wind speed if the rotor is turned at $\omega_{m\ opt}$ [123].

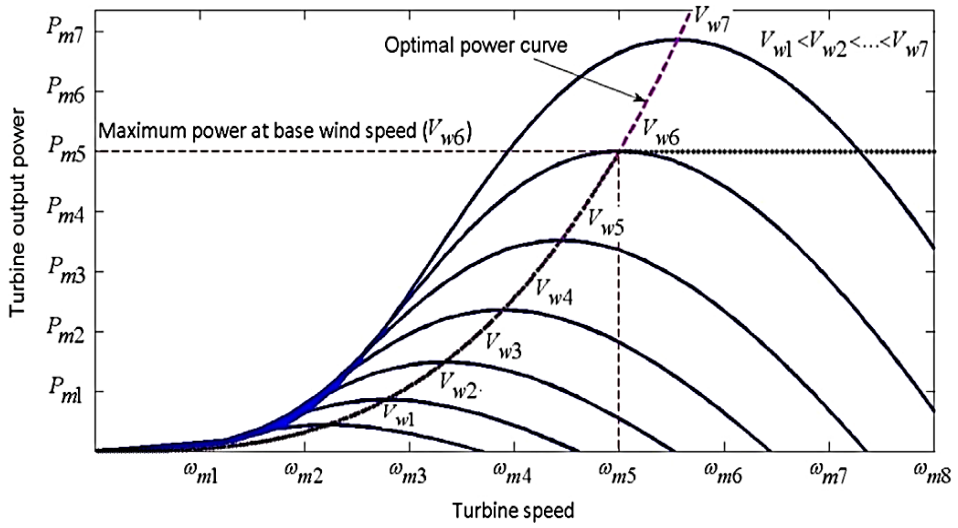

Figure 2.8. Mechanical power function of the rotor speed.

The subsections below provide an explanation of the three most common MPPT techniques [124]: perturb and observe (PO), power signal feedback (PSF), and tip speed ratio (TSR).

2.2.1. TSR Algorithm

The TSR control regulates the wind turbine rotor speed to maintain an ideal TSR. The wind speed and turbine speed must be measured using the MPPT approach. An anemometer is typically used to measure wind speed, which raises system costs and makes it nearly impossible to get an accurate reading in practice [125]. The block diagram in Figure 2.9 depicts a WECS with TSR control. In this diagram, the optimum and actual rotational speeds are compared. The controller then adjusts the generator's speed to minimize the error based on the difference. It is concluded that this technique compels the generator's mechanical power to track its maximum mechanical power. The TSR algorithm is highly effective and responsive [126], but it is more expensive since an accurate anemometer is required to measure wind speed in small-scale WECS.

Furthermore, these MPPT control algorithms only offer details on the system's optimal power-harvesting operating point. To run the system at its MPP, WECS needs a controller [127].

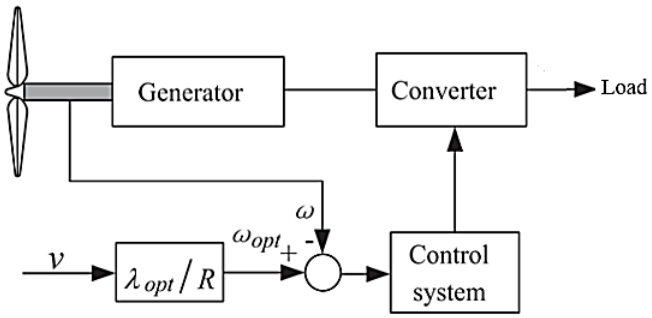

Figure 2.9. The control diagram of the optimum TSR MPPT method [125].

2.2.2. PSF Algorithm

Mathematically, the PSF control can be determined by using (2.1) and (2.2) as follows

$$P_t = 0.5\ \rho \pi\ r^2\ (\frac{\omega_m\, r}{\lambda})^3\ c_P \tag{2.6}$$

The maximum power can be found by substituting the maximum value of the c_p and the optimum value of the TSR at (6) [128].

$$P_{\max} = 0.5\ \rho\ \pi\ r^5\ \frac{\omega_m^3}{\lambda^3}\ c_P = K_{opt}\ \omega_m^3 \tag{2.7}$$

$$K_{opt} = \frac{0.5\ \rho\ \pi\ r^5}{\lambda_{opt}^3}\ \mathrm{c}_{\mathrm{p\_max}} \tag{2.8}$$

From Eq. 2.7, it can be concluded that the maximum power is proportional to the cube of the mechanical speed. Using $\mathrm{c}_{\mathrm{p\_max}}$ and λ_{opt}, the K_{opt} (maximum power coefficient) can be obtained. The ideal power curve consists of the rotational speed, and electrical power can be obtained by using knowledge of $\mathrm{c}_{\mathrm{p\_max}}$ and λ_{opt} or by the experimental

study [129]. The optimal power curve also needs a measured mechanical speed to produce the reference of the MPP. Comparing the measured turbine power and reference turbine power makes an error, which is then delivered to the controller, so the WES is controlled based on the directive of the controller. The control block diagram of this method is given in Figure 2.10.

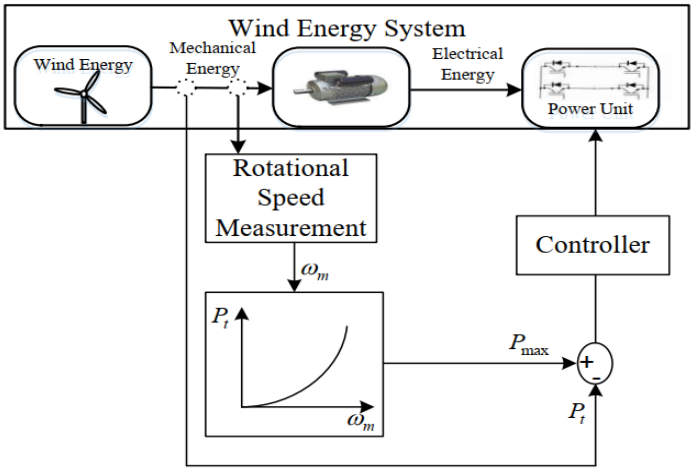

Figure 2.10. The control block diagram of the PSF method [129].

2.2.3. Perturb and Observe (PO) Control

A mathematical optimization methodology known as PO or the hill-climb searching (HCS) method is utilized to find the local maximum point [130]. First, the controlled system is used to choose the control and output parameters. The output parameter is then observed after perturbing the control parameter. This process is continued until the slope equals zero, as shown in Figure 2.11. The WES control parameter (ω) is raised if the slope is positive. Otherwise, it is decreased. According to the literature, this method's control parameter can be the converter's duty cycle, input current, or input voltage.

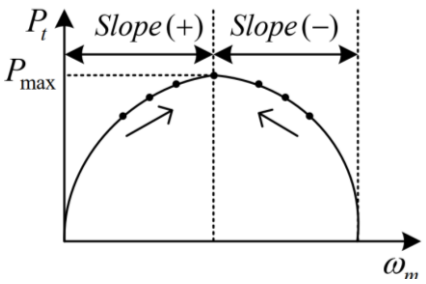

Figure 2.11. P&O method graph [129].

2.3. POWER CONVERTERS IN WECS

Important WECS components include converters and electric generators because they link the turbine's mechanical energy to the electric load. Therefore, using the right kinds of these devices and control systems is crucial to ensure both perform as efficiently as possible [131]. Power converters, which are semiconductor-based devices that alter the type or level of an electrical signal, are a must for achieving this. According to the current input-output relationship, power converters are categorized into four groups: (i) inverter (input DC/output AC), (ii) rectifier (input AC/output DC), (iii) chopper (input DC/output DC), and (iv) frequency converter (input AC/output AC), called a phase converter or a cycloconverter [132].

There are three different classes of semiconductors used in power converters based on how tightly controlled they are: 1) Diodes, which only allow electricity to travel in one direction, and they can't be controlled. 2) Grid-commutated components called thyristors or semi-controllable switches, which must be set "off" by the power circuit but latch "on" by control signal 3) Bidirectional devices that can be turned "on" or "off" by control signals are self-commuted converter systems, also known as controllable switches. Active/reactive power is transferrable in either direction (DC/AC or AC/DC) using controllable switches. They are composed of the bipolar junction transistor (BJT), the metal oxide semiconductor field effect transistor (MOSFET), and the insulated-gate bipolar transistor (IGBT) [131]. An AC/DC and DC/AC converter-equipped power electronic interface is then used to link an asynchronous or synchronous generator to the electrical grid.

The power electronics converter is becoming increasingly crucial as wind power generation capacity and technology advance quickly. On the other hand, the standards for power electronics converters are significantly more stringent than ever. In Type 1, power converters only utilize slick grid hookups. After connecting the generator to the grid, the power converters are then removed [111]. For current Type 3 and Type 4 WECS, the following technical, operational, and regulatory requirements must be met by power converters [133]:

- **General requirements:** To manage the electromagnetic torque on the generator side, the current needs to be adjusted. This is required to balance the energy in the event of dynamics brought on by an imbalance in inertia between mechanical and electrical power conversions and maximize the power collected from wind turbines. The converter on the grid side needs to operate similarly to conventional power plants. This implies that it should aid in maintaining the grid's frequency and voltage amplitude and survive grid faults and potentially contribute to their recovery [111,113].
- **Initial Cost:** In order to compete with other energy sources and achieve a low cost of energy (COE), this component is crucial. A power converter's starting cost makes up a small part (about 7–12%) of the WT costs [134]. Despite the minor portion of the cost, a wind farm with hundreds of WTs can achieve significant cost reductions.
- **Reliability and Maintenance Cost:** To achieve low COE, a power converter's maintenance costs must to be as low as possible. Power converters and electric generators lead the list of turbine failures (average failure rate: 13-20%), according to the most recent reports [135]. Power converter issues lengthen the time the WT is not operational and raise the COE. Thus, excellent reliability is required for WT power converters. Modular power converters are preferred because they can still function with a reduced capacity even if one fails, reducing downtime.
- **Efficiency:** Efficiency is crucial for reducing COE at the MW power level. Just a 1% power converter efficiency gain translates into substantial cost savings in a wind farm with hundreds of WTs [136]. Conduction and switching losses are the two forms of losses in power converters. Switching devices produce conduction losses. It is necessary to reduce power losses, which directly impact efficiency, by employing effective switching devices and the best switching device design, control strategies, and a cooling system.
- **Power Quality:** The numerous power converter parameters are responsible for power quality, which is the number of steps in the waveform’s output voltage (dv/dt) [137], specifying whether the output voltage waveform must resemble a sinusoidal waveform. The necessity for a harmonic output filter and the dv/dt ratio both drops as the waveform's step size increases. Additionally, as dv/dt

lowers, the electromagnetic interference also does. The total harmonic distortion (THD) must be low to supply quality currents and decrease generator shaft oscillations [133].

- **Grid Code Compliance: It is** a key prerequisite for grid-connected WTs. Grid current harmonic control must adhere to tight requirements set forth in utility standards like IEEE 519-1992. Power converters must, among other things, maintain voltage and frequency, feed the grid with currents that offer reactive power whenever needed, have a low THD (lower than 5%), and provide ride-through during disruptions [138]. The power converters must fulfill these requirements without the aid of additional hardware or parts, such as a static VAR compensator (SVC), static synchronous compensator (STATCOM), or flexible alternating current transformer (FACTS).
- **Footprint and Weight:** Unlike electric drives, the nacelle of WTs has a restricted amount of room. Power converters must have a high power density for a small footprint and weight, particularly for offshore WTs [133].
- To achieve the goals as mentioned earlier, WT manufacturers and the power converter companies that support them have developed a variety of generator-conversion configurations. To differentiate themselves, some WT manufacturers are creating cutting-edge power conversion methods [17]. Modern WECS power converter classification is a complex topic to master. Below is a quick overview of each converter category:

2.3.1. Back-to-Back Connected Power Converters

Back-to-back (BTB) connected power converters are identical on the grid and generator sides. They are connected through a DC link. They can be current or voltage source converters; both contain a DC link comprised of inductors or capacitors. BTB converters transform the generator's output from AC to DC, and then DC to AC, with a constant frequency and voltage for connection to the grid. Since power conversion occurs in two stages, BTB converters are called two-stage power converters. In addition, power travels from the generator to the grid and back again; therefore, BTB converters are usable with DFIG, SCIG, WRSG, or PMSG. The MSC and GSI are identical, so their development and application are simple and valuable. They hold the largest market share and are used by most Type 3 and Type 4 WTs currently in use [17].

- **Full-Scale BTB:** A complete BTB has two levels (2L-VSC). A Type 4 WECS is depicted in Figure 2.12. Both MSC and GSC are implemented, respectively, using the voltage source inverter (2L-VSI) and 2L voltage source rectifier. A DC-link capacitor couples the MSC and GSC. The 2L-VSR and 2L-VSI are implemented using matrix-arranged low-voltage IGBTs [139].

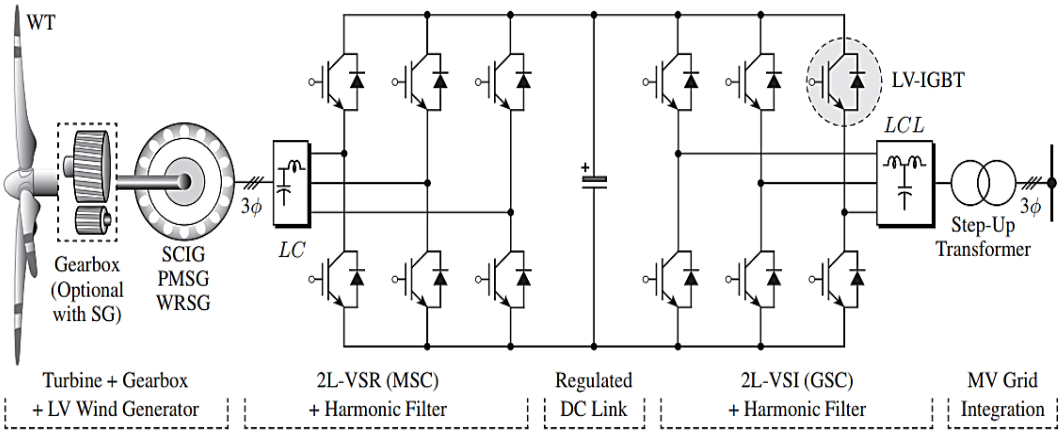

Figure 2.12. Full-scale BTB coupled to 2L-VSC and WECS [17].

- **BTB 2L-VSCs in parallel with separate DC links:** It is used to link identical power converter modules in parallel to lessen the stress on WECS components

for a high-power application. This structure benefits from redundancy, modularity, and scalability [113].

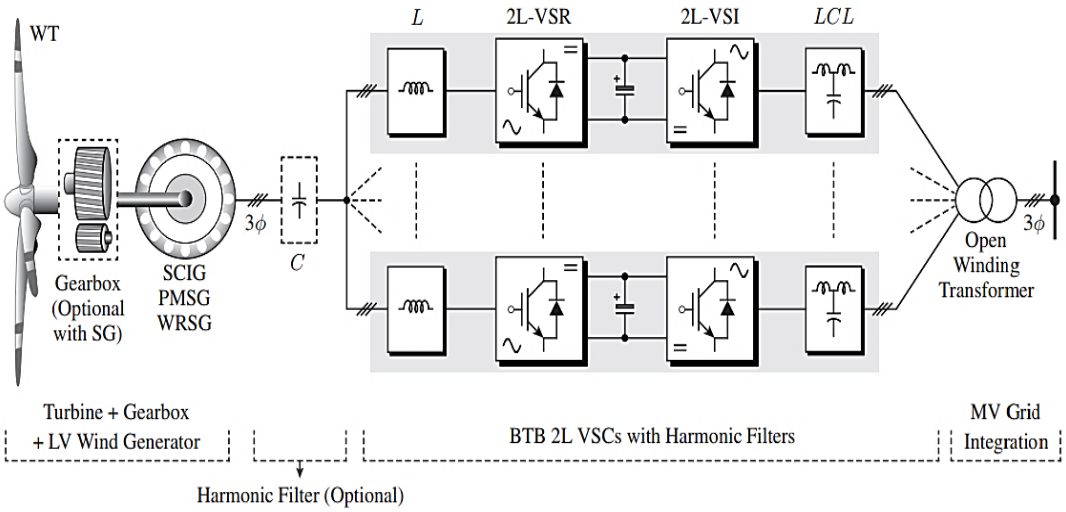

Figure 2.13. Multiple power converters are connected in parallel to connect a wind turbine [17].

On the grid side, open-winding transformers are utilized to lower circulating currents. Each GSC employs its own set of LCL filters. However, Type 4 WECS continue to use this setup as their principal technology.

2.3.2. Unidirectional Power Converter

Power in WECS only flows in one direction, from the generator to the grid. As a result, the AC to DC conversion on the generator's side can be accomplished using diode-bridge rectifiers, sometimes referred to as passive generators (PG), as opposed to pulse-width-modulated (PWM) active converters [132]. Diode-bridge rectifiers' affordability and inherent dependability are unmatched by PWM converters. In PMSG and WRSG, permanent magnets and rotor field excitation produce the rotor flux. Therefore, diode-bridge rectifiers can implement the generator-side power conversion system in PMSG/WRSG WTs. On the generator side, diode-bridge rectifiers are not allowed since induction generators like SCIG and DFIG needs magnetizing currents to operate.

- **Diode Rectifier + 2L-VSI:** Compared to the BTB 2L-VSC, this topology offers a cheap, lightweight alternative. The diode rectifier converts the generator's output's AC voltage to DC. The DC voltage is then converted back to AC voltage via the 2L-VSI. The inductor in the DC link smoothes down the output current of the diode rectifier.

Figure 2.14 shows how a three-phase diode rectifier and 2L-VSI are used in the power converter setup for PMSG/WRSG WECS.

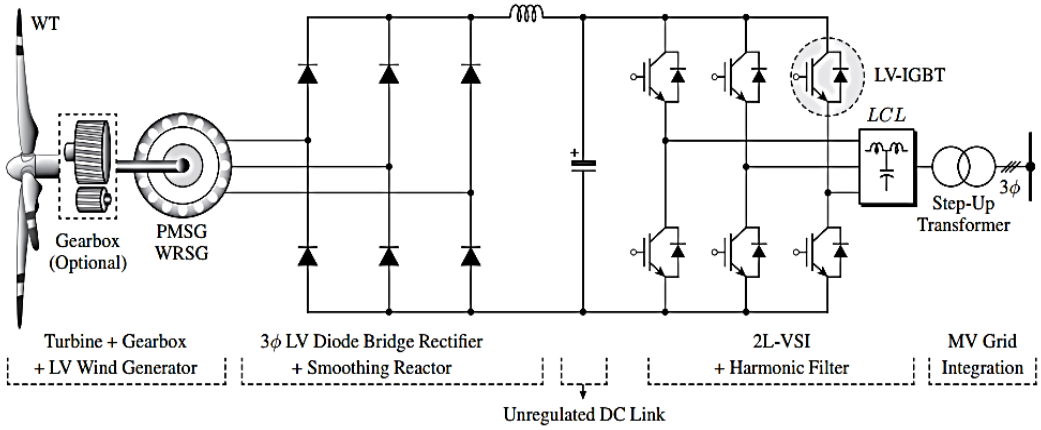

Figure 2.14. Type 4 SG WECS with a 2L-VSI and a diode bridge rectifier [17].

The wind generator and diode rectifier's output voltage changes in response to the changing wind speed conditions. However, the highest diode rectifier output voltage value is constrained by the generator's rated speed. As a result, the first DC link is identified as an unregulated DC link. The diode rectifier's output voltage drastically decreases when there is minimal wind. The DC-link voltage must be higher than the grid's peak line-to-line voltage in order to transfer the generated electricity to the grid. The generator should be overestimated in order to ensure this situation.

- **B) Diode Rectifier + 2L-Boost Converter + 2L-VSI** Figure 2.15 depicts the WECS with a diode rectifier, a 2L boost converter, and a 2L-VSI. The diode rectifier converts the generator's variable output voltage to DC. To increase the unregulated DC-link voltage and enable variable-speed operation for the PMSG/WRSG WECS, the boost converter conducts MPPT. They are referred to as (AC/DC + DC/DC + DC/AC) three-stage power converters as a result.

An optional component that filters the ripple in the DC voltage generated by the diode rectifier is the capacitor in the first DC connection. The boost converter also enables the PMSG/WRSGWECS to run at various speeds by performing MPPT. As a result, the efficiency of converting wind energy rises, particularly during times of low wind speeds [17].

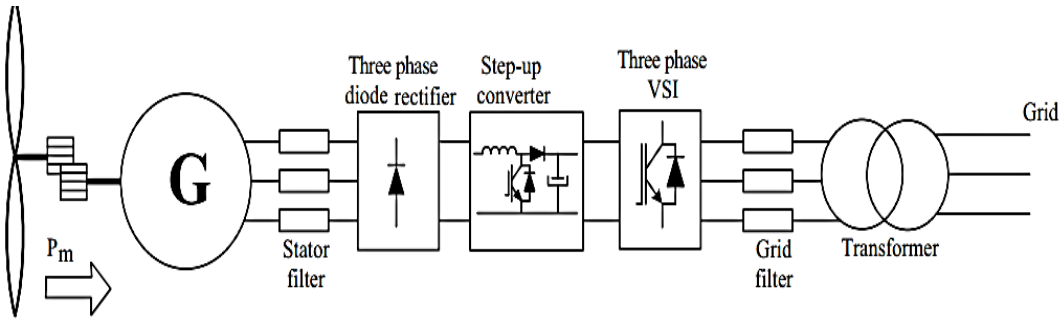

Figure 2.15. Diode rectifier WECS with a 2L boost converter and a 2L-VSI [140].

The generator's variable output voltage is converted to DC by a diode rectifier. The diode rectifier converts the variable output voltage of the generator to DC. With the help of the boost converter, the unregulated DC-link voltage is raised to a level suitable for the 2L-VSI [141]. The capacitor in the first DC link is an optional part that filters the ripple in the DC voltage generated by the diode rectifier. The boost converter also enables the PMSG/WRSG WECS to run at various speeds by performing MPPT. A constant DC input voltage is maintained by managing the DC/AC converter [119]. As a result, the efficiency of converting wind energy rises, especially during times of low wind speed.

2.3.3. Multilevel Power Converter

It becomes increasingly difficult for a traditional 2L-BTB solution to offer reasonable performance with the existing switching devices as wind turbine power capacities rise. Because of its ability to provide more output voltage levels, greater voltage amplitude, and higher output power, multi-level converter topologies are quickly displacing rivals as the favored option for wind turbine applications [142]. Generally, multilevel converters can be classified into three categories: Multilevel converters can typically

be split into three categories: neutral-point diode clamped structures, flying capacitor clamped structures, and cascaded converter cells structures [143].

2.3.4. Power Converters without a median DC Link

In this topology, the generator-side variable voltage/frequency can be changed to a grid-side fixed voltage/frequency without using any bulky, short-lived DC link components like electrolytic capacitors. Instead, direct AC/AC power conversion is carried out using matrix converters (MCs) [17]. Typical MCs, often called direct matric converters (DMCs), are single-stage converters that link an m-phase voltage source to an n-phase output load via an $m \times n$ array of bidirectional switches. For the voltage and current conversion, however, an indirect matrix converter (IMC) needs separate stages [144]. However, MCs can be used with both induction and synchronous wind generators.

2.4. REQUIREMENTS OF WTS INTEGRATION AND GRID CODE

When compared to traditional power plants, wind energy systems provide different obstacles for efficient and cost-effective grid integration, including intermittent, uncontrolled wind speed, turbine technology, and protection issues [27]. Because the output power of a wind turbine is proportional to the cube of the wind speed, any minor change in wind speed results in a significant change in the generated output power. As a result, fluctuations in wind speed induce power fluctuation on the grid [145]. These variations impact the grid's losses and have an impact on power quality parameters, including frequency and voltage aberrations. Several technological aspects, including active and reactive power control, fault ride-through (FRT) capability, and power quality, should be considered when integrating WECS into the grid network. The operational parameters of WECS should be as similar to those of the utility grid to maintain the power supply's stability, dependability, and availability [146]. Transmission system operators (TSOs) and/or distribution system operators (DSOs) in a variety of nations have developed and frequently updated various particular technical specifications, referred to as "grid codes," to guarantee grid stability and consumer power quality [147].

In this context, it must be highlighted that a Type 4 arrangement best conforms with all applicable grid code standards [132]. The main takeaway from the grid code is that massive synchronous generator-based conventional power plants should behave as similarly as possible to wind power plants (WPP) in normal operations and during faults [138]. The applicable grid codes, which include standards for network frequency and voltage variation, should be followed by all wind energy providers [27]. The following subsections discuss the effects of integrating wind energy on grids, which must be taken into account to preserve the consistency and quality of the electricity supplied to customers.

2.4.1. Fault Ride-Through Capability

A WECS must maintain connectivity to the network and stability throughout network faults in order to have fault-ride-through (FRT) capability. This happens because of the possibility of a system cascading failure or a threat to security requirements when there is substantial wind penetration [148]. Therefore, if the voltage at the point of common coupling (PCC) goes below its nominal value for a brief period of time during a fault, a WECS should continue to be stable and connected. In order to enable voltage recovery during asymmetrical and symmetrical faults and voltage dips, WECS are also expected to continue operating. Low Voltage Ride-Through (LVRT) capability refers to a wind turbine-based power plant's capacity to maintain a fixed grid connectivity across failures or voltage dips [149]. Several novel techniques have been published in the literature to improve the system ride-through capabilities, including a variety of control methodologies [27]. The typical FRT specifications for grid-connected wind power plants are shown in Figure 2.16.

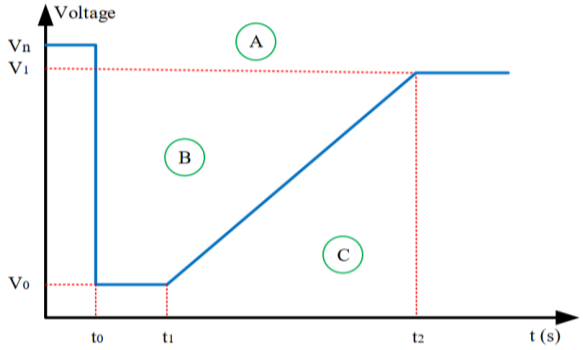

Figure 2.16. General curve limits for fault ride-through requirements [150].

The WT must constantly operate in region A, which depicts the nominal voltage at the connecting point, also known as the point of common collection (PCC). However, the WTs have to withstand voltage dip and remain connected to the system for a period of time ($t_0 \rightarrow t_1$) if the voltage is in area B; otherwise, they must be disconnected. The voltage at the connection point in area C recovers to V_1 within time t_2 after a fault has occurred. It is essential when a wind power plant remains under continuous operation without disconnection. The values of V_0, V_1, t_2, and t_2 differ from the grid code based on the standards and characteristics of the national grid [150].

2.4.2. Frequency Control

The performance of the active power output offered by wind power plants is an issue for the active power control requirements. As a result, WPPs must produce as much active power as possible. However, TSOs have developed numerous control functions of active power, such as frequency control and power gradient restriction, which must be applied since wind energy penetration has increased quickly [151]. The system's frequency regulation is essential for an electrical network to run steadily. It makes sure that power generation and consumption are continuously adapted. The power balance in the electrical network is coupled to the network frequency through all of the synchronous generators connected to it. For instance, a rise in load slows down the synchronous generators, causing the frequency to fall, and a strong wind energy injection into the system can also affect the grid's frequency [152]. Frequency stability is the capacity of a system to keep its frequency within a predetermined tolerance level. Figure 2.17 depicts the characteristic of frequency supports in the Danish grid

regulations, which state that depending on the power reserving strategy, the active power should be reduced when the frequency exceeds 48.7 or 50.15 Hz [153].

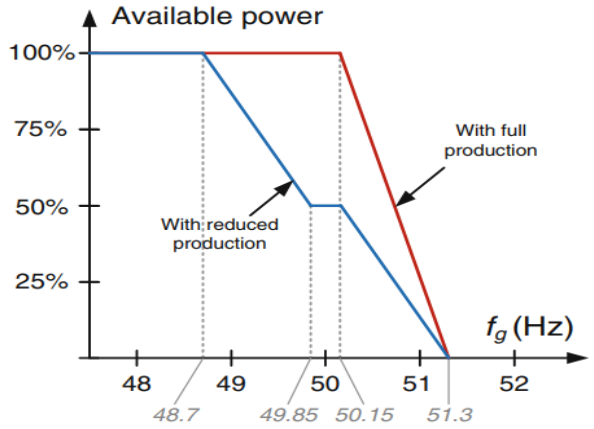

Figure 2.17. Frequency control profiles for the wind turbines connected to the Danish grid [153].

2.4.3. Voltage and Reactive Power Control

Voltage stability can be significantly impacted by wind power penetration, which thus makes these jobs more challenging [154,155]. Therefore, maintaining steady voltages within acceptable limits in various operational scenarios has proven difficult for power system operators. One option is to regulate the power factor at the PCC using either the active power or terminal voltage; Figure 2.18 and Figure 2.18, respectively, show the typical requirements for power factor control based on the active power and terminal voltage to support grid stability [156].

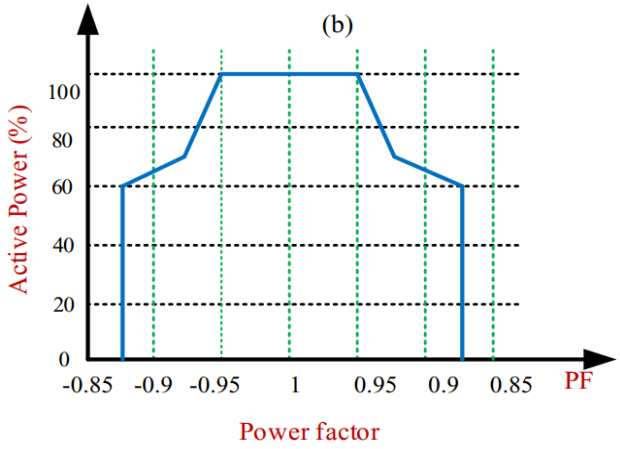

Figure 2.18. Typical power factor deviation range with regard to the active power [157].

2.5. POWER QUALITY

Maintaining the nearly sinusoidal waveform of the node voltages and line currents during rated operating circumstances is referred to as maintaining power quality (PQ). In general, voltage quality concerns variations in the voltage from the ideal waveform [158]. Therefore, PQ also can be defined as a set of electrical constraints (reference limits) that permits equipment to function as intended without experiencing significant operational losses or lifetime degradations. To put it another way, PQ is based on the measurements of four crucial electrical characteristics: voltage, current, frequency, and phase. As a result, both the voltage and current should have a sinusoidal form with a set magnitude at a fixed frequency without changing in phase [159].

The power-quality parameters of the output power from the wind farm at the PCC should be governed by applicable IEC 61400 standards (International Electrotechnical Commission). The purpose of IEC 61400-21 is to develop a uniform methodology for measuring and assessing the power quality parameters of grid-connected WTs to provide consistency and accuracy. The WT's electric characteristics that affect the grid's voltage quality are included in the definition of "power quality" in this context. IEC61400-21 [160] is the relevant IEC standard. Figure 2.19 shows the most typical criteria for the power-quality parameters of the output power that emanates from the wind power.

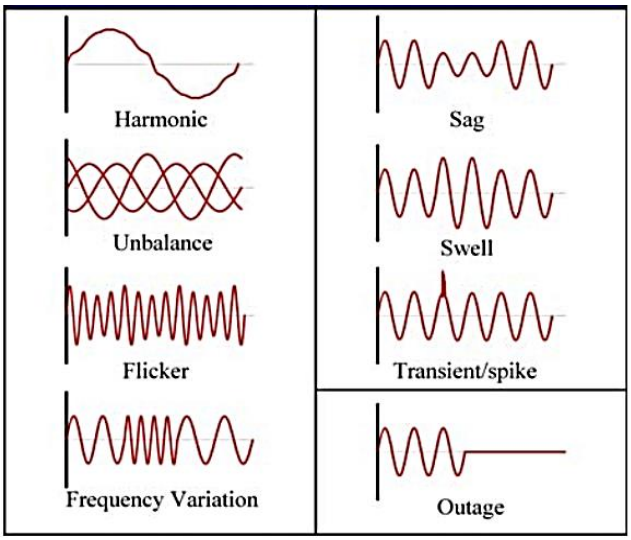

Figure 2.19. The common power quality problems.

2.5.1. Flicker

When a wind turbine is operating continuously or switchingly, flicker is the visible variations in light intensity brought on by voltage fluctuations. In all situations, the calculating method for wind turbine flicker emission is defined by IEC61400-21. The PCC's approved threshold for flicker output is 4% [161]. Rapid voltage fluctuations cause the phenomenon known as power line flicker. These voltage changes might result in the irritating and unsettling flickering of electric light.

Additionally, this phenomenon poses a risk to delicate technological equipment. Therefore, a standard was required for flicker measurement equipment to ensure measurement coherence amongst devices because of the human eye sensitivity involved in measuring voltage fluctuations [162]. The structural and functional requirements of a flicker measurement device known as a flicker meter are described in detail in IEC 61000-4-15 [163]. This monitoring instrument provides both a short p_{st} and long-term p_{lt} signal for the link between voltage variations and human discomfort [164].

2.5.2. Frequency Deviation

The definition of power frequency fluctuations is the departure of the power system's fundamental frequency from the frequency value set (50 or 60 Hz). Frequency variations result from malfunctions in the bulk power transmission system, the disconnection of a sizable portion of the load, or the shutdown of a sizable generation source [160].

2.5.3. Transient

Transients, sometimes known as "surges," are brief sub-cycle disturbances with a wide range in amplitude. A single transient can produce thousands of voltages into the electrical system, which can damage the installed equipment [12]. In power systems, transients, which can be categorized into two classes, oscillatory and impulsive, are undesired brief occurrences. These events occurred in less than half a period [160].

2.5.4. Power Outages

Total interruptions of the electrical supply happen as a result of power outages. Power is briefly cut off by various utilities with protection equipment installed so that disruption can pass. Ice storms, lightning, wind, and utility equipment failure are the causes effects: Complete operation disruption.

2.5.5. Harmonics

Power systems' harmonics are characterized by nonlinear components, particularly power electronics and reactive power compensators, distorting the voltage or current's waveform. [165‑167]. There are two sources of harmonics: one is from the inverters, and the other is from the loads or the grid. WECS produce harmonics due to the power electronics in the interacting inverter switching. The overall harmonic distortion at PCC is determined by the interface inverter's topology, control scheme, and component choice [148]. Specifications for voltage and current harmonics up to 50 times the fundamental power frequency are required by IEC61400-21. Subsequently, according to generally accepted standards, the PCC's total harmonic distortion (THD) from these harmonics should be less than 5% [161]. In order to suit the needs of the operator, the controllers with a filter employed should have excellent harmonic rejection capabilities due to the cumulative nature of harmonics in power systems. [168]. voltages or currents that have frequency components that are not integer multiples of the frequency are known as interharmonics; static frequency converters, cyclo converters, induction furnaces, and arcing apparatus are some examples of interharmonics sources.

2.5.6. Voltage Unbalance

When the three-phase voltage varies in magnitude or exhibits a nominal phase shift (120^0), there is a voltage imbalance, which can be identified by the ratio of the positive to negative sequence voltage component [169]. The voltage unbalance factor (VUF) is used to check the quality of voltage unbalance and can be expressed as follows [157,170]:

$$VUF = \frac{V^+}{V^-} \times 100\% \tag{2.9}$$

where V^+ and V^- are the positive and negative voltage sequences, respectively. Since voltage imbalance is a reliable indicator of the quality of the power supplied to the grid, some standards and grid codes limit the VUF at the PCC and ensure that a balanced three-phase voltage is injected into the grid. For instance, IEEE Standard [171] calls for a maximum voltage imbalance of 3%.

2.5.7. Voltage Fluctuations

Voltage fluctuations result from changes or swings in the steady-state voltage, which is above or below the designated input voltage range of equipment. Sags and swells are both variations.

- **Voltage Sag**

A short-term, abrupt drop in the electrical grid's voltage is referred to as a voltage sag or dip. It can occur anytime, often between 10 and 90 percent of the nominal voltage. It usually lasts one-half cycle and one minute and can impact amplitude or phase [172]. It usually occurs when large wind turbines are started together – in which case, the current drawn from the electric grid will rise to a high value for milliseconds. Voltage sag can also occur as a result of the startup of large motors or when there is a grid short circuit. The acceptable voltage dip limiting value is ≤ 3% [173,174].

- **Voltage Swell**

Voltage swell is defined as a temporary increase in the supply voltage's RMS value that lasts between 0.5 cycles and a minute and remains between 110 and 180 percent [173]. Voltage rise for grid-connected WT can occur due to inrush currents or shutting down of the big capacity of the WTs. Grid lightning, faults on other phases, and faulty substation tuning are additional sources of voltage rise. However, less than 2% is the permissible rate for a voltage swell [174,175].

PART 3

CONTROL SYSTEM OF WECS GRID CONNECTION AND OPTIMIZATION

3.1. CONTROL ALGORITHM FOR GSI

A grid-side controller primarily assures the generated power quality, DC-link voltage control, grid synchronization, grid code compliance, and control of reactive power transfer between the DPGS and the grid [176]. This type of control is independent of the type of generator control used and the arrangement of the WECS power conversion stages. In a grid-connected inverter, the inverter performs as a current-regulated source that produces output current, which is based on the reference current signal. The current regulatory algorithm regulates how much-intended output power is sent to the utility. The linear PI controller has been selected for the GCI application, as explained in Section 3.2.1. Translating the dynamic variables into the synchronous reference frame is beneficial for controlling the sinusoidal inverter's output current. The grid' voltage and current waveforms are transformed into a reference frame, which synchronously rotates with the grid voltage, applying a reference frame transformation module, which is also called the Park Transformation [5]. Instead of sinusoids with a certain frequency, the control variables are DC quantities (while a synchronous PI controller is operational). The PI compensators can make the fundamental component's stationary error zero [177].

3.2. PI CONTROLLER

The controllers are one of the main components of the systems. These structures make sure that the associated systems function as intended. The study and design of these circuits are crucial since controllers with quite various architectures and features have been created for this purpose. In the industrial sector, the standard controller that is

widely used is PID (proportional-integral-derivative). These controllers are typically employed in P, PI, PD, and PID combinations [178]. They work to reduce error by executing multiplication, integral, and derivative functions, keeping the system response at the intended value. A proportional-integral controller, or PI controller, is frequently used to correct offset errors [179] when a derivative controller cannot be utilized because of the slow response. As a result, in this study, the PI controller is considered in the grid-connected DPGS' GSI. In industrial control applications, PID controllers are frequently employed. In this case, the r-value, reference setpoint, and the measured process output value (m) are compared by the controller. Later, the control signal is calculated for the modified process inputs using the error signal (e). It ensures that the system output approaches the reference value. In contrast, a PID controller modifies process inputs based on the rate of change in the error signal and history for reliable and precise control [180]. In other words, the PI controller's responsibility is to keep the output at a level where there is no deviation from the setpoint (r) between the measured variable (m) and the measured variable (r) [181]. Because of its efficiency and simplicity, PI control is the most helpful type of controller. Additionally, it lowers the system's offset and noise signals [182]. Figure 3.1 provides the PI controller's general control closed loop system architecture.

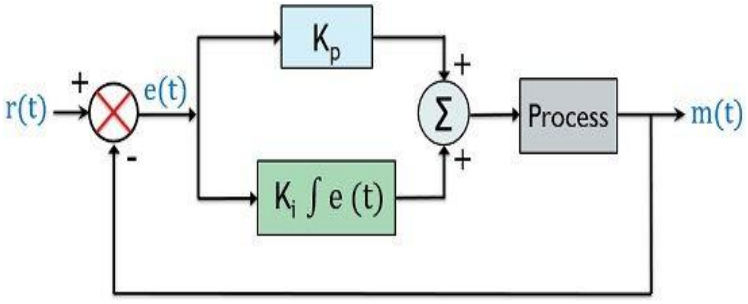

Figure 3.1. Control system with PI controller

The PI controller's mathematical equation is given below:

$$u(t) = K_p\, e(t) + K_i \int_0^t e(t) \tag{3.1}$$

$$e(t) = m(t) - r(t) \tag{3.2}$$

Here, K_p represents proportional gain, $e(t)$ is the error value, $u(t)$ is a control variable, and K_i shows an integral gain. The controller maintains the optimum output, so an appropriate controller needs to be designed. It is possible by selecting a PI controller's tuning parameters K_p and K_i [183]. A controller that can minimize the error between an output value and the actual input is necessary for a controlled process. PI controllers are frequently used for this purpose, but a primary issue with PID controllers is they need tuning. Several methods, including classical and metaheuristics, help tune PID controllers and find their optimal parameter values [88]. The traditional approaches call for mathematical system modeling and response analysis, whereas metaheuristic technique-based optimization algorithms are Stochastic methods to address the issue by utilizing natural laws. The standard techniques for locating the global optimum include GA, Particle Swarm Optimization (PSO), Ant Colony Optimization (ACO), Simulated Annealing, Differential Evolution (DE), and Grey Wolf Optimizer (GWO). These techniques are also popular in this area. The following sections address optimization strategies based on metaheuristics.

3.3. OPTIMIZATION METHODS FOR DESIGNING OF PI CONTROLLER

To find the optimal solution when one or more criteria are given, an optimization must consider the system's characteristics and any external limitations. Using random processes, the best answer is selected from solutions. Based on the generation of new solutions, the search for the optimal solution is conducted [184]. Numerous optimization algorithms developed up to this point have drawn inspiration from the collective behavior of living creatures in their search for food or in the development of their breed [185]. These algorithms rely on collective intelligence, which is generated by adding up the individual behaviors of its pieces and following fundamental laws. In load frequency management, optimal size, power flow, voltage regulation, and optimization techniques are frequently used [186–188]. The integral absolute error (IAE), integral square error (ISE), integral time multiplied absolute error (ITAE), and integral multiplied time square error (ITSE) are commonly applied objective functions to adjust the PI controller's gains [84,189]. Their mathematical expressions are presented in (3.3)-(3.6).

Integral Absolute Error

$$IAE = \int_0^T |e(t)| \tag{3.3}$$

Integral Time Absolute Error

$$ITAE = \int_0^T t|e(t)| \tag{3.4}$$

Integral Square Error

$$ISE = \int_0^T |e(t)|^2 \tag{3.5}$$

Integral Time Square Error

$$ITSE = \int_0^T t|e(t)|^2 \tag{3.6}$$

However, the effectiveness of beneficial algorithms is reliant on an appropriate search technique, which necessitates the accurate description of the objective function, search limitations, the setup of the search algorithm control parameters, and the complexity of the analysis system [190].

3.3.1. Genetic Algorithm (GA)

The foundation of the general algorithm is the simulations of biological evolution and the underlying genetic selection process. The GA algorithm mathematically models the genes' crossover and mutation activities. These mechanisms allow the species to have better genes in every generation and make them suitable for the environment. The objective function of the optimization problem will be satisfied by the best genes after n generations [191].

3.3.2. Particle Swarm Optimization (PSO)

The fundamental idea of this algorithm is inspired by the group migration of birds, where a leader precedes each feature. The fitness of each particle in the PSO may be calculated using this space, which is made up of a collection of particles traveling in a specific search space. The velocity and position vectors correspond to a position for each particle. Every particle remembers its optimum position following each iteration. Additionally, the group's local relationship is established. The following value is saved as the position vector that is the best among all neighbors. The relationship can be used to calculate each particle's position and speed of motion. The optimum solution may also vary for each particle depending on the number of particles and iterations. Obviously, as the integration and particle count rise, the solution will improve; however, constraints must be considered, including the computational load and required time. The velocity and intelligence of the particles determine the optimal spot to reach, and each particle in this area might hold the answer. The fundamental idea behind PSO is to randomly assess each particle's acceleration toward its optimal location and the optimal global position at each time step [192].

3.3.3. Grey Wolf Optimizer (GWO)

It was first developed by Mirjalili et al. as a structure that mimics the social leadership and hunting behaviors of grey wolves to solve optimization problems. This algorithm works based on the hunting skills of a pack of 5-12 wolves.

The GWO algorithm updates the wolves' locations and hierarchy and searches for an optimal solution in a pre-defined search space. Engineering is a required field in optimization in the real world. It has many important uses that directly affect how well people live. Therefore, it's interesting that GWO has been adapted to numerous engineering applications [76,191]. These applications, which include designing and tuning controllers, power dispatch issues, robotics and path planning, and many others, are thoroughly and in-depth explored in the first chapter. Thus, GWO, a recent addition to the population-based swarm intelligence optimization algorithms, is distinguished by several attractive benefits, including simplicity, derivation-free process, local

optima avoidance, and flexibility. Additionally, it has fewer control parameters to alter, is simple to implement, and exhibits a quick convergence property [74].

- **Inspiration**

Wolf packs are in a hierarchical structure; the leading wolves are the alpha (α) wolves; followers of alpha are beta (β) wolves; subordinates are delta (δ) wolves, and familiar followers are omega (ω) wolves, as Figure 3.2 illustrates.

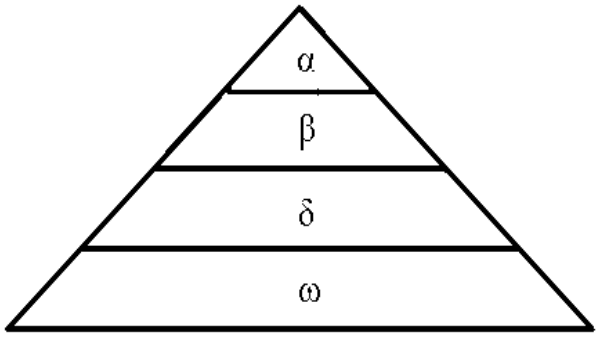

Figure 3.2. Grey wolves' hierarchy.

Here, Figure 3.3 depicts how Alpha selects a target and asks Beta to join, who notifies the whole pack, updates Alpha about all pack activities, and helps Alpha make decisions. Delta wolves are under the control of both alpha and beta wolves. In a typical pack, delta sub-types like scouts, hunters, sentinels, caregivers, and elders can be found. The least dominant Omega follows all others and is nonetheless important despite a low hierarchical standing. Interns become cranky when Omega is absent. When omega is absent, internal conflict develops that sabotages the hierarchical social structure of wolves. When hunting, wolves approach, track, chase, harass and encircle their prey before attacking it when it stops moving. By breaking down the exploration of the search area into three phases that resemble the wolf's three stages of hunting—encircling, hunting, and attacking the prey—the search for the best answer can be realized [191].

- **Encircling Prey**

Wolves encircle their prey before they hunt it. Their encircling behavior can be mathematically described using the following model: study [70]:

$$D = \left| C \times x_P(t) - x(t) \right| \tag{3.7}$$

$$x(t+1) = x_p(t+1) - A \times D \tag{3.8}$$

Here t is the present iteration, $x_P(t)$ which shows the leading wolves' positions, $x(t)$ is the arbitrary wolf's position $x(t+1)$ is the random position of the wolf, D represents the distance, and both A and C are coefficient vectors [193]:

$$\begin{gathered} A = (2r_1 - 1) \times a(t) \\ C = 2r_2 \\ a(t) = 2 - 2 \times t / T \qquad t = 1, 2, 3, \ldots\ldots T \end{gathered} \tag{3.9}$$

Here, $a(t)$ a variable represented has a linear iteration number lowered from 2 to 0, and T displays the maximum number of iterations. The r_1 and r_2 are random values between [0, 1]. All the wolves (including Omega) change their places about the three ideal positions. The following set of equations can mathematically depict where a candidate wolf stands concerning the three best positions [72]:

$$\begin{aligned} D_\alpha &= \left| C \times x_\alpha(t) - x(t) \right| \\ D_\beta &= \left| C \times x_\beta(t) - x(t) \right| \\ D_\delta &= \left| C \times x_\delta(t) - x(t) \right| \end{aligned} \tag{3.10}$$

$$\begin{aligned} x_1(t+1) &= x_\alpha(t) - A \times D_\alpha \\ x_2(t+1) &= x_\beta(t) - A \times D_\beta \\ x_3(t+1) &= x_\delta(t) - A \times D_\delta \\ x(t+1) &= \frac{x_1(t+1) + x_2(t+1) + x_3(t+1)}{3} \end{aligned} \tag{3.11}$$

In this case, the wolf's location is denoted by $x(t)$, and his alternative positions are $x_1(t+1)$, $x_2(t+1)$, and $x_3(t+1)$. Here $x_\alpha(t)$, $x_\beta(t)$ and $x_\delta(t)$ are the alpha, beta, and delta wolves' positions, and during the next iteration, $x(t+1)$ shows the candidate wolf's position. In GWO, the coefficients A and C govern the search. Here, $|A| \geq 1$ means that the wolves were given the command to leave the under-appreciated target. Then, they will explore the search space and find a suitable target; however, the $|A| \leq 1$ shows how the wolves approach and catch prey [194], as Figure 3.3 shows.

Figure 3.3. Mechanisms used by wolves to exploit and explore their search areas [94].

An exploration-exploitation balance is created by reducing A, concerned with iterations within the already established range [-2, 2]. The uniform distribution of the coefficient C lies in the range [0, 2]. The stochastic variable C1 in this situation supports the exploitation process, but C >1 focuses on exploration. In this case, C behaves stochastically independently of the number of iterations, preventing local minima-trapping during optimization [193].

3.4. PROXY MODEL CONCEPT

Proxy models have drawn much attention lately because they are sophisticated non-linear interpolation tables to simplify computations and approximate complex models. High-fidelity models allow data collection to build a proxy model. They can be a fantastic option once they've been built for various jobs like uncertainty analysis, optimization, forecasting, etc. [91]. Comparing numerical models to more

conventional trial-and-error techniques can save time and cost [195]. Nevertheless, getting precise findings rapidly has never been easy. In a particularly complex process, numerous data sources are rapidly gathered and may modify the circumstances and uncertainties. Field development plans must also be updated more frequently, and real-time analysis can be quite helpful in gaining insight into how the situation is changing as it happens. However, these pricey models, or software to build them, have been constrained by having a real-time analysis. As a result, recent years have seen an increase in research to make and use efficient proxy models (PMs) [91]. PMs are also known as meta or surrogate models because they replace mathematical models, numerical models, combinations of these models, or even experimental tests. Proxy models might be characterized as sophisticated interpolation tables to make us swiftly interpolate non-linear data and find a rough solution.

In proxy modeling, the high-fidelity model is run within the specified space of the input parameters to generate outputs. An appropriate sample consisting of input parameters was selected. The PM will then fit these facts. Only the specified input set and associated search space are valid for this PM. A PM's benefit is that it can be designed quickly and run in a matter of seconds. PMs offer a faster decision-making pace than high-fidelity models, which is necessary, yet, the models' accuracy continues to be an issue. A high-fidelity model nevertheless yields the most accurate answers across all the geographical and temporal locations, notwithstanding the speed advantage of utilizing a PM. Optimization, uncertainty quantification, Sensitivity Analysis (SA), and risk analysis are a few of the aims of applying PMs [196].

3.5. ARTIFICIAL NEURAL NETWORK (ANN)

ANNs are a mathematical model of the human brain that can imitate how the brain functions. The perceptions of the human nervous system serve as the foundation for the ANN data processing paradigm and interpretations of information [197]. Figure 3.4 depicts the ANN architecture, which has many layers.

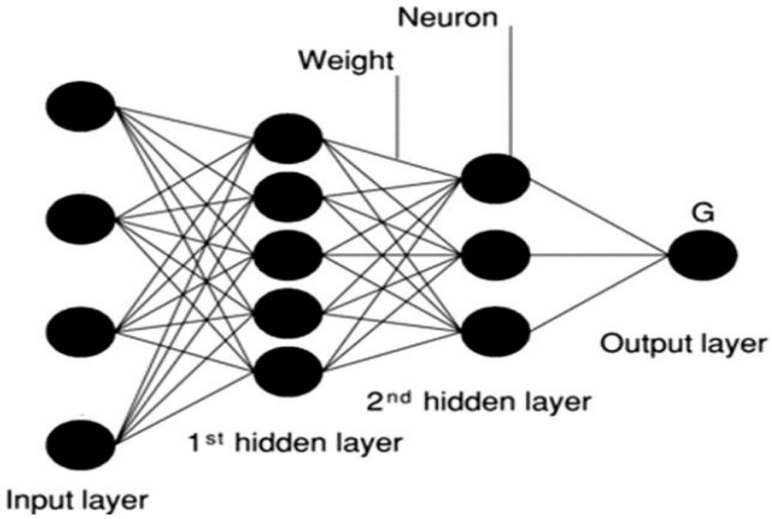

Figure 3.4. Structure of a typical ANN.

Like the nervous system, an information system's network has a finite number of artificial neurons. The cornerstone of neural network training is to change the parameters to map the input-output relationship that has been established. Through training and learning, ANN models may extract the dependence between variables and reflect a complicated nonlinear connection. A network's hidden layers, composed of nodes, connect the input and output layers in many ways. For example, a ten-input network has ten nodes in the input layer because each node has a unique input value. Training is the term used to describe the process that teaches a NN. The task of training NNs to operate at their best under fresh sets of input conditions falls to a trainer. Learning frequently uses ANNs. The ability of a NN to learn from experience is referred to as learning. The ANN has been designed with mechanisms to adapt to a set of provided inputs, just like biological neurons do. Unsupervised learning and supervised learning are the two main categories. In supervised learning, NNs are first given a collection of samples known as training samples via a training method. In order to enhance performance, the trainer subsequently alters the structural characteristics of the NN in each training stage. When the training stage is over, the trainer is removed, and NN is then ready for use. Any NN's trainer might be thought of as its most crucial element. Deterministic and stochastic learning methods are two different categories. Methods such as back-propagation stochastic trainers can be deterministic, which begins the training process with a random solution and then evolves it [198].

3.6. PROXY MODEL-BASED ANN

Calculations for the under-consideration power system (DPGS) are quite numerous. With a simulation length of 10 seconds and a sample time of 1 microsecond, it is, therefore, computationally intensive. Additionally, when GWO is used to optimize the PI controller of the aforementioned system, this problem will worsen as simulations get more high-fidelity. The proxy model is then made to lessen this issue. Powerful machine learning technologies like neural networks are trained to predict relationships without mimicking any underlying behavior. The trained neurons accurately predict the output using the input and linking the input-output data. Consequently, a trained neural network can be utilized in this study to forecast errors that would come from a set of given PI controller gain values (Kp, Ki) without performing the time-consuming calculations that would be required using a direct model. Because of its great accuracy, quick computation speeds, and ability to be integrated with optimization methods, this surrogate model would be helpful [199] . A feed-forward neural network (FFNN) is one of the often-employed ANN. As shown in Figure 3.5, a multi-layered FFNN is used with two hidden layers in this study, with input cascading throughout the networks in a single direction.

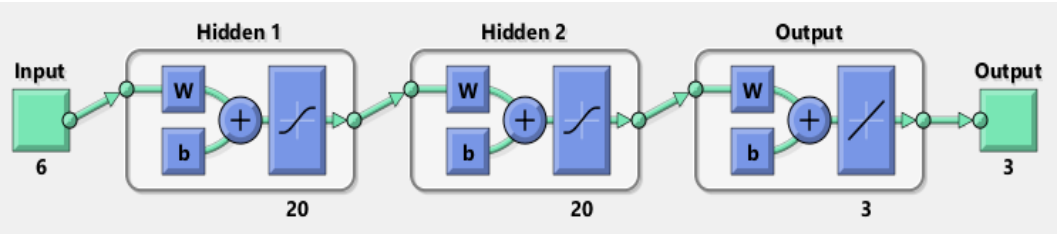

Figure 3.5. Structure of FFNN network.

As shown in the above figure, the FFNN is developed with an input layer, two hidden layers, and an output layer. The input layer contains six input neurons, and the hidden layers comprise 20 neurons each, whilst the output layer consists of 3 neurons. The output of each hidden layer is followed by a Tanh activation function and a linear transfer function in the output layer.

Among NNs, fully-connected layers are the most prevalent kind of hidden layer. In a fully connected layer, each node is linked to every other node, with the layer above and below. Each node's value is a weighted sum of nodes in the layer above added to the internal bias, which is then used to produce the output after passing it through a nonlinear activation function. The data input-output relationship in any two FFNN layers is mathematically expressible [94,200]:

$$y_j = f\left(\sum_{i=1}^{n} w_{ij} x_i + b_j\right) \qquad \begin{bmatrix} i = 1, 2, 3, \ldots\ldots n \\ j = 1, 2, 3, \ldots\ldots k \end{bmatrix} \tag{3.12}$$

Here, y_j shows the output value at the j^{th} neuron, n is the number of input-layer neurons in total., and k shows the total neurons in an output/hidden layer. In this case, b_j is the bias, x_i shows the input value at j^{th} neuron, w_{ij} represents the weight coefficients of the input x_i and output y_j and f shows the activation function. The ANN computes the learnable parameters' optimal values (w_{ij} and b_j) by minimizing the error function. The error function between the predicted and actual trajectory can be expressed in terms of mean squared error (MSE) as given below [201]:

$$MSE = \frac{1}{m} \sum_{J=1}^{m} (y_j^p - y_j^a)^2 \tag{3.13}$$

Here, m the total number of outputs y_j^a is the actual data and y_j^p shows the ANN's predicted output data.

The input parameters must first be determined in order to create the ANN model as an approximate representation of DPGS. The network structure should then be created with an appropriate training technique in order to get the best prediction result. Additionally, network training requires a set of input and output data. Following the training data entry, the experience values are saved in the network structure as weights and thresholds. New outputs are calculated after the network weights are updated

during the training phase. The approach is repeated until the network learns the issue and its error (difference between the network output and target value) falls within acceptable bounds [202]. An essential limitation of this approach is that a trained model is fixed for a specific set of input conditions. To evaluate the solution for different initial inputs, a new model would have to be trained on the new data.

3.7. MODEL DEVELOPMENT

3.7.1. Using ANN to Approximate the DPGS Model

- Input Dataset: It consists of independent variables $[x_1, x_2, x_3, x_4, x_5, x_6]$ in the range of minimum and maximum variables, as depicted in Table 3.2.

Table 3.1. Input dataset.

	x_1	x_2	x_3	x_4	x_5	x_6
$x_{\min}$	6	250	0.1	3	0.1	3
$x_{\max}$	15	500	2	9	2	9

The input dataset corresponding to the controllers gains PI1, PI 2 and PI 3, which can be mentioned as: $[K_{p1}, K_{i1}, K_{p2}, K_{i2}, K_{p3}, K_{i3}]$. The input dataset is bounded by the lowest and maximum gains of the controller produced at random.

- Output Dataset: This dataset consists of dependent variables' values, which are the standard deviation of the errors (e, e_1, e_2). It generated using the formula [203]:

$$\sigma = \sqrt{\frac{\sum_{i=1}^{N} (x_i - \mu)^2}{N}} \tag{3.14}$$

σ = Set standard deviation, N = the size of the samples, x_i = each value from the samples set, μ = the samples set mean. The output dataset is generated by executing 27 random runs to the original DPGS model using the random input dataset for a simulation time 10 seconds with 1 μs sample time. The total number of the dataset is 243 divided by the input dataset is 162 and 81 as the output dataset.

- Versus the ANN model to the DPGS model, input/output datasets are used to evaluate the trained ANN model by following the mentioned mechanism in section 3.6. The performance of the ANN model is evaluated using the mean square error (MSE) and correlation coefficient (R). Figure 3.6 demonstrates that the correlation coefficient (R) is 1. It is also observed that the ANN model is computationally more efficient than the DPG model. The execution time of GWO with the original model in the specified parameters takes approximately. Correspondingly, by coupling ANN-GWO, the execution time is shortened.

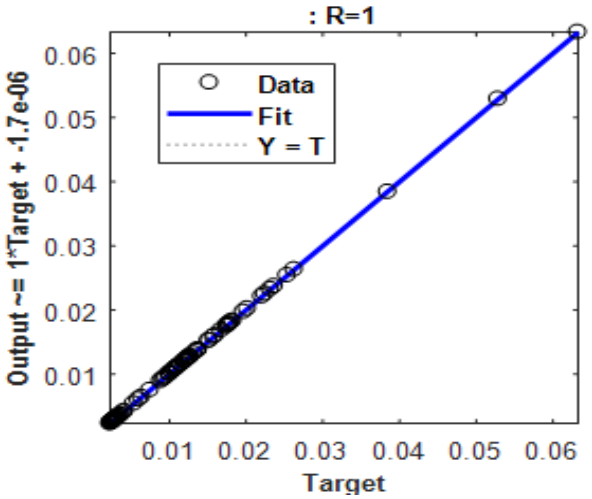

Figure 3.6. ANN and DPGS output relationship shown in a scatter plot.

3.7.2. GWO Development

- Set each wolf's starting places at random. The decision variable vector displays the location of each wolf (x).
- Determine the fitness value for each wolf (F).

- Three best values should be set as Alpha fitness (F_α), beta fitness (F_β), and delta fitness (F_δ).
- Put the appropriate Alpha (x_α), Beta (x_β), and Delta (x_δ) in the respective locations.
- Calculate the coefficients a, A, and C for each wolf (x) using Eq (3.9).
- Update the positions of each wolf using Eqs. 3.10 and 3.11.
- Repeat steps 2 through 6 until the maximum number of iterations have been made (T).

PART 4

METHODOLOGY

The modeling of a DPGS system is the subject of this investigation. The mentioned system will be integrated with an AC grid. An intermediate direct current-link circuit, a 2-level PWM inverter, and a 2-level three-phase rectifier make up the fully-rated power electronic interface used by the under-consideration power system, equipped with a variable-speed directly driven PMSG (DD-PMSG-VSWT). Three control techniques were employed when the suggested system was applied to the grid-side inverter. To analyze the entire system's performance, the voltage source converters, control algorithms, and proposed wind turbine model were developed in MATLAB/Simulink [204]. The main emphasis of this research study is the grid side controller, which concentrates on the quality of current waveforms, which are injected for power exchange between the grid and DPGS-based power plants. We used the grid-side current control approach to complete this challenge. The current controller reduces the overall harmonic distortion by attenuating the inverter output current harmonics. Additionally, the controller controls the power transfer between the DG plant and grid, and compensates for reactive power. A high-output power factor is another goal of this work [205].

4.1. SYSTEM DESCRIPTION

According to Figure 4.1, the model's sub-parts consist of a wind turbine (WT), a PMSG, a boost converter, an unregulated rectifier, an LCL filter, a GSI, a DC-link capacitor, a three-phase transformer, a transmission line, and a grid. A local AC bus has been connected to a local AC load with 380V line-to-line voltage.

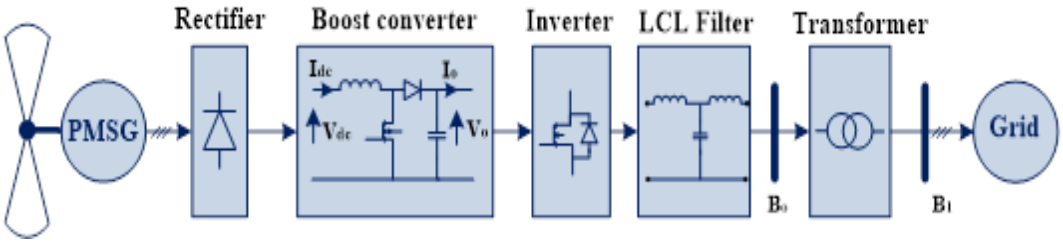

Figure 4.1. Boost converter, diode rectifier, and grid-side inverter combination in a WECS design.

LCL filter is placed between the GSI and the grid to lower the harmonics produced by the high-frequency inverter. The power quality therefore increased. Finally, a 380V/33kV transformer and a local bus were connected to a distribution grid (three-phase 33kV).

4.1.1. Wind Turbine Model

WT converts the wind's energy into mechanical power (P_m) in this model. It is seen by the relationship considering the changing wind speed (v_ω) [102,206]:

$$P_m = 0.5\ \rho A v_\omega^3 c_P \tag{4.1}$$

Here, A shows the turbine's swept area in m^2, ρ shows the air density (kg/m^3), c_p stands for the performance factor, c_p is a function of pitch angle (β) and tip speed ratio (λ), and is described as in (4.2)-(4.4):

$$C_p(\lambda,\beta) = C_1\left(\frac{C_2}{\lambda_i} - C_3\,\beta - C_4\right)\exp\left(\frac{-C_5}{\lambda_i}\right) + C_6\,\lambda \tag{4.2}$$

$$\frac{1}{\lambda_i} = \left(\frac{1}{\lambda + 0.08\beta} - \frac{0.035}{\beta^3 + 1}\right) \tag{4.3}$$

$$\lambda = r\,\omega / v_\omega \tag{4.4}$$

Here, r implies the blade radius (m), $C_1, C_2 \ldots . C_6$ are constant coefficients, and ω shows the rotational speed (rad/s) of blades. The constant coefficients' values are 0.5176, 116, 0.4, 5, 21, and 0.0068, depending on the blades' mechanical structure [207]. For the MPPT control region, the blade's pitch angle β is zero.

Eq. 4.4 shows that the rotor speed can be maintained to keep λ at an optimum value λ_{opt}. The power efficiency remains the maximum, demonstrated by $c_{p\max}$. The turbine's maximum power output is as follows:

$$P_{\max} = 0.5\ \rho\ \pi\ r^5\ \frac{\omega_m^3}{\lambda^3}\ c_P = K_{opt}\ \omega_m^3 \tag{4.5}$$

$$K_{opt} = \frac{0.5\ \rho\ \pi\ r^5}{\lambda_{opt}^3}\ \mathrm{c_{p\_max}} \tag{4.6}$$

In this case, wind turbine characteristics determine the constant K_{opt}, and the dotted lines in Figure 4.2 show the maximum power curve.

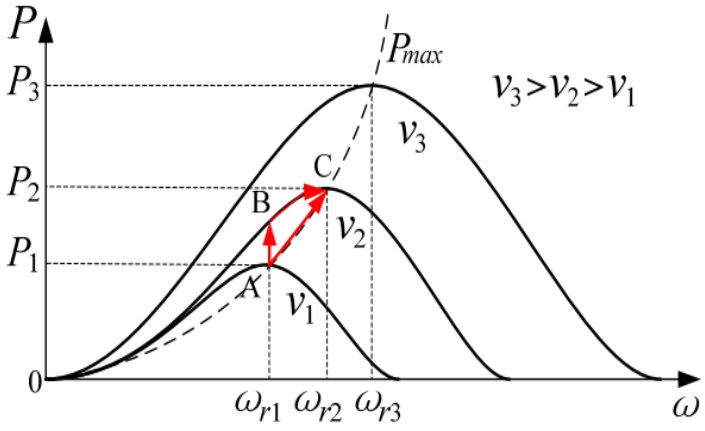

Figure 4.2. Wind turbine characteristics Power versus rotor speed.

Figure 4.2 shows that if v_1 is the wind speed, the rotor's maximum power will be at rotor speed ω_{r1} while the system's operating point is A. In case the wind speed changes from v_1 to v_2 but there is a fixed rotor speed ω_{r1}, and the system's operating point

jumps to B, that does not correspond to the maximum power tracking. In that case, the rotor speed should be controlled to manage the increase from ω_{r1} to ω_{r2}.

4.1.2. PMSG

Because of its reliability and high power density, self-excitation, low maintenance costs, the ability to couple directly to a WT (gearbox elimination), and operating with high efficiency; PMSG is the most common and preferred over DFIG based WECS for a full variable speed operation [204,208]. Since direct drive PMSG systems are the most prevalent on the small and medium scale, they are the only systems this research focuses on [209]. The PMSG voltage in the d-q reference frames is given below [210,211]:

$$V_d = -R_s i_d - L_d \frac{di_d}{dt} + \omega_e L_q i_q \tag{4.7}$$

$$V_q = -R_s i_q - L_q \frac{di_q}{dt} + \omega_e L_d i_d + \omega_e \lambda_m \tag{4.8}$$

where R_s is machine resistance per phase, V_d; V_q; i_d; i_q; L_d, and L_q are two-axis machine voltages, currents, and inductances, $\omega_e = P\,\omega_m$ is electrical angular velocity , P is pole pairs, and λ_m is the amplitude of the flux linkages provided by the permanent magnet.

4.1.3. Uncontrolled Rectifier

A three-phase bridge rectifier that generates six-pulse ripples in the output voltage is frequently used in small-scale WECS. The diodes with line-to-line voltage amplitude are conducted [20]. The mentioned bridge rectifier is depicted in Figure 4.3.

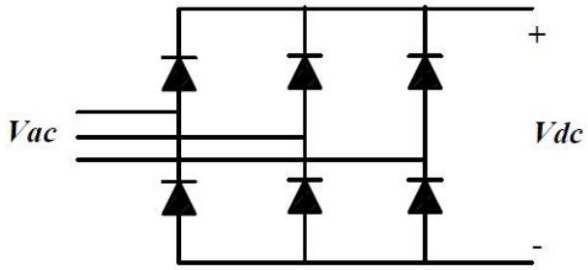

Figure 4.3. Three-phase bridge rectifier.

If it is assumed that V_m is the phase voltage's maximum value, the average output voltage can be calculated as follows:

$$V_{dc} = \frac{3\sqrt{3}}{\pi} V_m = 1.654 V_m \tag{4.9}$$

4.1.4. LCL Filter

Grid-tied inverters need a filter to link VSI to the grid for feedback control, lower output current harmonics [212]. There are four groups of inverter output filters: L, LC, LCL, and LLCL. Comparing different filters, there are pros and downsides. A straightforward series inductor can be employed; however, this results in a high voltage drop, a weak harmonic attenuation, and a bulky inductor that is needed for the design [213]. Second-order filters, such as the LC filter, are frequently chosen in power supply and off-grid systems. A second-order filter called the LC filter causes some issues when utilized in grid-tied systems. High-frequency harmonics that happen when an inductor is connected in parallel to the filter capacitor is one of these issues. In high-power quality applications, LCL filters are increasingly popular as an alluring substitute for conventional series inductance output filters. LCL filters have the capacity to precisely control the output current as well as the ability to attenuate

harmonics at lower frequencies which is significant for high-power applications, but control systems employing LCL filters are unavoidably complex, so special consideration must be given to their design in order for them to function when terminal voltage is distorted [214]. The LLCL filter has a small size and low cost, and it filters harmonics more effectively. The system, however, has a very difficult time maintaining a steady state [215]. In this study, Figure 4.4 shows a three phase LCL filter circuit modeling between output the inverter and the grid. The main benefits of using this filter over standard "L" and "LC" filters include its advantages in terms of filter size, its lower voltage drop, improved damping, and the ability to operate at low switching frequencies [216]. Besides, this type of filters is excellent to for meeting the harmonic constraints as specified by standards like IEEE-1547 and IEEE-519 [217].

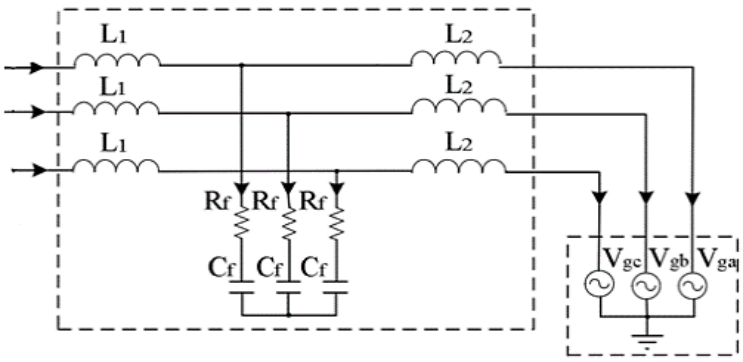

Figure 4.4. LCL Configuration [216].

LCL Filter Design

For an LCL filter design, some input data are needed, which include the line-to-line RMS grid voltage U_{gn}, the rated active power of the system P_n, the rated angular frequency of grid voltage f_g and the switching frequency of the converter f_{sw} and then, the mentioned LCL filter parameters are tuned according to the following formulas [212,217,218]:

$$Z_b = \frac{(V_n)^2}{P} \tag{4.10}$$

$$C_b = \frac{1}{\omega_g . Z_b} \tag{4.11}$$

$$I_{\max} = \frac{P.\sqrt{2}}{3.V_f} \tag{4.12}$$

Here, P is the active power, V_n is one-phase effective voltage, ω_g is the grid's angular velocity, Z_b is base impedance, C_b is base capacitance, and V_f shows filter voltage. For the design parameters, if the rated current is allowed to fluctuate by 10%, the values can be obtained through Eq. 4.13 and 4.14.

$$\Delta I_{L\_\max} = 10\%.I_{\max} \tag{4.13}$$

$$L_1 = \frac{V_{DC}}{6.f_{sw}\Delta I_{L\_\max}} \tag{4.14}$$

where, f_{sw} is switching frequency, V_{DC} represents DC link voltage, and L_1 is value inverter side inductance. Consequently, the filter capacitor's maximum value can be calculated using Eq. 4.15.

$$C_{f\max} = 5\% \frac{P_n}{2\pi f_g U_{gn}^2} \tag{4.15}$$

For beginning, it is advised to start with a half-of-the-maximum capacitor value before increasing or reducing it without going above the maximum value if some requirements cannot be satisfied [90].

$$L_2 = \frac{\sqrt{\frac{1}{K_a^2}} + 1}{C_f . \omega_{sw}^2} \tag{4.16}$$

$$\omega_{res} = \sqrt{\frac{L_1 + L_2}{L_1 . L_2 C_f}} \tag{4.17}$$

$$f_{res} = \frac{\omega_{res}}{2\pi} \tag{4.18}$$

Here C_f is the filter capacitance; the attenuation factor is K_a = 0.2 (20%), f_{res} which is resonance frequency. ω_{res} is the resonance angular velocity, and L_2 is the grid side inductance. To prevent resonance issues for the filter (caused by low and high harmonic ratings), the resonance frequency should be half of the switching frequency and ten times the grid frequency. Below is a diagram illustrating switching frequency and grid frequency range [212]:

$$10\, f_g < f_{res} < 0.5\, f_{sw} \tag{4.19}$$

To avoid resonance and eliminate some of the ripple at the switching frequency, a series resistor connection is necessary with the capacitor. At a specified frequency, this resistor should have an impedance of a maximum of one-third of the filter capacitor's impedance. Eq. 4.20 provides a formula for calculating resistor value.

$$R_f = \frac{1}{3.C_f . \omega_{res}} \tag{4.20}$$

The LCL filter was created using the computation techniques mentioned above. Table 4.1 contains the parameter values for the filter and other derived parameters.

Table 4.1. calculated parameters of the LCL filter.

1	U_{gn}	**380 V**	**6**	V_{DC}	**700 V**
2	f_{sw}	$15\,KHz$	7	L_1	17 mH
3	P_n	$2.2\,KW$	8	L_2	0.3 mH
4	f_g	$50\,Hz$	9	C_f	1.9 μF
5	f_{res}	$6173\,Hz$	10	R_d	4 Ω

4.2. CONTROL STRATEGY OF WECS

4.2.1. Boost Converter

Due to several benefits, including lower cost, improved reliability, and a simple control structure with only one power-switching device, the three-phase unregulated rectifier and the Boost Converter (BC) were selected for this study. [211]. To achieve the MPPT, the PMSG can be managed using a power electronic interface. [219]. Machine side converter with Uncontrolled Rectifier, Boost Converter, and PMSG are shown in Figure 4.5.

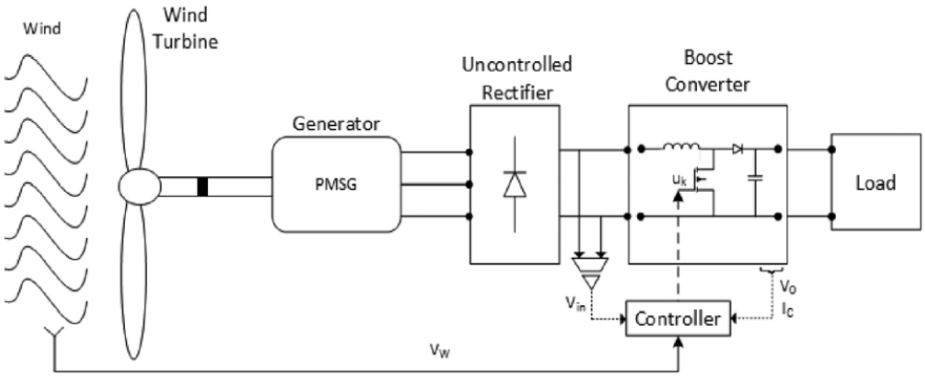

Figure 4.5. PMSG, uncontrolled rectifier, and boost Converter [219].

The DC-DC boost converter's standard unidirectional topology, also referred to as a chopper or a step-up, has a switching-mode power device that has two energy storage components (an inductor and a smoothing capacitor) and two semiconductor switches (a power transistor with a corresponding anti-parallel diode and a rectifier diode) to produce higher output DC voltage than the input DC voltage [8]. To obtain MPPT control, the BC's switching device is used [220]. The relationship between the input and output DC voltages for a boost converter is as follows:

$$V_0 = \frac{V_{in}}{1-D} \tag{4.21}$$

where, V_0 is the output voltage, V_{in} is the input voltage, where D is a value oscillating between 0 and 1 (0,1) called duty cycle.

4.2.2. Grid-Side Inverter

Grid synchronization, high-quality power delivery, grid code compliance, and control of electricity injected into the grid are the primary goals of grid-side controllers [221]. Thus, the capacitor voltages and the d- and q-axis currents are controlled by the GSI control system. Reactive power is governed by the quadratic component i_q of the grid current. Subsequently, to guarantee a unity power factor, it should be set to zero. The GSI control system's foundation is vector orientation control (VOC). Figure 4.6 depicts a GSI control's outer loop for modifying DC-link voltages and the inner control loops to control the active and reactive power.

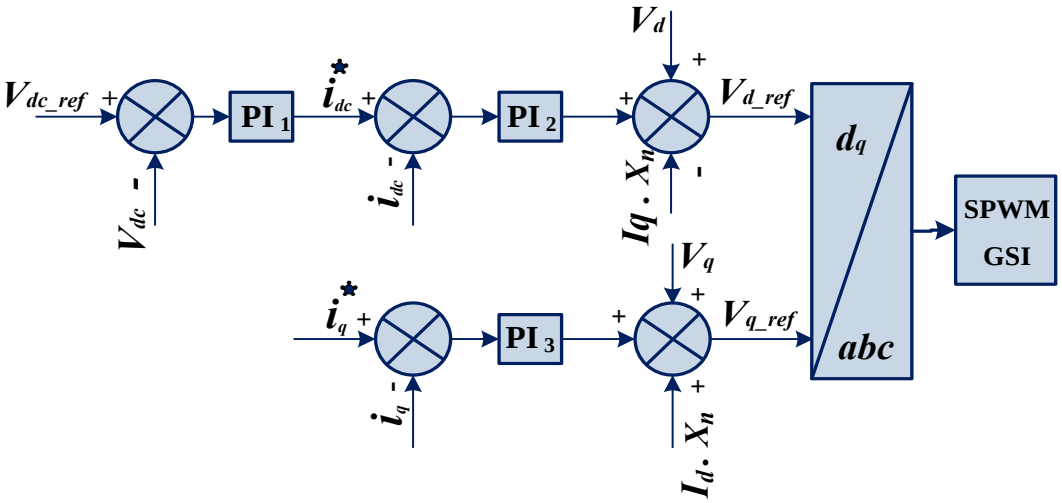

Figure 4.6. The cascaded GSI control system.

Using PI controllers, three control loops are used in a grid-side inverter control method developed by VOC. Both measured and transformed grid phase currents i_d and i_q were first compared to the reference values of grid currents i_d^* and i_q^*. For promising ontrol system attributes, there is a need to use special decoupling circuits, which are used in a control system. The reference voltages V_{q-ref} and V_{d-ref} later translate into the system's a, b, and c before passing on to the SPWM block. The active/reactive powers can be directly regulated through i_d and i_q.

4.2.3. DQ Transformation

At the point of common coupling, a three-phase balanced voltage system operates at 120◦ between the phases to make up the voltage. The sine law governs how the three-phase voltages change over time. Simple voltage control cannot directly decouple the control of reactive and actual power. We require a decoupled control system. There are two benefits to the park makeover. The time-varying three-phase voltage system V_{abc} is the first one that has been transformed into a non-time varying d and q components so that the low bandwidth controllers can be used. A decoupled control scheme is the second advantage, which is achieved by carrying out independent real and reactive power flows without disturbing each other [222,223].

$$\begin{bmatrix} V_d \\ V_q \\ V_0 \end{bmatrix} = \frac{2}{3} \begin{bmatrix} \cos(\theta) & \cos(\theta - \frac{2\pi}{3}) & \cos(\theta + \frac{2\pi}{3}) \\ -\sin(\theta & -\sin(\theta - \frac{2\pi}{3}) & -\sin(\theta + \frac{2\pi}{3}) \\ \frac{1}{2} & \frac{1}{2} & \frac{1}{2} \end{bmatrix} \begin{bmatrix} V_a \\ V_b \\ V_c \end{bmatrix} \tag{4.22}$$

4.2.4. Grid Synchronization

In order to acquire synchronized values for the inverted voltage's amplitude, phase, and frequency—regarded as variables and essential data for the grid-connected inverter systems—a synchronization technique is required. The synchronization method connects the magnitude and angle of the VSI reference currents with the grid voltage [224]. To ensure proper production of reference signals and abide by grid-connected system regulations, this equipment and its operation require quick and accurate detection of the amplitude, phase angle, and frequency of the VSI's inverted voltage. However, to fulfill minimum power dissipation requirements and adhere to grid code rules, grid-connected WECS have been managed to function as closely as possible to the unity power factor [225]. Two essential synchronization methods that can be used for this are Phase Locked Loop (PLL) and Filtered Zero Cross Detection (ZCD) [226]. A feedback control mechanism provided by the PLL automatically aligns the generated signals phase with the input signals. The goal of the PLL is to achieve a

power factor that is as close to unity as is practical. This procedure synchronizes the inverter current's angle θ_{inv} with the grid voltage angle θ_{grid}. The angle θ_{inv} determines the reference current compared to the actual value of the inverter output current. From three-phase systems representation, the space vector voltage V_{abc} can be represented by two orthogonal voltages V_d and V_q which should be easily obtained to satisfy the PLL algorithm [227]. When there is a phase difference between the grid voltage and the inverter current, the PLL's fundamental principle is to change the frequency of the inverter current. For three-phase grid-connected systems, the most widely used PLL method is based on an algorithm used in a synchronous reference frame's dq axis.

4.3. OPTIMIZATION METHODOLOGY

The optimization methodology of the cascaded controllers' parameters in GSI control is achieved as follows:

- Development of the approximated ANN model of the original power system DPGS regarding the explained mechanism in section 3.6.
- Generating a MATLAB code of GWO by following the procedure in 3.7.2.
- Execution of the GWO code for optimizing the cascaded PI controllers gains in the GSI side by considering three cases of optimization as follows:

Case 1 – Applying the GWO on the original power system by considering the standard deviation of the error as an objective function.
Case 2 – Applying the GWO on the original power system by considering the integral time absolute error (ITAE) as an objective function.
Case 3 – Applying the conjunction of ANN - GWO by considering the standard deviation of the error as an objective function.

The number of agents and iterations is selected by running the GWO with many values of them to compare their performance according to minimum fitness. The obtained results are illustrated in Figure 4.7.

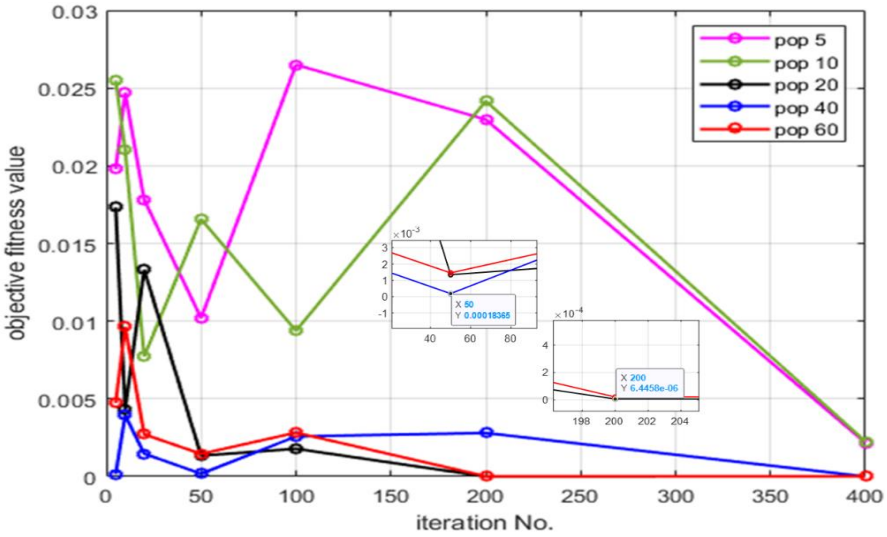

Figure 4.7. Objective fitness function and iteration values.

As seen from the above figure, the minimum value of the objective function was (6.4458e-5), which corresponds to the population size of 20 and 200 iterations. These values of population size and iterations are applied for 3 cases.

4.4. SIMULATION RESULTS AND DISCUSSION

The parameters used for the simulation of DPGS is shown in Table 1. The simulations have been done using MATLAB programming environment R2021a for examining the PI controllers' performance under the same variable wind speed, as shown in Figure 4.8.

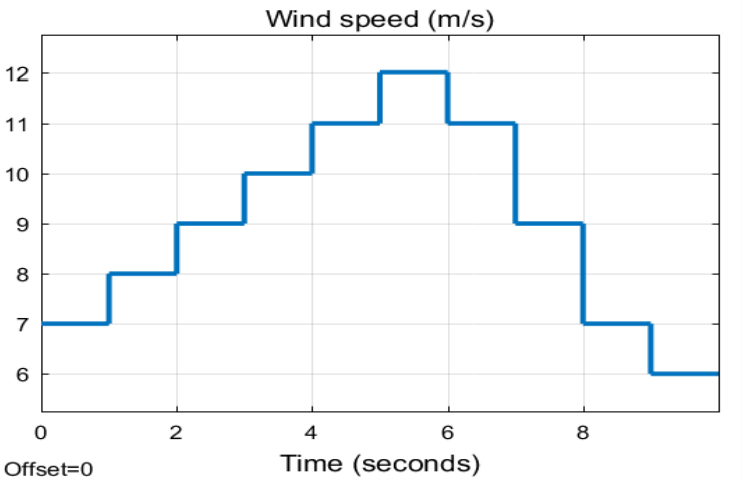

Figure 4.8. Wind speed variation with time.

The optimum gains of each controller in each case are depicted in Table 4.2.

Table 4.2. Optimum gains of PI controllers.

Case 1	K_{P1}	K_{I1}	K_{P2}	K_{I2}	K_{P3}	K_{I3}
	8.59	424.36	1.41	5.17	1.65	2.30
Case 2	K_{P1}	K_{I1}	K_{P2}	K_{I2}	K_{P3}	K_{I3}
	7.996	335.22	1.226	3.616	0.906	3.524
Case 3	K_{P1}	K_{I1}	K_{P2}	K_{I2}	K_{P3}	K_{I3}
	6.488	337.511	1.988	6.959	0.994	7.953

The Figures (4.9)-(4.11) shows the whole constructed blokes for system simulation.

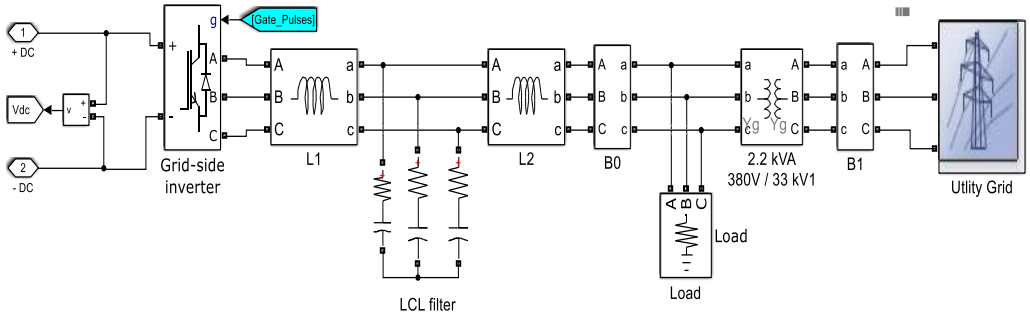

Figure 4.9. Grid side inverter components.

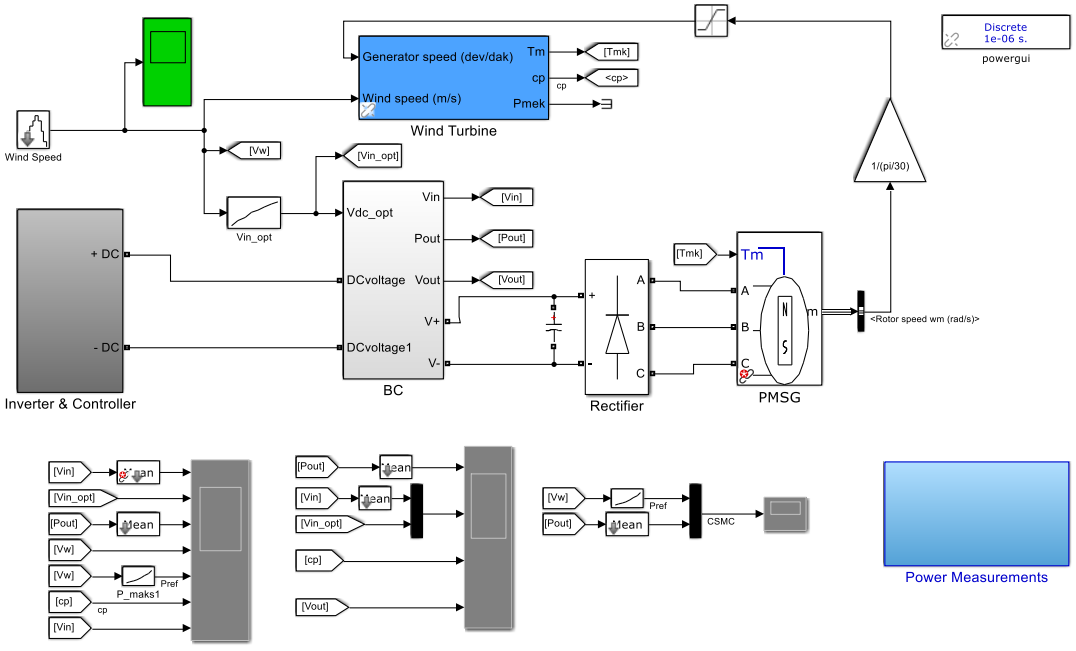

Figure 4.10. Overall simulation blocks of grid-connected DPGS.

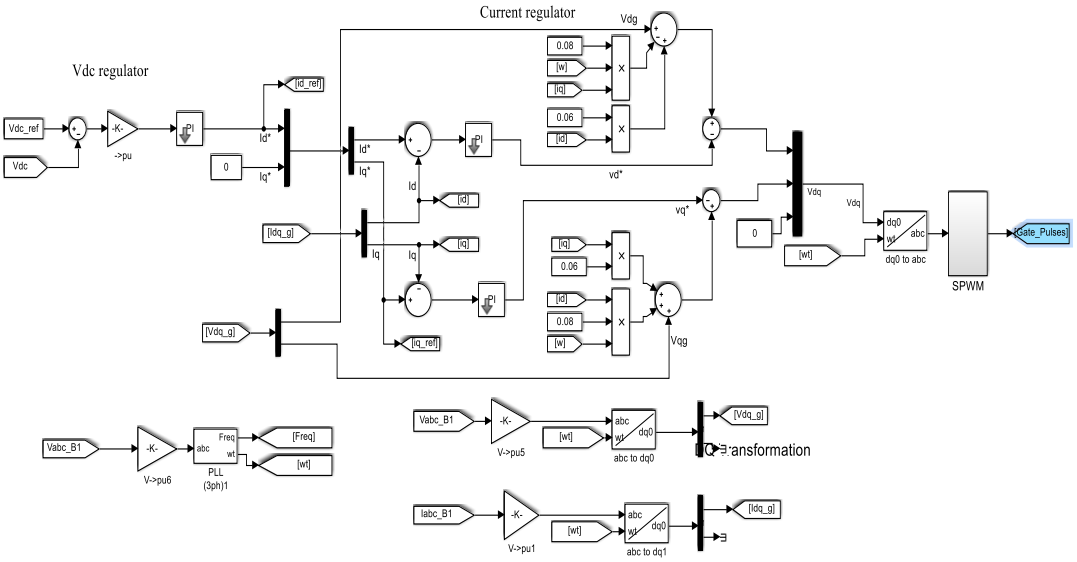

Figure 4.11. Components of grid side control algorithm.

The voltage and current smoothness have a big impact on the grid-connected system. Figure 4.12 (a) shows the 3-phase current/voltage on the inverter side. In 3 instances, a very brief, minor fluctuation in the voltage and current signals was found to be caused by rapidly varying wind speed, especially at wind speeds 7 m/s and 8 m/s. Both the current and the wind speed rise as the wind speed rises and vice versa. The output voltage and inverter current signals for phase A are shown in greater clarity in Figure 4.12 (b). The phase voltage is steady-state and smooth. Additionally, it demonstrates how each case's voltage and current are matched.

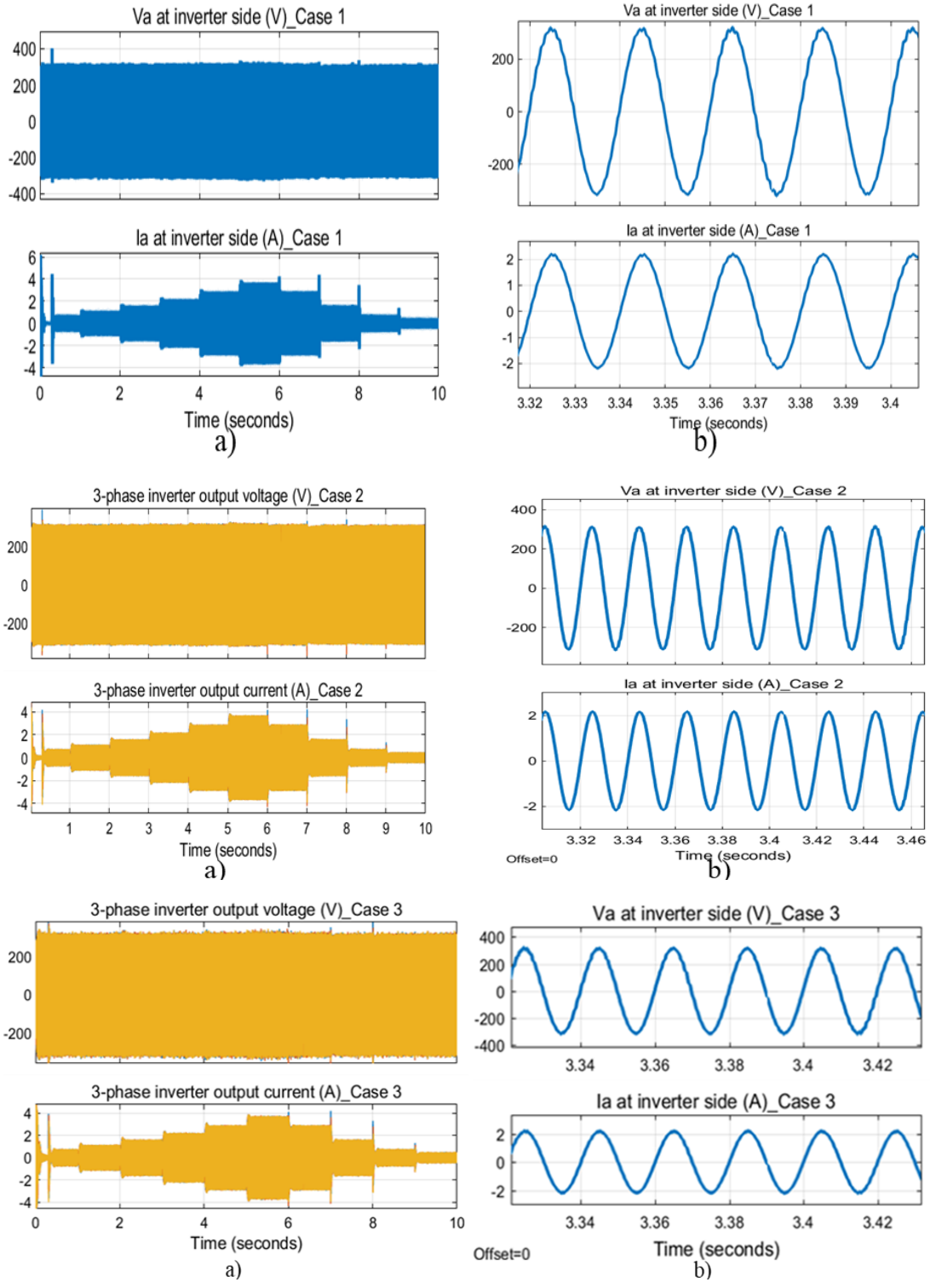

Figure 4.12. (a) voltage and current in three phases on the inverter side, (b) zoomed Voltage and current of phase A on the inverter side.

The voltage fluctuation of the RMS value of phase A is always kept within allowable bounds regarding the inverter output nominal voltage [228] (Vnom=220V) as

illustrated in Figure 4.13. This proves the effectiveness of the established controller systems.

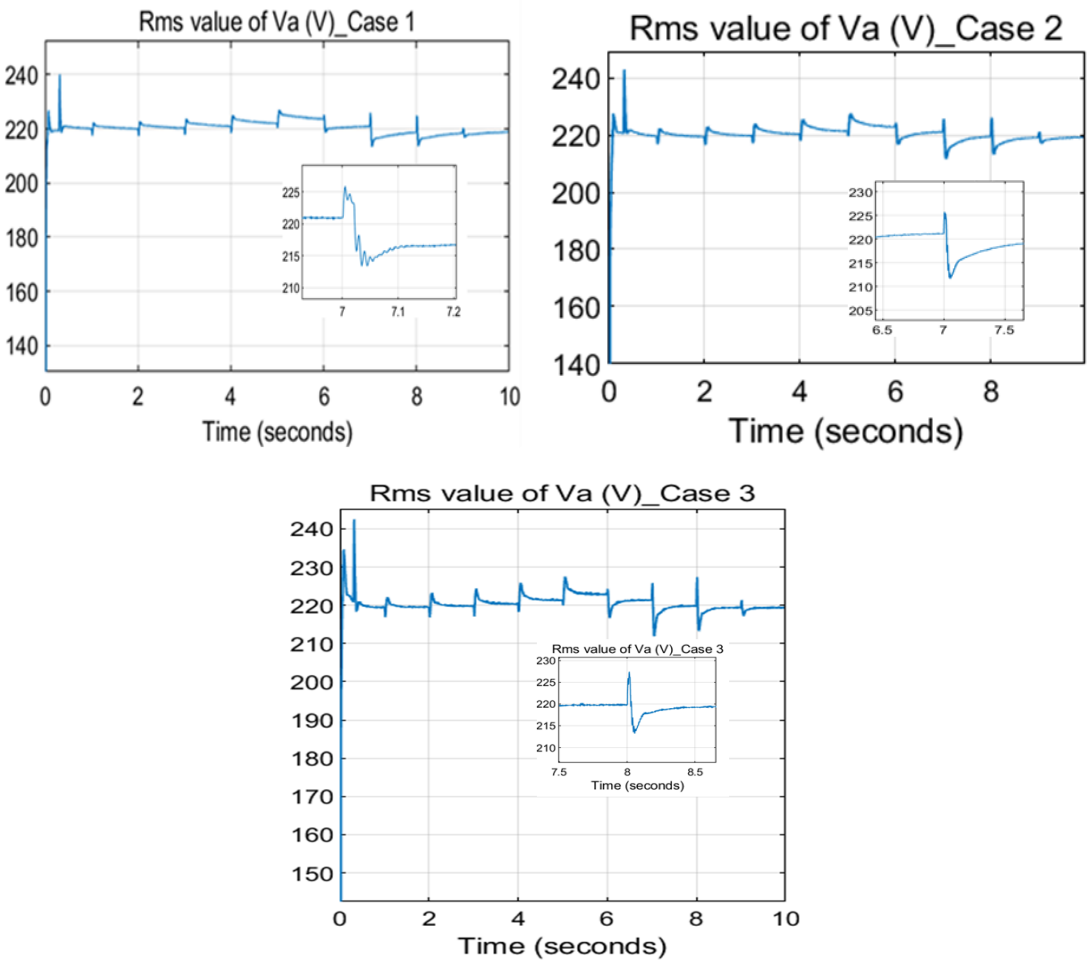

Figure 4.13. Rms value of phase voltage a of the inverter side.

The phase voltage A waveforms for the inverter and the grid in case 1, case 2 and case 3 are shown in Figure 4.14. The waves' stability and phase coherence can be observed.

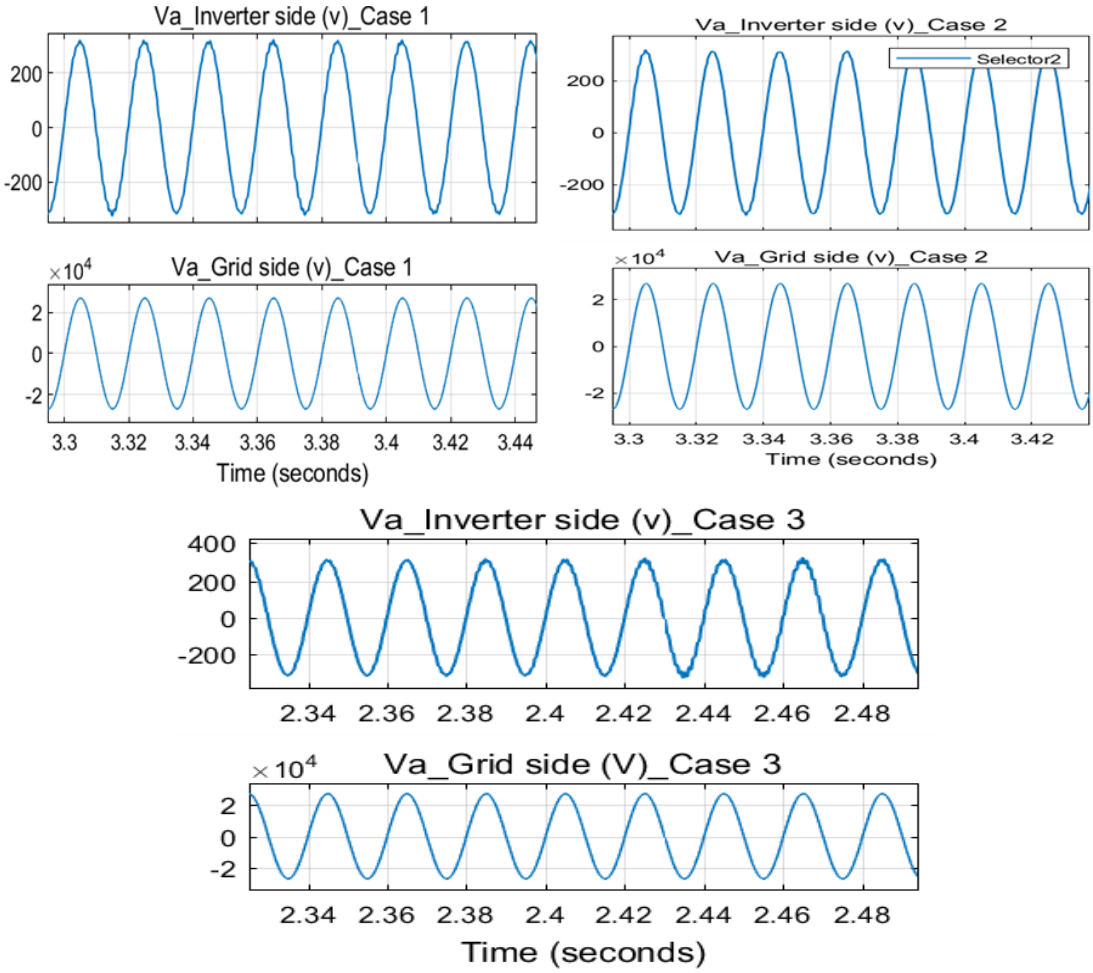

Figure 4.14. Phase voltage Va at the inverter side and the grid side.

The frequency variations for the same wind profile have also been looked at figure 4.15 (a) makes it clear that differences in wind speed typically result in very small frequency oscillations. The Figure concludes that the frequency fluctuation is acceptable for the IEEE Std 1547standard [229]. As was previously noted, the 700 V DC bus reference voltage should be roughly the same for the control activities. The bus voltage varies within acceptable bounds even while the wind speed varies significantly, as shown in Figure 4.15 (b).

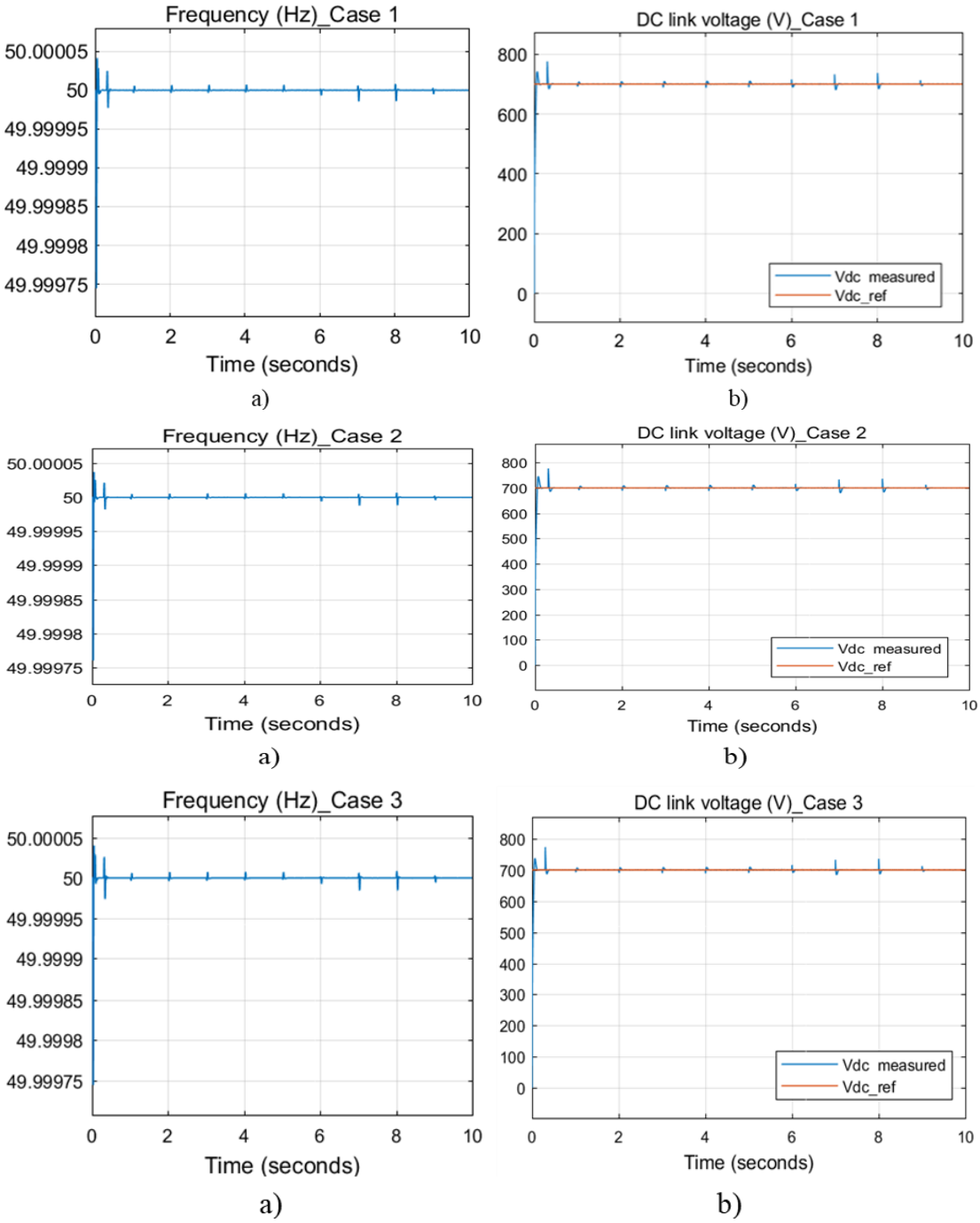

Figure 4.15. (a) Frequency of the injected power (Hz), b) DC link voltage (V).

There is an IEEE-519 standard for THD, which must be less than 5% [206][217]. Figure 4.16 is presented in this work to evaluate THD. It is clear from this figure that the proposed controller ensured the standard limit despite changing wind speed.

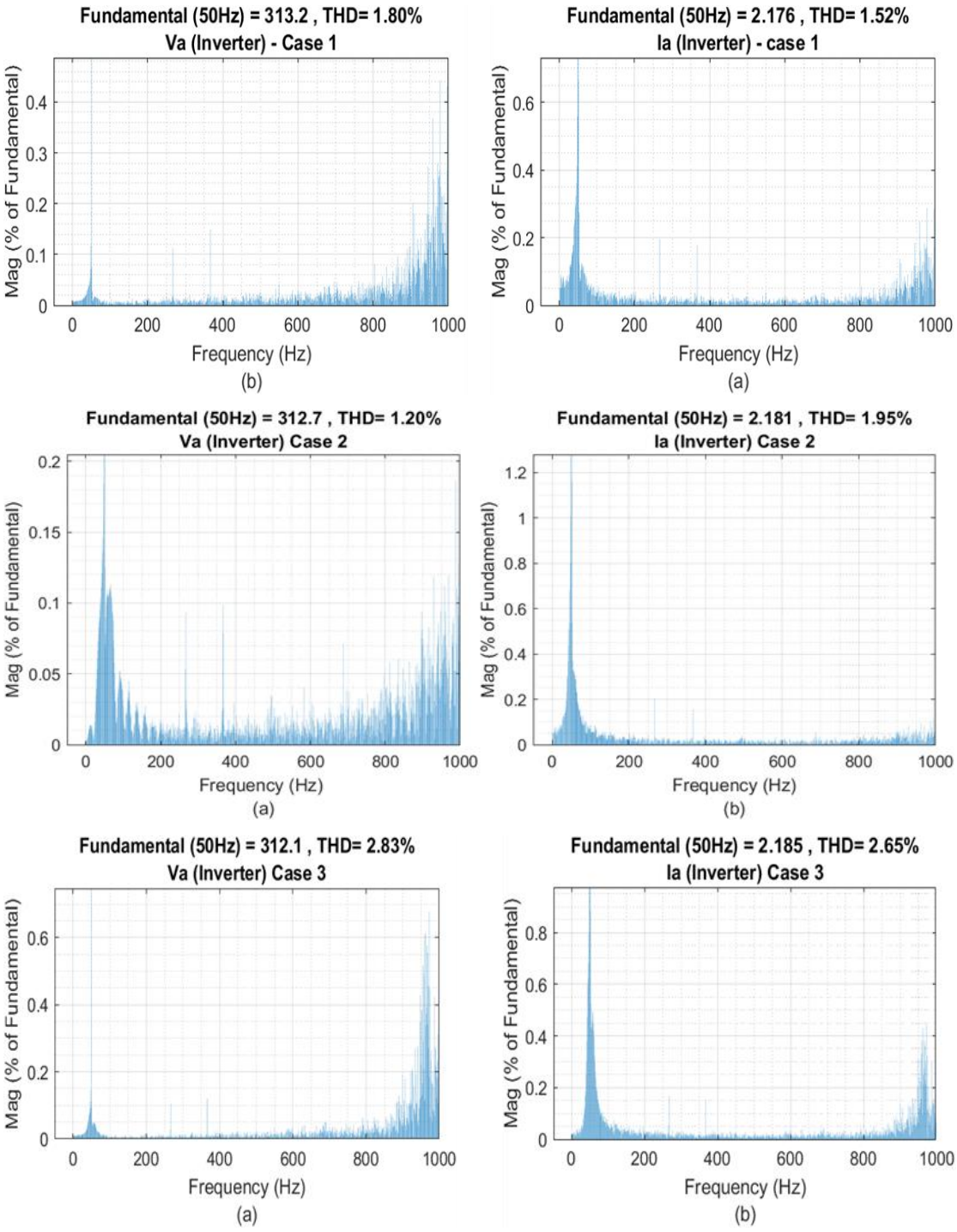

Figure 4.16. (a) THD of voltage at the inverter side, (b) THD of current at the inverter side.

Figure 4.17 depicts the power exchange between the wind turbine and the grid. If the equipped power from the inverter exceeds the load, the grid absorbs the overflowing power. Correspondingly, if the generated power does not do enough to the load, the rest is absorbed from the grid.

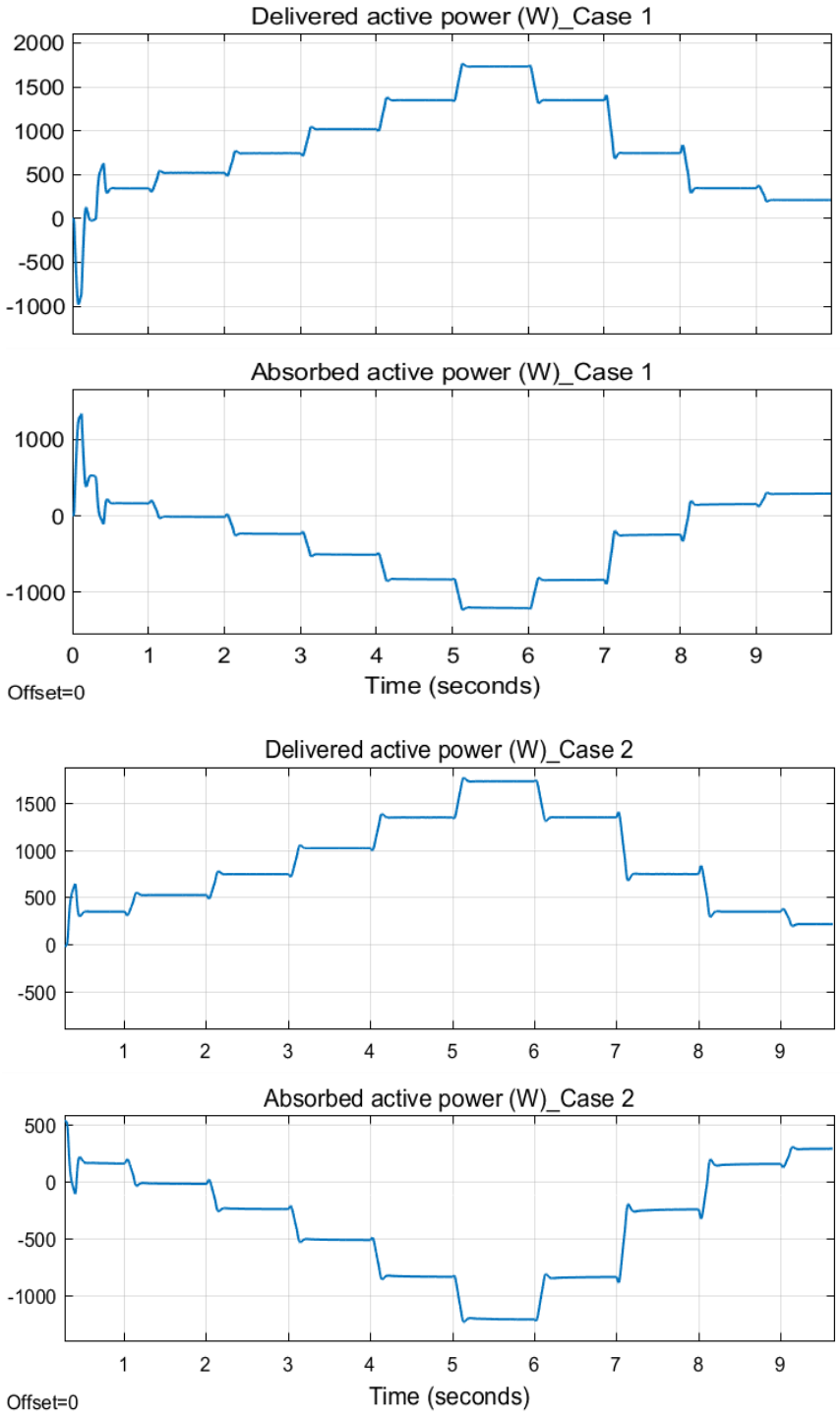
Delivered active power (W)_Case 1
2000
1500
1000
500
0
-500
-1000
Absorbed active power (W)_Case 1
1000
0
-1000
0 1 2 3 4 5 6 7 8 9
Time (seconds)
Offset=0
Delivered active power (W)_Case 2
1500
1000
500
0
-500
1 2 3 4 5 6 7 8 9
Absorbed active power (W)_Case 2
500
0
-500
-1000
1 2 3 4 5 6 7 8 9
Time (seconds)
Offset=0

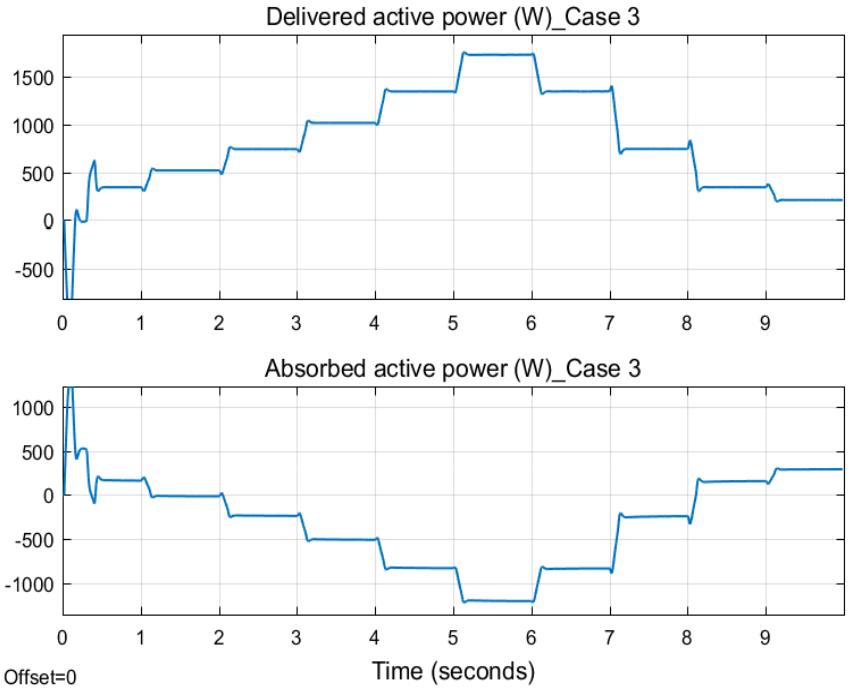

Figure 4.17. Delivered power at the inverter and absorbed power from the grid.

PART 5

SUMMARY

The ANN-based GWO algorithm has been suggested in this research to adjust the cascaded PI controllers' coefficients in the GSI of grid-connected DPGS, thereby enhancing the quality of the power injected into the electric grid. The suggested GWO technique has demonstrated well-organized exploitation and exploration; on top of that, it can avoid local optimum. This approach can be used for complex systems because it is reliable and straightforward. Further, there is no mathematical model required for the suggested algorithm. The ANN model is used as an alternative to DPGS. The ANN model is constructed using the range of the input parameters for the controllers and the standard deviation of the related errors previously obtained by running the DPGS model. The ANN model is also well suited to the creation of simulation-optimization systems due to its computational effectiveness. The ANN-GWO technique's influence can save time for parameters selection. The controller's performance is examined with the optimum gains obtained from GWO under different criteria of the objective function. The results were close in all the cases. Correspondingly, the ANN-GWO was very effective according to the time consumed in the optimization process. According to the simulation findings, the PI controller is effective at generating a high output power quality with low THD values within the international standards bounds during steady state operation. It also shows superior performance by regulating power exchange between the grid and the source during a variety of wind speed conditions.

Moreover, the suggested approach performs well in terms of steady-state voltage, frequency constancy, and DC link voltage stability. Therefore, a grid-tied wind energy system can benefit from using a GWO-based strategy to tune numerous PI controllers. The technique can be used for various power systems and renewable energy applications.

5.1. THESIS CONTRIBUTIONS

The following contributions have been made in this research work:

- The modeling of the grid-connected DPGS-based WECS is developed and analyzed.
- The control algorithm of GSI is carried out with cascaded PI controllers to improve the injected power quality injected into the grid.
- The PI controllers' parameters are optimized using grey wolf optimization under different criteria for the objective function.
- ANN model was developed as an alternative representation for a DPGS, which is considered a salient feature of the presented work.

5.2. RECOMMENDATION FOR FUTURE WORKS

Summarizing the contributions of the thesis, the following suggestions might be made for future works:

- Applying various optimization strategies with swarm intelligence optimization techniques such as particle swarm optimization, genetic algorithms, and fox optimization, etc.
- Using various methods to create a proxy model for the power system under consideration.
- • Experimenting with the work that has been provided.

REFERENCES

1. Maihemuti S, Wang W, Wang H, Wu J, Zhang X. Dynamic Security and Stability Region under Different Renewable Energy Permeability in IENGS System. **IEEE Access**. 2021;9:19800–17.

2. Jones D, Graham E, Tunbridge P, Ilas A. **Global Electricity Review 2022**. 2022.

3. Novakovic B, Nasiri A. Introduction to electrical energy systems. In: Electric Renewable Energy Systems. first edit. **Elsevier Inc**.; 2016. p. 1–20.

4. Manzano-agugliaro F, Alcayde A, Montoya FG, Zapata-sierra A, Gil C. Scientific production of renewable energies worldwide : An overview. **Renew Sustain Energy Rev**. 2013;18:134–43.

5. Hernandez RR, Easter SB, Murphy-Mariscal ML, Maestre FT, Tavassoli M, Allen EB, Barrows CW, Belnap J, Ochoa-Hueso R, Ravi S, Allen MF. Environmental impacts of utility-scale solar energy. **Renew Sustain Energy Rev**. 2014;29(2014):766–79.

6. Luis F, Moncayo G. Advances in Renewable Energies and Power Technologies. first edit. **Elsevier**; 2018.

7. Members R. global status report 2022. **REN21**; 2022.

8. Patel MR, Beik O. Wind and Solar Power Systems Design, Analysis, and Operation. Third edit. **Taylor & Francis**; 2021.

9. Al-Dousari A, Al-Nassar W, Al-Hemoud A, Alsaleh A, Ramadan A, Al-Dousari N, Ahmed M. Solar and wind energy: Challenges and solutions in desert regions. **Energy**. 2019;176:184–94.

10. International Renewable Energy Agency. Renewable Power Generation Costs in 2021. **International Renewable Energy Agency**. Abu Dhabi; 2022.

11. Lee J, Zhao F. GWEC Global Wind Report. **Glob Wind Energy Counc**. 2022;75.

12. Gupta A. Integration Challenges of Wind Power on Power System Grid A Review. **2018 Int Conf Adv Comput Telecommun**. 2018;1–7.

13. Energy F. Future Energy Improved, Sustainable and Clean Options for our Planet. Third Edit. Letcher TM, editor. **Elsevier**; 2020.

14. Kumar D, Chatterjee K. A review of conventional and advanced MPPT algorithms for wind energy systems. **Renew Sustain Energy Rev**. 2016;55:957–70.

15. T M. Study of Power Quality Issues in Grid Connected Wind Farms. **Anna University**, Chennai; 2016.

16. Eltamaly AM, A. I. Alolah, Farh HM. Maximum Power Extraction from Utility-Interfaced Wind Turbines. In: New Developments in Renewable Energy. **IntechOpen**; 2013. p. 159–92.

17. Yaramasu V, Wu B. Model Predictiv Control of Wind Energy Conversion Systems. First edit. Hoboken, New Jersey: **John Wiley & Sons**, Inc.; 2017.

18. Blaabjerg F, Ionel DM. Renewable Energy Devices and Systems with Simulations in MATLAB® and ANSYS®. 1st Editio. **Taylor & Francis Group**,; 2017.

19. Engleitner R, Nied A, Cavalca MSM, Da Costa JP. Dynamic Analysis of Small Wind Turbines Frequency Support Capability in a Low-Power Wind-Diesel Microgrid. **IEEE Trans Ind Appl**. 2018;54(1):102–11.

20. Mariam L, Basu M, Conlon MF. A Review of Existing Microgrid Architectures. **J Eng**. 2013;2013:1–8.

21. Jiayi H, Chuanwen J, Rong X. A review on distributed energy resources and MicroGrid. **Renew Sustain Energy Rev**. 2008;12(9):2472–83.

22. Cao W, Hu Y. Renewable Energy - Utilisation and System Integration. first. Renewable Energy - Utilisation and System Integration. **ExLi4EvA**; 2016.

23. Iqbal MM, Kumar S, Lal C, Kumar C. Energy management system for a small - scale microgrid. **J Electr Syst Inf Technol**. 2022;9(1):1–17.

24. XIAO Z, WU J, JENKINS N. An Overview Of Microgrid Control. **Intell Autom Soft Comput**. 2010;16(2):199–212.

25. Kobayakawa T, Kandpal TC. Optimal resource integration in a decentralized renewable energy system : Assessment of the existing system and simulation for its expansion. **Energy Sustain Dev**. 2016;34(2016):20–9.

26. Zhou X, Guo T, Ma Y. An overview on microgrid technology. In: **2015 IEEE International Conference on Mechatronics and Automation, ICMA** 2015. Beijing, China; 2015. p. 76–81.

27. Ahmed SD, Al-ismail FSM. Grid Integration Challenges of Wind Energy : A Review. **IEEE Access**. 2020;8:10857–78.

28. Kumar KSVP, Venkateshwarlu S. A Review on Power Quality in Grid Connected Renewable Energy System. **CVR J Sci Technol**. 2013;5:57–61.

29. Reilly JT. From microgrids to aggregators of distributed energy resources . The microgrid controller and distributed energy management systems. **Electr J**. 2019;32(5):30–4.

30. Hossain J, Mahmud A. Renewable Energy Integration Challenges and Solutions. first edit. 21st PPA Annual Conference. **Springer**; 2012.

31. Qais MH, Hasanien HM, Alghuwainem S. Output Power Smoothing of Grid-Connected Permanent Magnet Synchronous Generator Driven Directly by Variable Speed Wind Turbine : a Review. **J Eng**. 2017;3(November):1755–9.

32. Bhadane K V, Jaware TH, Patil DP, Nayyar A. Wind Energy System Grid Integration and Grid Code Requirements of Wind Energy System. In: Control and Operation of Grid-Connected Wind Energy Systems. **Springer**; 2021.

33. Ackermann T. Wind Power in Power Systems. Second edi. United Kingdom: **John Wiley & Sons Ltd**; 2012.

34. Nirosha C, Patra PSK. Power Quality Issues of Wind and Solar Energy Systems Integrated into the Grid. **Adv Sci Lett**. 2020;26(5):514–23.

35. Jeremiah M, Kabeyi B, Olanrewaju OA. Relationship Between Electricity Consumption and Economic Development. In: **International Conference on Electrical, Computer and Energy Technologies (ICECET)**. South Africa: IEEE; 2021. p. 1–8.

36. Dehghanzadeh AR, Behjat V, Banaei MR. Dynamic modeling of wind turbine based axial flux permanent magnetic synchronous generator connected to the grid with switch reduced converter. **Ain Shams Eng J**. 2018;9(1):125–35.

37. William Shepherd, Zhang L. Electricity Generation using Steam Turbines. second edi. **World Scientific Publishing Co. Pte. Ltd**. 2017.

38. Gwóźdź M, Krystkowiak M, Ciepliński Ł, Strzelecki R. A wind energy conversion system based on a generator with modulated magnetic flux. **Energies**. 2020;13(12).

39. Errami Y, Obbadi A, Sahnoun S, Ouassaid M, Maaroufi M. Power Extraction Control of Variable Speed Wind Turbine Systems Based on Direct Drive Synchronous Generator in All Operating Regimes. **J Electr Comput Eng**. 2018;2018:1–17.

40. Urtasun A, Sanchis P, San Martín I, López J, Marroyo L. Modeling of small wind turbines based on PMSG with diode bridge for sensorless maximum power tracking. **Renew Energy**. 2013;55(2013):138–49.

41. Farh HMH, Eltamaly AM. Fuzzy Logic Control of Wind Energy Conversion System. **J Renew Sustain Energy** ·. 2013;5(2014):023125.

42. Marmouh S, Boutoubat M, Mokrani L. MPPT fuzzy logic controller of a wind energy conversion system based on a PMSG. **Proc 2016 8th Int Conf Model Identif Control ICMIC** 2016. 2017;296–302.

43. Li Z, Member S, Zang C, Zeng P, Yu H. Control of A Grid-Forming Inverter Based on Sliding Mode and Mixed H2 / H∞ Control. **IEEE Trans Ind Electron**. 2016;0046(c).

44. Ali SM, Jawad M, Guo F, Mehmood A, Khan B, Glower J, Khan SU. Exact feedback linearization-based permanent magnet synchronous generator control. **Int Trans Electr Energ Syst**. 2016;26(9):1917–39.

45. Alrifai M, Zribi M, Rayan M, Department. Feedback Linearization Controller for a Wind Energy Power System. **MDPI**. 2016;9(10):1–23.

46. Abdalrahman A, Zekry A. Control of the grid-connected inverter using dsPIC microcontroller. In: **2nd International Japan-Egypt Conference on Electronics, Communications and Computers, JEC-ECC**. 2013. p. 159–64.

47. Agarwal J, Parmar G, Gupta R, Sikander A. Analysis of grey wolf optimizer based fractional order PID controller in speed control of DC motor. **Microsyst Technol**. 2018;24(12):4997–5006.

48. Joseph E, Olaiya OO. Cohen-coon PID Tuning Method ; A Better Option to Ziegler Nichols-PID Tuning Method. **IJRERD**. 2017;02(11):141–5.

49. Hasanien HM, Member S, Muyeen SM, Member S. A Taguchi Approach for Optimum Design of Proportional-Integral Controllers in Cascaded Control Scheme. **IEEE Trans Power Syst**. 2013;28(2):1636–44.

50. Wang Z, Qiu S, Song R, Wang X, Zhu B, Li B. Research on PID parameter tuning of coordinated control for ultra-supercritical units based on Ziegler Nichols method. **IEEE. 2019;(Imcec)**:1155–8.

51. Przystupa K. Tuning of PID Controllers – Approximate Methods. **Adv Sci Technol Res J**. 2018;12(4):56–64.

52. Pajchrowski T, Zawirski K, Member S, Nowopolski K. Neural Speed Controller Trained Online by Means of Modified RPROP Algorithm. **560 IEEE Trans Ind INFORMATICS**. 2015;11(April):560–8.

53. KUSHWAH M, ASHISH PATRA. PID Controller Tuning using Ziegler-Nichols Method for Speed Control of DC Motor. **Int J Sci Eng Technol Res**. 2018;3(13):2924–9.

54. Muyeen SM. An Affine Projection Algorithm based Adaptive Control Scheme for Operation of Variable-Speed Wind Generator. **IET Gener Transm Distrib**. 2015;9(August 2017):2611–6.

55. Qais MH, Hasanien HM, Alghuwainem S. A Grey Wolf Optimizer for Optimum Parameters of Multiple PI Controllers of a Grid-Connected PMSG Driven by Variable Speed Wind Turbine. **IEEE Access**. 2018;6(January 2020):44120–8.

56. Leandro B, Costa G, Bacon VD, Oliveira SA. Tuning of a PI-MR Controller Based on Differential Evolution Metaheuristic Applied to the Current Control Loop of a Shunt-APF. **IEEE Trans Ind Electron**. 2017;64(6):4751–61.

57. Petchinathan G, K. Valarmathi, T. K. Radhakrishnan. Optimal Tuning of Fractional Order PI Controller using Particle Swarm Optimization for pH process. **Int J Appl Eng Res**. 2017;12(1):1–7.

58. Mirjalili S, Lewis A. The Whale Optimization Algorithm. **Adv Eng Softw**. 2016;95:51–67.

59. Niu Xiang-jie. The optimization for PID controller parameters based on Genetic Algorithm. **Trans Tech Publ**. 2014;(2014):4102–5.

60. Sen R, Pati C, Dutta S, Sen R. Comparison Between Three Tuning Methods of PID Control for High Precision Positioning Stage. **J Metrol Soc India**. 2014;30(1):65–70.

61. Nicola M, Nicola CI. Improved Performance of Grid-Connected Photovoltaic System Based on Fractional-Order PI Controller and Particle Swarm optimization. **Proc 2021 9th Int Conf Mod Power Syst MPS**. 2021;(July):1–5.

62. Ulusoy S, Nigdeli SM, Bekdaş G. Novel metaheuristic-based tuning of PID controllers for seismic structures and verification of robustness. **J Build Eng**. 2021;33:1–29.

63. Sabir MM, Khan JA. Optimal Design of PID Controller for the Speed Control of DC Motor by Using Metaheuristic Techniques. **Adv Artif Neural Syst.** 2014;2014:1–8.

64. Fethia H, Amel A, Ahmed M. Tuning gain of PI controller based on Meta-heuristic techniques. In: **2018 International Conference on Applied Smart Systems (ICASS)**. ALGERIA: IEEE; 2018. p. 1–6.

65. Hasanien HM, Muyeen SM. Design Optimization of Controller Parameters Used in Variable Speed Wind Energy Conversion System by Genetic Algorithms. **IEEE Trans Sustain Energy**. 2012 Apr;3(2):200–8.

66. Haridy AL. The Whale Optimization Algorithm based controller forfor PMSG wind energy generation system. **2019 Int Conf Innov Trends Comput Eng**. 2019;(February):438–43.

67. Pareek S. Optimal Tuning Of PID Controller Using Meta Heuristic Algorithms. In Unnao, India: **IEEE International Conference on Advances in Engineering & Technology Research (ICAETR - 2014)**; 2014. p. 3–7.

68. Cong CN, Anh NN, Trong CT, Ba NN. Tuning Pi Controller Bases on Chemical Reaction Optimization Algorithm. **Am J Electr Comput Eng**. 2019;3(1):46–52.

69. Costa BLG, Graciola CL, Angélico BA, Goedtel A, Castoldi MF. Metaheuristics optimization applied to PI controllers tuning of a DTC-SVM drive for three-phase induction motors. **Appl Soft Comput J**. 2018;62:776–88.

70. Mirjalili S, Mirjalili SM, Lewis A. Grey Wolf Optimizer. **Adv Eng Softw**. 2014;69:46–61.

71. Nimma KS, Al-Falahi MDA, Nguyen HD, Jayasinghe SDG, Mahmoud TS, Negnevitsky M. Grey Wolf optimization-based optimum energy-management and battery-sizing method for grid-connected microgrids. **Energies**. 2018;11(4):1–27.

72. Hassan HA, Zellagui M. Application of grey wolf optimizer algorithm for optimal power flow of two-terminal HVDC transmission system. **Adv Electr Electron Eng**. 2017;15(5):701–11.

73. Tripathi AK, Sharma K, Bala M. A Novel Clustering Method Using Enhanced Grey Wolf Optimizer and MapReduce. **Big Data Res**. 2018;14:93–100.

74. Song X, Tang L, Zhao S, Zhang X, Li L, Huang J, Cai W. Grey Wolf Optimizer for parameter estimation in surface waves. **Soil Dyn Earthq Eng**. 2015;75:147–57.

75. Kandasamy P. Literature Review on Grey Wolf Optimization Techniques. **Int J Sci Res**. 2020;9(12):1765–9.

76. Faris H, Aljarah I, Azmi M, Mirjalili A betar S. Grey wolf optimizer : a review of recent variants and applications. **Neural Comput Appl**. 2017;30(July 2018):413–35.

77. Li S xia, Wang J sheng. Dynamic Modeling of Steam Condenser and Design of PI Controller Based on Grey Wolf Optimizer. **Hindawi Publ Corp**. 2015;2015:1–9.

78. Yang B, Zhang X, Yu T, Shu H, Fang Z. Grouped grey wolf optimizer for maximum power point tracking of doubly-fed induction generator based wind turbine. **Energy Convers Manag**. 2017;133:427–43.

79. Sule AH, Mokhtar AS, Bin Jamian JJ, Sheikh UU, Khidrani A. Grey Wolf Optimizer Tuned PI Controller for Enhancing Output Parameters of Fixed Speed Wind Turbine. In: **2020 IEEE International Conference on Automatic Control and Intelligent Systems, ICACIS** 2020 - Proceedings. Shah Alam, Malaysia; 2020. p. 118–22.

80. Joseph SB, Dada EG, Abidemi A, Oyewola DO, Khammas BM. Metaheuristic algorithms for PID controller parameters tuning: review, approaches and open problems. **Heliyon**. 2022;8(5):1–29.

81. Qais MH, Hasanien HM, Alghuwainem S, Elgendy MA. Output Power Smoothing of Grid-Tied PMSG-Based Variable Speed Wind Turbine Using Optimal Controlled SMES. **2019 54th Int Univ Power Eng Conf**. 2019;1–6.

82. Precup RE, David RC, Petrin EM. Grey Wolf Optimizer-Based Approach to the Tuning of PI-Fuzzy Controllers with a Reduced Process Parametric Sensitivity. **IFAC**. 2016;49(5):55–60.

83. Mahmoud HY, Hasanien HM, Besheer AH, Abdelaziz AY. Hybrid cuckoo search algorithm and grey wolf optimiser-based optimal control strategy for performance enhancement of HVDC-based offshore wind farms. **IET Gener Transm Distrib Res**. 2020;14(10):1902–11.

84. Safawi A, Mokhtar BIN, Hamza A, Pke S. Optimal tuning of proportional integral controller for fixed-speed wind turbine using grey wolf optimizer. **Int J Electr Comput Eng**. 2020;10(5):5251–61.

85. Şen MA, Kalyoncu M. Optimal Tuning of PID Controller Using Grey Wolf Optimizer Algorithm for Quadruped Robot. **Balk J Electr Comput Eng**. 2018;6(1):29–35.

86. Hatta NM, Zain AM, Sallehuddin R, Shayfull Z, Yusoff Y. Recent studies on optimisation method of Grey Wolf Optimiser (GWO): a review (2014–2017). **Artif Intell Rev**. 2019;52(4):2651–83.

87. Al-shamma AA, Omotoso HO, Noman AM, Alkuhayli AA. Grey Wolf Optimizer Based Optimal Control for Grid-Connected PV System. In: **IECON 2020 The 46th Annual Conference of the IEEE Industrial Electronics Society**. Singapore; 2020. p. 2863–7.

88. Vargas-Salgado C, Hurtado-Perez E, García EXM. Optimal PID Parameters Tunning for a DC-DC Boost Converter. In: **2020 IEEE Conference on Technologies for Sustainability (SusTech)**. Santa Ana, CA USA; 2020. p. 1–6.

89. Qais MH, Hasanien HM, Alghuwainem S. A Grey Wolf Optimizer for Optimum Parameters of Multiple PI Controllers of a Grid- Connected PMSG Driven by Variable Speed Wind Turbine. **IEEE Access**. 2018;PP(c):1.

90. Liserre M, Frede Blaabjerg, Steffan Hansen. Design and Control of an LCL-filter based Three-phase Active Rectifier. **IEEE Trans Ind Appl**. 2001;41(5):299–307.

91. Peyman Bahrami, Moghaddam FS, Lesley A. James. A Review of Proxy Modeling Highlighting Applications for Reservoir Engineering. **energies Rev**. 2022;15(14):1–32.

92. Shohreh Amini, Shahab Mohaghegh. Application of Machine Learning and Artificial Intelligence in Proxy Modeling for Fluid Flow in **Porous Media. Fluids**. 2019;4(3):1–17.

93. Aydin H, Akin S, Senturk E. A proxy model for determining reservoir pressure and temperature for geothermal wells. **Geothermics**. 2020;88(2020):1–9.

94. Majumder P, Eldho TI. Artificial Neural Network and Grey Wolf Optimizer Based Surrogate Simulation-Optimization Model for Groundwater Remediation. **Water Resour Manag**. 2020;763–83.

95. Nosratabadi S, Szell K, Beszedes B, Imre F, Ardabili S, Mosavi A. Comparative Analysis of ANN-ICA and ANN-GWO for Crop Yield Prediction. In: **International Conference on Computing and Communication Technologies (RIVF)**. Ho Chi Minh, Vietnam; 2020. p. 1–5.

96. Sun H, Qiu C, Lu L, Gao X, Chen J, Yang H. Wind turbine power modelling and optimization using artificial neural network with wind field experimental data. **Appl Energy**. 2020;280(October):1–12.

97. Gasparis G, Lio WH, Meng F. Surrogate Models for Wind Turbine Electrical Power and Fatigue Loads in Wind Farm. **energies Artic**. 2020;13(23):1–15.

98. Göçken M, Boru A, Dosdogru AT, Özçalici M. Integrating metaheuristics and artificial neural network for weather forecasting. **Int J Glob Warm**. 2018;14(4):440–61.

99. Alizadeh N. Artificial Neural Network With Experimental Design : A Fast Tool for Risk Analysis and Forcasting in an Oil Reservoir, A Case Study. **Int J Eng Sci Technol**. 2020;4(5):40–50.

100. Kalaam RN, Muyeen SM, Al-Durra A, Hasanien HM, Al-Wahedi K. Optimisation of controller parameters for gridtied photovoltaic system at faulty network using artificial neural network-based cuckoo search algorithm. **IET Renew Power Gener**. 2017;11(12):1517–26.

101. Kumar D, Chatterjee K. A review of conventional and advanced MPPT algorithms for wind energy systems. **Renew Sustain Energy Rev**. 2016;55:957–70.

102. Devashish, Thakur A. A comprehensive review on wind energy system for electric power generation: Current situation and improved technologies to realize future development. **Int J Renew Energy Res**. 2017;7(4):1787–805.

103. Sunderland KM, Mills G, Conlon MF. Estimating the wind resource in an urban area : A case study of micro-wind generation potential in Dublin , Ireland. **Jnl Wind Eng Ind Aerodyn**. 2013;118(2013):44–53.

104. Mahela OP, Shaik AG. Comprehensive overview of grid interfaced wind energy generation systems. **Renew Sustain Energy Rev**. 2016;57:260–81.

105. Machowski J, Lubosny Z, Bialek JW, Bumby JR. Power System Dynamics Stability and Control. Third Edit. **WILEY**; 2020.

106. Franco JA, Jauregui JC, Toledano-Ayala M. Optimizing wind turbine efficiency by deformable structures in smart blades. **J Energy Resour Technol Trans ASME**. 2015;137(5):1–8.

107. Muyeen SM. Wind Energy Conversion Systems Technology and Trends. First edit. **Springer**; 2012.

108. Duran MJ, Barrero F, Member S, Pozo-ruz A, Guzman F, Fernandez J. Understanding Power Electronics and Electrical Machines in Multidisciplinary Wind Energy Conversion System Courses. **IEEE Trans Educ**. 2013;56(2):174–82.

109. Ibrahim RA, Zakzouk NE. A PMSG Wind Energy System Featuring Low-Voltage Ride-Through via Mode-Shift Control. **Appl Sci**. 2022;12(3).

110. JEEVAJOTHI R. Impact of Wind Turbine Generators on Power System Stability. **KALASALINGAM UNIVERSITY**, Tamil Nadu; 2014.

111. Orłowska-kowalska T, Rodríguez J, Blaabjerg F. Advanced and Intelligent Control in Power Electronics and Drives. First edit. Vol. 531. Switzerland: **Springer**; 2014.

112. Asuhaimi A, Zin BM, A MPH, Khairuddin AB, Jahanshaloo L, Shariati O. An overview on doubly fed induction generators ′ controls and contributions to wind based electricity generation. **Renew Sustain Energy Rev**. 2013;27(2013):692–708.

113. Blaabjerg F, Ke Ma. Future on Power Electronics for Wind Turbine Systems. **IEEE J Emerg Sel Top POWER Electron**. 2013;1(3):139–52.

114. Gireeshma K, Chandramohan S. Enhancing LVRT capability of DFIG using cooperative control of BTFCL and RPC. **J Control Meas Electron Comput Commun**. 2022;64(1):51–62.

115. MET SJ, LCG F. Power Electronics for Modern Sustainable Power Systems : Distributed Generation , Microgrids and Smart Grids — A Review. **Sustain Rev**. 2022;14(1–22).

116. Machines E, Wybrze T. Advanced control of direct-driven PMSG generator in wind turbine system. **Arch Electr Eng**. 2016;65(4):643–56.

117. Qiu Z, Zhou K, Yingtao LI. Modeling and Control of Diode Rectifier Fed PMSG Based Wind Turbine. In: **4th International Conference on Electric Utility Deregulation and Restructuring and Power Technologies (DRPT)**. Weihai, China; 2011. p. 1384–8.

118. Duong MQ, Le KH, Grimaccia F, Leva S, Mussetta M, Zich RE. Comparison of power quality in different grid-integrated wind turbines. In: **Proceedings of International Conference on Harmonics and Quality of Powe**r, ICHQP. 2014. p. 448–52.

119. Koutroulis E. Energy Management in Wind Energy Systems. In: Comprehensive Energy Systems. **Elsevier Ltd**.; 2018. p. 707–41.

120. Mourabit Y El, Derouich A, Allouhi A, Ghzizal A El, Ouanjli N El, Zamzoumyes O. Sustainable production of wind energy in the main Morocco ' s sites using permanent magnet synchronous generators. **John Wiley Sons Ltd**. 2020;30(6):1–26.

121. Lydia M, Kumar SS, Selvakumar AI, Prem GE. A comprehensive review on wind turbine power curve modeling techniques. **Renew Sustain Energy Rev**. 2014;30:452–60.

122. Dı E, Cidra J, Carrillo C, Montan AFO. Review of power curve modelling for wind turbines. **Renew Sustain Energy Rev**. 2013;21:572–81.

123. Yaakoubi AE, Amhaimar L, Attari K, Harrak MH, Halaoui ME, Asselman A. Non-linear and intelligent maximum power point tracking strategies for small size wind turbines : Performance analysis and comparison. **Energy Reports**. 2019;5:545–54.

124. İrfan Yazici, Ersagun Yaylaci. Maximum power point tracking for the permanent magnet synchronous generator- based WECS by using the discrete-time integral sliding mode controller with a chattering-free reaching law. **IET Power Electron**. 2017;10(13):1751–8.

125. Cheng M, Zhu Y. The state of the art of wind energy conversion systems and technologies: A review. **Energy Convers Manag**. 2014;88(2014):332–47.

126. Nasiri M, Milimonfared J, Fathi SH. Modeling , analysis and comparison of TSR and OTC methods for MPPT and power smoothing in permanent magnet synchronous generator-based wind turbines. **ENERGY Convers Manag**. 2014;86:892–900.

127. Ullah A, Khan L, Khan Q, Ahmad S. Variable gain high order sliding mode control approaches for PMSG based variable speed wind energy conversion system. **Turkish J Electr Eng Comput Sci**. 2020;28(5):2997–3012.

128. Zhu Y, Cheng M, Hua W, Wang W. A Novel Maximum Power Point Tracking Control for Permanent Magnet Direct Drive Wind Energy Conversion Systems. **energies**. 2012;5(2012):1398–412.

129. Yaylaci EK, 2 İY. Maximum Power Point Tracking Algorithms for the Wind Energy Systems. **J New Results Sci**. 2016;12(2016):71–80.

130. Abdullah MA, Yatim AHM, Tan CW, Saidur R. A review of maximum power point tracking algorithms for wind energy systems. **Renew Sustain Energy Rev**. 2012;16(5):3220–7.

131. Han YH. Grid Integration of Wind Energy Onshore and Offshore Conversion System. Third Edit. Renewable Energy. **John Wiley & Sons, Ltd**; 2014.

132. Llorente R, Lacal R, Aguado M. Power electronics evolution in wind turbines — A market-based analysis. **Renew Sustain Energy Rev**. 2011;15(9):4982–93.

133. Yaramasu BV, Wu B, Sen PC, Kouro S, Narimani M. High-Power Wind Energy Conversion Systems : State-of-the-Art and Emerging Technologies. **Proc IEEE**. 2015;103(5):740–88.

134. Carrasco JM, Bialasiewicz JT, Guisado RCP, León JI. Power-Electronic Systems for the Grid Integration of Renewable Energy Sources : A Survey. **IEEE Trans Ind Electron**. 2006;53(4):1002–16.

135. Kusiak A, Li W. The prediction and diagnosis of wind turbine faults. **Renew Energy**. 2011;36(1):16–23.

136. Kouro S, Malinowski M, Gopakumar K, Pou J, Franquelo LG, Wu B, Rodriguez J, Pérez MA, Leon JI. Recent Advances and Industrial Applications of Multilevel Converters. **IEEE Trans Ind Electron**. 2010;57(8):2553–80.

137. Rodríguez J, Bernet S, Wu B. Multilevel Voltage-Source-Converter Topologies for Industrial Medium-Voltage Drives. **IEEE Trans Ind Electron**. 2007;54(6):2930–45.

138. R. Teodorescu, M. Liserre PR. GRID CONVERTERS FOR PHOTOVOLTAIC AND WIND POWER SYSTEMS. First. **John Wiley and Sons**,; 2011.

139. Linus RM, Damodharan P. Maximum power point tracking method using a modified perturb and observe algorithm for grid connected wind energy conversion systems. **IET Renew Power Gener**. 2015;9(6):682–9.

140. Colak I, Fulli G, Bayhan S, Chondrogiannis S. Critical aspects of wind energy systems in smart grid applications. **Renew Sustain Energy Rev**. 2015;52:155–71.

141. Shukla RD, Tripathi PRK, Gupta S. Power Electronics Applications in Wind Energy Conversion System : A Review. In: **International Conference on Power, Control and Embedded Systems**. 2010. p. 1–6.

142. Blaabjerg F, Liserre M, Ma K. Power Electronics Converters for Wind Turbine Systems. **IEEE Trans Ind Appl**. 2012;48(2):708–19.

143. Rodriguez J, Bernet S, Steimer PK, Lizama IE. A Survey on Neutral-Point-Clamped Inverters. **IEEE Trans Ind Electron**. 2010;57(7):2219–30.

144. Trzynadlowski AM. Power Electronic Converters and Systems. Second edi. London,, United Kingdom: **Institution of Engineering and Technology** 2016; 2016.

145. Qais MH, Hasanien HM, Alghuwainem S. Output power smoothing of grid-connected permanent-magnet synchronous generator driven directly by variable speed wind turbine: a review. **J Eng**. 2017;3(October):1755–9.

146. Nobela ON, Bansal RC, Justo JJ. A review of power quality compatibility of wind energy conversion systems with the South African utility grid. **Renew Energy Focus**. 2019;31(00):63–72.

147. Papathanassiou MTS. A review of grid code technical requirements for wind farms. **IET Renew Power Gener**. 2009;3(March):308–32.

148. Ndirangu JG, Nderu JN, Muhia AM. Power Quality Challenges and Mitigation Measures in Grid Integration of Wind Energy Conversion Systems. **2018 IEEE Int Energy Conf**. 2018;1–6.

149. Mahela OMP, Gupta N, Khosravy M, Patel N. Comprehensive Overview of Low Voltage Ride Through Methods of Grid Integrated Wind Generator. **IEEE Access**. 2019;7:99299–326.

150. Al-Shetwi AQ, Sujod MZ. Modeling and Control of Grid-Connected Photovoltaic Power Plant with Fault Ride- Through Capability. **J Sol Energy Eng**. 2017;140:1–9.

151. Liu X, Xu Z, Wong KP. Recent advancement on technical requirements for grid integration of wind power. **J Mod Power Syst Clean Energy**. 2013;1(3):216–22.

152. Díaz-gonzález F, Hau M, Sumper A, Gomis-bellmunt O. Participation of wind power plants in system frequency control : Review of grid code requirements and control methods. **Renew Sustain Energy Rev**. 2014;34:551–64.

153. Ke Ma. Power Electronics for the Next Generation Wind Turbine System. First Edit. **Springer**; 2015.

154. Hossain J, Pota HR. Robust Control for Grid Voltage Stability : High Penetration of Renewable Energy. **Springer** Singapore Heidelberg; 2014.

155. Hannan MA, Hussin I, Ker PJ, Hoque MM, Hossain Lipu MS, Hussain A, Rahman MSA, Faizal CWM, Blaabjerg F. Advanced control strategies of VSC Based HVDC transmission system: Issues and potential recommendations. **IEEE Access**. 2018;6(c):78352–69.

156. Sourkounis C, Tourou P. Grid Code Requirements for Wind Power Integration in Europe. In: **Hindawi Publishing Corporation**. 2013. p. 1–9.

157. Al-Shetwi AQ, Hannan MA, Jern KP, Mansur M, Mahlia TMI. Grid-connected renewable energy sources: Review of the recent integration requirements and control methods. **J Clean Prod**. 2020;253.

158. Zobaa AF, Ahmed I, Aleem SHEA. A Comprehensive Review of Power Quality Issues and Measurement for Grid-integrated Wind Turbines. **Recent Adv Electr Electron Eng**. 2019;12(2019):210–22.

159. Zobaa AF, Aleem SHEA. Power Quality in Future Electrical Power Systems. first. London, United Kingdom: **Institution of Engineering and Technology**; 2017.

160. BAYRAK G, YILMAZ A. Assesment of Power Quality Disturbances for Grid Integration of Pv Power Plants. **Sak Univ J Sci**. 2019;23(1):35–42.

161. Saqib MA, Saleem AZ. Power-quality issues and the need for reactive-power compensation in the grid integration of wind power. **Renew Sustain Energy** Rev. 2015;43:51–64.

162. Janik P, Kosobudzki G, Schwarz H. Influence of increasing numbers of RE-inverters on the power quality in the distribution grids : A PQ case study of a representative wind turbine and photovoltaic system. **Front Energy**. 2017;11(2):155–67.

163. IEC 61000-4-15. Part 4: Testing and measurement techniques – Section 15: Flickermeter – Functional and design specifications. **Electromagnetic compatibility (EMC)**. 2003.

164. Gutierrez JJ, Ruiz J, Saiz P, Azcarate I, Leturiondo LA, Lazkano A. Power Quality in Grid-Connected Wind Turbines. In: Wind Turbines. **IntechOpen**; 2008. p. 547–70.

165. Fida M, Ali M. Power Quality Improvement of Distribution Feeder Using Hybrid Series Active Power Filters with Sliding Mode Controller. **2018 Int Conf Power Gener Syst Renew Energy Technol**. 2018;(September):1–6.

166. Liang X. Emerging Power Quality Challenges Due to Integration of Renewable Energy Sources. **IEEE Trans Ind Appl**. 2016;53(2):1–9.

167. Javadi A, Hamadi A, Woodward L. Experimental Investigation on a Hybrid Series Active Power Compensator to Improve Power Quality of Typical Households. **IEEE Trans Ind Electron**. 2016;63(8):4849–59.

168. Zhong QC, Hornik T. CONTROL OF POWER INVERTERS IN RENEWABLE ENERGY AND SMART GRID INTEGRATION. first. **John Wiley & Sons, Ltd**; 2013.

169. Shang L, Hu J, Yuan X, Huang Y. Improved virtual synchronous control for grid-connected VSCs under grid voltage unbalanced conditions. **J Mod Power Syst Clean Energy**. 2019;7(1):174–85.

170. Kim YJ. Development and Analysis of a Sensitivity Matrix of a Three-Phase Voltage Unbalance Factor. **IEEE Trans Power Syst**. 2018;33(3):3192–5.

171. IEEE standards Coordinating Committee 21. IEEEStandard for Interconnecting Distributed Resources with Electric Power Systems - Amendment 1," in **IEEE Std 1547a-2014 (Amendment to IEEE Std 1547-2003)**. Vol. 2014. 2014.

172. Engineering E, Engineering F, Qena SV. Power Quality Issues of Grid Connected DFIG Wind Farm System. **Electr Eng Appl Sci**. 2019;2(2):49–56.

173. Kadandani NB, Maiwada YA. Impact of Voltage Sag and Swell on the Power Quality of Grid Connected Wind Power Plant. **Int J Eng Sci**. 2015;4(7):56–64.

174. Babaei E, Shahir FM, Tabrizi SD, Sabahi M. Compensation of voltage sags and swells using photovoltaic source based DVR. In: **14th International Conference on Electrical Engineering/Electronics, Computer, Telecommunications and Information Technology (ECTI-CON)**. Phuket, Thailand; 2017. p. 903–6.

175. Thirupathaiah M, Prasad PV. Analysis of Various Compensation Devices for Power Quality Improvement in Wind Energy System. **Int J Electr Eng Technol**. 2016;7(3):25–39.

176. Blaabjerg F, Teodorescu R, Liserre M, Timbus A V. Overview of control and grid synchronization for distributed power generation systems. **IEEE Trans Ind Electron**. 2006;53(5):1398–409.

177. Sozer Y, Torrey DA. Modeling and control of utility interactive inverters. **IEEE Trans Power Electron**. 2009;24(11):2475–83.

178. VATANSEVER F, HACIİSKENDEROGLU E. PID TUNING WITH UP-TO-DATE METAHEURISTIC ALGORITHMS. **Bursa Uludağ Univ J Fac Eng**. 2022;27(2):573–84.

179. Singh, Rajat Kumar SY. Optimized PI Controller for an Interacting Spherical Tank System. In: **1st International Conference on Electronics, Materials Engineering and Nano-Technology (IEMENTech)**. Kolkata, India; 2017. p. 1–6.

180. Yucelen T, Kaymakci O, Kurtulan S. Self-tuning PID controller using Ziegler-Nichols method for programmable logic controllers. **IFAC Proc Vol**. 2006;39(14):11–6.

181. Shabnam P, Priyanka AK, Vijay Muni T, Rajasekhar S. PID controller based grid connected wind turbine energy system for power quality improvement. **J Crit Rev**. 2020;7:31–5.

182. Jaikhang W, Tunyasrirut S, Permpoonsinsup W. Optimization PI Controller of Grid Connected for Wind Turbine Based on PMSG. In: **International Electrical Engineering Congress (iEECON)**. Pattaya, Thailand; 2017. p. 1–4.

183. Agalya KNBNA. Tuning of a PID controller using evolutionary multi objective optimization methodologies and application to the pulp and paper industry. **Int J Mach Learn Cybern**. 2018;10:2015–2025.

184. Belgaid Y, Helaimi M, Taleb R, Youcef MB. Optimal tuning of PI controller using genetic algorithm for wind turbine application. **Indones J Electr Eng Comput Sci**. 2019;18(1):167–78.

185. ÖZDEMIR MT, ÖZTÜRK D. Comparative Performance Analysis of Optimal PID Parameters Tuning Based on the Optics Inspired Optimization Methods for Automatic Generation Control. **energies**. 2017;12(10):1–19.

186. Reddy SS, Rathnam CS. Optimal Power Flow using Glowworm Swarm Optimization. **Int J Electr POWER ENERGY Syst**. 2016;80(2016):128–39.

187. Zeng G qiang, Xie X qing, Chen M rong. An Adaptive Model Predictive Load Frequency Control Method for Multi-Area Interconnected Power Systems with Photovoltaic Generations. **Energies**. 2017;10(11):1–23.

188. Sawle Y, Ferrão P, Fournier J, Lacarrière B, Corre O Le. Optimal sizing of standalone PV/Wind/Biomass hybrid energy system using GA and PSO optimization technique. **Energy Procedia**. 2017;117:690–8.

189. Soued S, Ebrahim MA, Ramadan HS, Becherif M. Optimal blade pitch control for enhancing the dynamic performance of wind power plants via metaheuristic optimisers. **IET Electr Power Appl**. 2017;11(8):1432–40.

190. Aguilar-Mejía O, Minor-Popocatl H, Tapia-Olvera R. Comparison and ranking of metaheuristic techniques for optimization of PI controllers in a machine drive system. **Appl Sci**. 2020;10(18):1–27.

191. Aguila-Leon J, Chinas-Palacios CD, Vargas-Salgado C, Hurtado-Perez E, Garcia EXM. Optimal PID Parameters Tunning for a DC-DC Boost Converter. In: **IEEE Conference on Technologies for Sustainability**,. Santa Ana, CA USA: IEEE; 2020. p. 1–6.

192. Amini B, Roshanfekr R, Hajipoor A, Yousef S, Mousavi M. Interface converter control of distributed generation in microgrids using fractional proportional — Resonant controller. **Electr Power Syst Res**. 2021;194(February):1–12.

193. Sulaiman MH, Mustaffa Z, Mohamed MR, Aliman O. Using the gray wolf optimizer for solving optimal reactive power dispatch problem. **Appl Soft Comput J**. 2015;32:286–92.

194. SEZER K, BAYHAN N. Comparison of Metaheuristic Algorithm Performances for Optimization of Fractional Order PID Controllers Applied to Gas Turbine Power Plant. **Aeronaut Sp Technol**. 2021;14(2):209–19.

195. Antunes JS. Physical Modelling vs . Numerical Modelling : Complementarity and Learning. **Preprints**. 2020;

196. Forrester AIJ, Sóbester A, Keane AJ. Engineering Design via Surrogate Modelling A Practical Guide. First Edit. **John Wiley & Sons Ltd**; 2008.

197. Fonseca RW Da, Didoné EL, Pereira FOR. Using artificial neural networks to predict the impact of daylighting on building final electric energy requirements. **Energy Build**. 2013;61(2013):31–8.

198. Mirjalili S. How effective is the Grey Wolf optimizer in training multi-layer perceptrons. **Appl Intell**. 2015;43(1):150–61.

199. Lalonde ER, Vischschraper B, Bitsuamlak G, Dai K. Comparison of neural network types and architectures for generating a surrogate aerodynamic wind turbine blade model. **J Wind Eng Ind Aerodyn**. 2021;216(2021):1–15.

200. Nouali S, Ouali A. Multi- layer neural network forsensorless MPPT control for wind energy conversion system using doubly fed twin stator induction generator. In: **8th International Multi-Conference on Systems, Signals & Devices**. 2011.

201. Ghasemiyeh R, Moghdani R, Sana SS. A Hybrid Artificial Neural Network with Metaheuristic Algorithms for Predicting Stock Price. **Cybern Syst AN Int J**. 2017;48(4):365–92.

202. Legaard CM, Schranz T, Schweiger G, Drgoňa J, Falay B, Gomes C, Iosifidis A, Abkar M, Larsen PG. Constructing Neural Network-Based Models for Simulating Dynamical Systems. **ACM Comput Surv**. 2021;1(1):1–35.

203. Morrison SJ. Statistics for Engineers an Introduction. first edit. **John Wiley & Sons, Ltd**; 2009.

204. Hamatwi E, Davidson IE, Gitau MN, Adam GP. Modeling and Control of Voltage Source Converters for Grid Integration of a Wind Turbine System. In: **IEEE PES Power Africa Confer**. Livingstone, Zambia; 2016. p. 98–106.

205. Chatterjee A, Mohanty K, Kommukuri VS, Thakre K. Power quality enhancement of single phase grid tied inverters with model predictive current controller. **J Renew Sustain Energy**. 2017;9(1):1–17.

206. Alremali FAM, Yaylacı EK, Uluer İ. Optimization of Proportional-Integral Controllers of Grid-Connected Wind Energy Conversion System Using Grey Wolf Optimizer based on Artificial Neural Network for Power Quality Improvement. **Adv Sci Technol Res J**. 2022;16(3):295–305.

207. Ersagun K. YAYLACI. Rüzgar enerji sistemlerinde maksimum güç noktasi takibi için kayan kipli denetleyici tasarimi. **SAKARYA ÜNİVERSİTESİ**; 2017.

208. Sarrias-Mena R, Fernández-Ramírez LM, García-Vázquez CA, Jurado F. Advanced Control and Optimization Paradigms for Wind Energy Systems. Power Systems. **Springer**; 2019. 189–212 p.

209. Zhou D, Blaabjerg F, Franke T, Tønnes M, Lau M. Comparison of Wind Power Converter Reliability with Low-Speed and Medium-Speed Permanent-Magnet Synchronous Generators. **IEEE Trans Ind Electron**. 2015;62(10):6575–84.

210. Saad NH, El-sattar AA, Marei ME. Improved bacterial foraging optimization for grid connected wind energy conversion system based PMSG with matrix converter. **Ain Shams Eng J**. 2017;9(4):2183–93.

211. Yazici I, Yaylaci EK, Cevher B, Yalçln F, Yüzkollar C. A new MPPT method based on a modified Fibonacci search algorithm for wind energy conversion systems. **J Renew Sustain Energy**. 2021;13(1):013304.

212. Reznik A, Simões MG, Al-durra A, Muyeen SM. LCL Filter Design and Performance Analysis for Grid Interconnected Systems. **IEEE Trans Ind Appl**. 2013;50(2):1225–32.

213. Karafil A, Ozbay H, Oncu S. Design and Analysis of Single-Phase Grid-Tied Inverter with PDM MPPT-Controlled Converter. **IEEE Trans Power Electron**. 2020;35(5):4756–66.

214. Papavasiliou A, Papathanassiou SA, Manias SN, Demetriadis G. Current control of a voltage source inverter connected to the grid via LCL filter. In: **IEEE Power Electronics Specialists Conference**. Orlando, FL, USA; 2007. p. 2379–84.

215. Lahlou T, Abdelrahem M, Valdes S, Herzog H georg. Filter Design for Grid-Connected Multilevel CHB Inverter for Battery Energy Storage Systems. In: **International Symposium on Power Electronics, Electrical Drives, Automation and Motion (SPEEDAM)**. Capri, Italy; 2016. p. 831–6.

216. Dursun M, DÖŞOĞLU MK. LCL Filter Design for Grid Connected Three-Phase Inverter. In: **2nd International Symposium on Multidisciplinary Studies and Innovative Technologies (ISMSIT)**. Ankara, Turkey; 2019. p. 1–4.

217. Saïd-Romdhane M Ben, Naouar MW, Belkhodja IS, Monmasson E. Simple and systematic LCL filter design for three-phase grid-connected power converters. **Math Comput Simul**. 2016;130:181–93.

218. Musunuri SK. CONTROL AND INTERFACE DESIGN FOR COST REDUCTION OF A LOW POWER GRID-CONNECTED WIND-PHOTOVOLTAIC SYSTEM. **Mississippi State University**; 2011.

219. Yazici I, Yaylaci EK. Improving Efficiency of the Tip Speed Ratio-MPPT Method for Wind Energy Systems by Using an Integral Sliding Mode Voltage Regulator. **J Energy Resour Technol**. 2018;140(5):051203–6.

220. Yaylacı E, Yazici İ. Sensorless double integral sliding mode MPPT control for the WECS. **J Renew Sustain Energy**. 2018;10(2):023301–14.

221. Jain B, Jain S, Nema RK. Control strategies of grid interfaced wind energy conversion system : An overview. **Renew Sustain Energy Rev**. 2015;47(2015):983–96.

222. Eswaran T, Kumar VS. Particle swarm optimization (PSO) -based tuning technique for PI controller for management of a distributed static synchronous compensator (DSTATCOM) for improved dynamic response and power quality. **J Appl Res Technol**. 2017;15:173–89.

223. Zhao H, Wu Q. Status of Wind Power Technologies. In: Modeling and Modern Control of Wind Power. 1st ed. **WILEY**; 2017. p. 1–10.

224. Zhong QC, Hornik T. CONTROL OF POWER INVERTERS IN RENEWABLE ENERGY AND SMART GRID INTEGRATION. first edit. **John Wiley & Sons, Ltd**; 2013.

225. Ciobotaru M, Remus T, Vassilios G Agelidis. Offset rejection for PLL based synchronization in grid-connected converters. In: **Twenty-Third Annual IEEE Applied Power Electronics Conference and Exposition**. Austin, TX, USA; 2008. p. 1611–7.

226. Wang J. The Control of Grid-Connected Invertrs in Microgrids. **University of Liverpol**; 2016.

227. Al-toma ASH. Hybrid Control Schemes for Permanent Magnet Synchronous Generator Wind Turbines. **Brunel University**; 2017.

228. Mohod SW, Aware M V. Power Quality and Grid Code Issues in Wind Energy Conversion System. In: An Update on Power Quality. **InTech**; 2013. p. 21–35.

229. Standards I, Committee C, Generation D, Storage E. IEEE Standard Conformance Test Interconnecting Distributed Energy. **IEEE Standards Coordinating Committee 21**; 2020.

APPENDIX A.

INPUT AND OUTPUT DATA SET FOR GENERATING ANN

X1 (6 – 15), X2 (250 - 500), X3 (0.1 - 2), X4 (3 - 9), X5 (0.1 - 2), X6 (3 - 9).

e1, e2, and e3 are the standard deviation of the output errors.

x1	x2	x3	x4	x5	x6	e1	e2	e3
12.0162	301.6941	1.3423	3.4323	0.8728	7.0016	0.0037	0.016	0.0121
14.4035	452.7375	1.0206	7.5405	0.8924	8.8307	0.0025	0.0107	0.0094
14.8918	466.0369	0.8389	5.7285	0.5687	7.7065	0.0024	0.0125	0.0125
13.9455	478.4279	1.1607	6.5932	0.3829	8.3983	0.0025	0.012	0.0197
10.0535	301.4181	1.8093	7.5755	1.7767	4.7097	0.0034	0.0089	0.0221
12.059	416.07	0.3333	5.4439	0.623	7.3	0.0025	0.011	0.012
8.5505	474.0497	1.6705	5.3402	1.046	7.1688	0.0032	0.0104	0.0128
13.5093	402.4074	1.192	4.9563	0.9672	7.2828	0.0028	0.0127	0.0122
13.9596	430.2139	0.1354	7.0487	0.9332	5.6269	0.0027	0.0177	0.0181
7.0533	453.6704	0.7172	4.4774	0.7512	5.2542	0.0031	0.0092	0.0168
10.919	390.48	0.8521	5.3888	1.0792	6.9452	0.0029	0.0096	0.0136
14.5582	430.5871	0.8602	7.9912	0.3552	3.3628	0.0029	0.0127	0.0237
6.7582	290.9746	0.716	4.8104	0.1222	6.2394	0.006	0.0232	0.0633
6.8584	286.6287	1.2992	8.1559	1.951	6.425	0.0041	0.0064	0.0175
14.9717	388.3854	1.0794	4.9841	0.917	5.9508	0.0028	0.0132	0.0158
6.6393	471.9348	0.2228	5.6171	1.6706	5.3672	0.0025	0.0138	0.0202
11.5213	454.6602	1.7838	8.5867	0.4625	4.5515	0.003	0.0101	0.0175
14.0808	398.3405	1.0573	6.6769	1.6569	6.1913	0.0027	0.0108	0.0179
7.8187	363.4734	0.913	8.7963	1.2781	7.1723	0.0037	0.0075	0.0138
12.4815	336.7238	1.0823	6.3402	0.3973	6.3723	0.0034	0.0115	0.0178
12.2532	356.6139	1.6889	7.3883	0.7841	5.7253	0.0034	0.0101	0.0152
9.4775	443.8887	1.4951	5.5817	1.4181	8.6713	0.0031	0.01	0.0116
13.0581	426.393	0.3077	5.3396	1.2227	5.7563	0.0023	0.0152	0.0183
6.4531	307.1719	1.685	3.0939	1.7411	3.4684	0.0042	0.0127	0.0254
12.0214	375.0528	0.5142	6.4297	0.3322	7.027	0.0031	0.0111	0.0225
11.3963	263.994	0.2071	3.915	0.1373	5.6111	0.0054	0.0385	0.0529
13.49	404.3475	1.0882	8.1832	0.2856	8.4483	0.0029	0.0111	0.0263

APPENDIX B.

SCREENSHOTS OF THE SIMULATION RUNNING

(Exchange power between the WT and the grid)

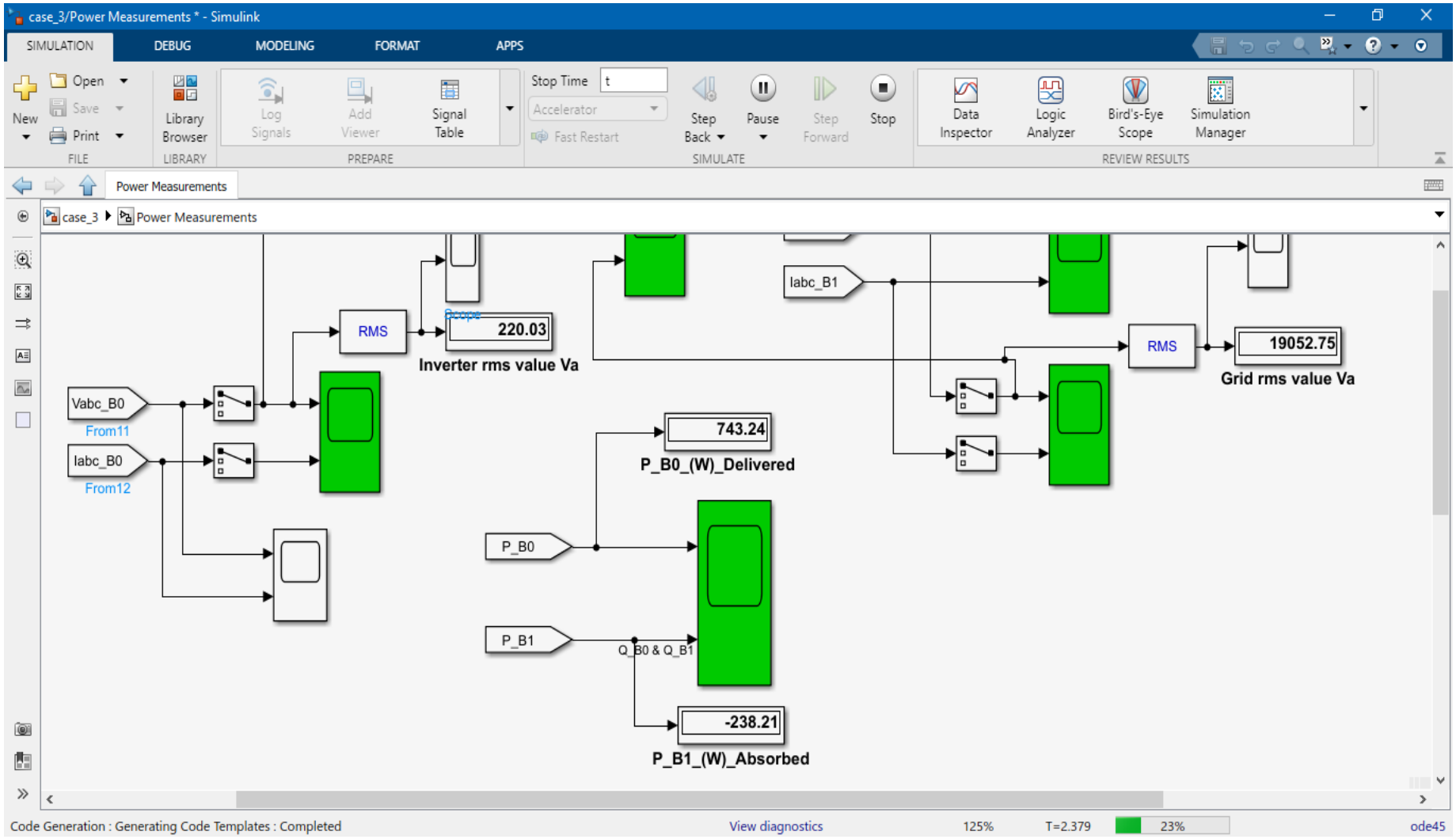
case_3/Power Measurements * - Simulink
SIMULATION
DEBUG
MODELING
FORMAT
APPS
New
Open
Save
Print
FILE
Library Browser
LIBRARY
Log Signals
Add Viewer
Signal Table
PREPARE
Stop Time
t
Accelerator
Fast Restart
Step Back
Pause
Step Forward
Stop
SIMULATE
Data Inspector
Logic Analyzer
Bird's-Eye Scope
Simulation Manager
REVIEW RESULTS
Power Measurements
case_3
Power Measurements
RMS
220.03
Inverter rms value Va
Vabc_B0
From11
Iabc_B0
From12
Iabc_B1
RMS
19052.75
Grid rms value Va
743.24
P_B0_(W)_Delivered
P_B0
P_B1
Q_B0 & Q_B1
-238.21
P_B1_(W)_Absorbed
Code Generation : Generating Code Templates : Completed
View diagnostics
125%
T=2.379
23%
ode45

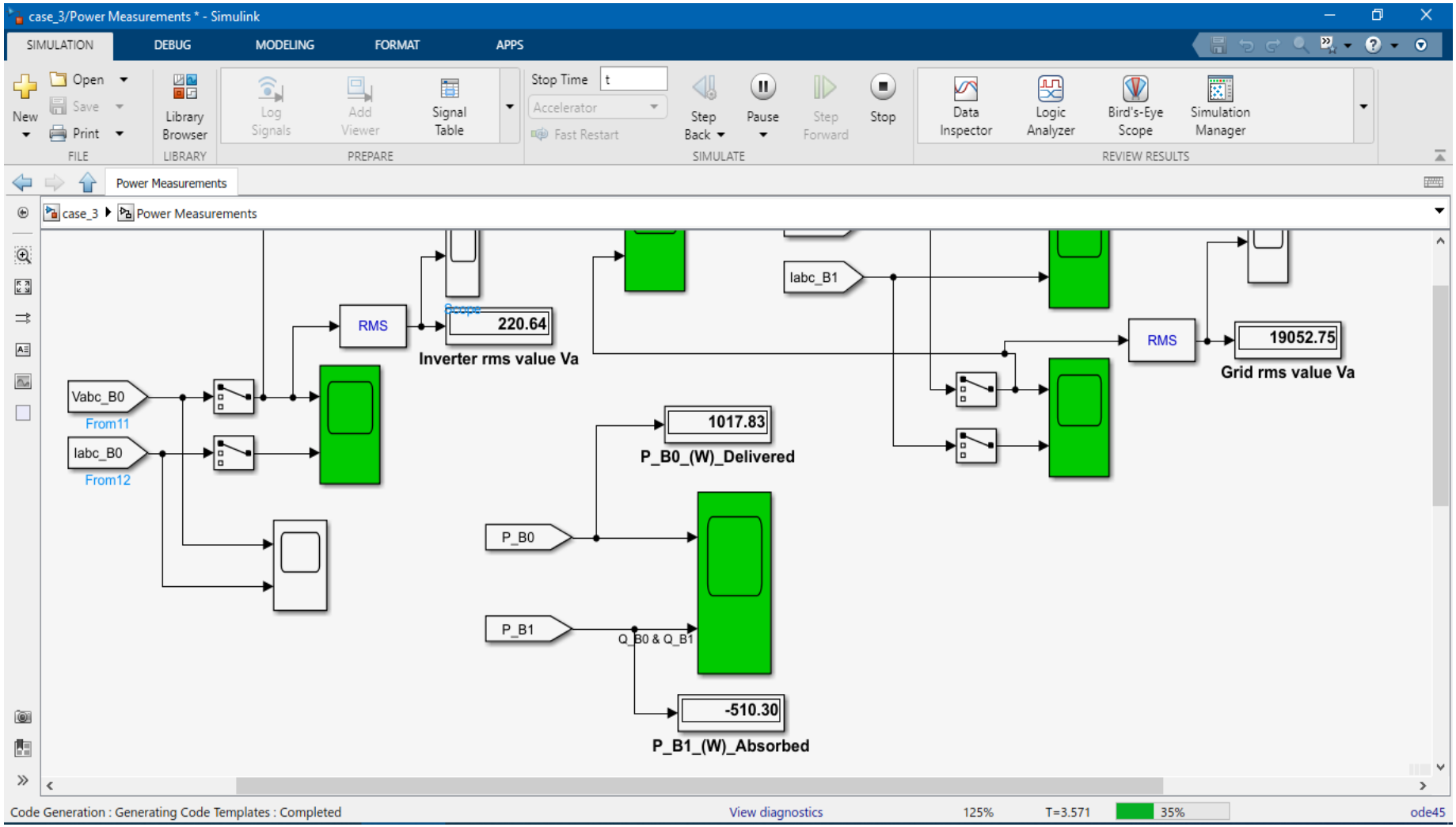
case_3/Power Measurements * - Simulink
SIMULATION
DEBUG
MODELING
FORMAT
APPS
New
Open
Save
Print
FILE
Library Browser
LIBRARY
Log Signals
Add Viewer
Signal Table
PREPARE
Stop Time
t
Accelerator
Fast Restart
Step Back
Pause
Step Forward
Stop
SIMULATE
Data Inspector
Logic Analyzer
Bird's-Eye Scope
Simulation Manager
REVIEW RESULTS
Power Measurements
case_3
Power Measurements
RMS
220.64
Inverter rms value Va
Iabc_B1
RMS
19052.75
Grid rms value Va
Vabc_B0
From11
Iabc_B0
From12
1017.83
P_B0_(W)_Delivered
P_B0
P_B1
Q_B0 & Q_B1
-510.30
P_B1_(W)_Absorbed
Code Generation : Generating Code Templates : Completed
View diagnostics
125%
T=3.571
35%
ode45

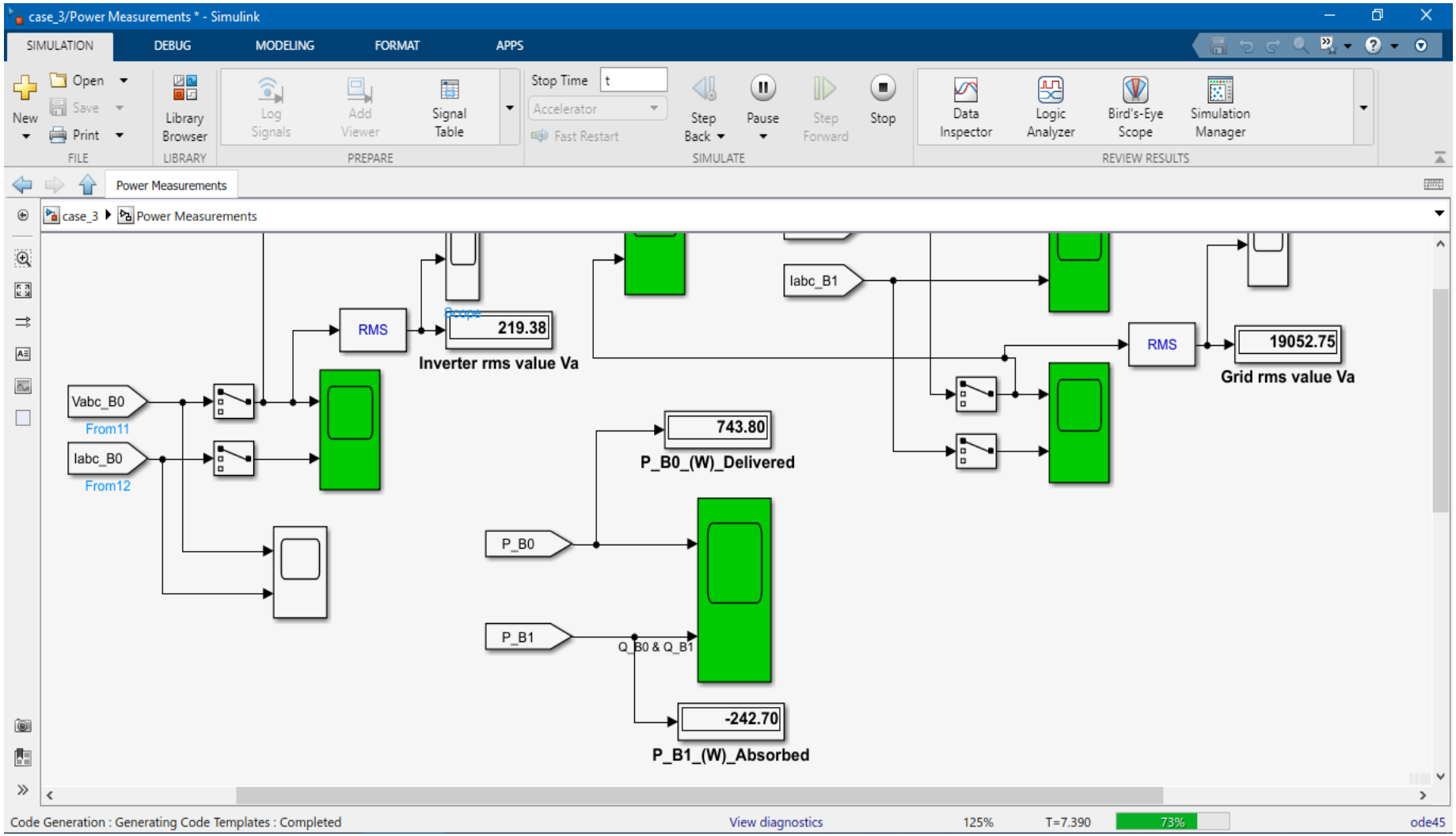
case_3/Power Measurements * - Simulink
SIMULATION
DEBUG
MODELING
FORMAT
APPS
New
Open
Save
Print
FILE
Library Browser
LIBRARY
Log Signals
Add Viewer
Signal Table
PREPARE
Stop Time
t
Accelerator
Fast Restart
Step Back
Pause
Step Forward
Stop
SIMULATE
Data Inspector
Logic Analyzer
Bird's-Eye Scope
Simulation Manager
REVIEW RESULTS
Power Measurements
case_3
Power Measurements
RMS
219.38
Inverter rms value Va
Vabc_B0
From11
Iabc_B0
From12
Iabc_B1
RMS
19052.75
Grid rms value Va
743.80
P_B0_(W)_Delivered
P_B0
P_B1
Q_B0 & Q_B1
-242.70
P_B1_(W)_Absorbed
Code Generation : Generating Code Templates : Completed
View diagnostics
125%
T=7.390
73%
ode45

RESUME

Fathi Abdulmajeed M. ALREMALI graduated primary and preparatory education in Alkhoms city (Libya). He completed his undergraduate program in College of Electronic Technology Department of Control Engineering in Bani Waleed (Libya). He graduated Master program in Libyan Academy for Postgraduate Studies, Department of Control Engineering and Measurements in Tripoli (Libya) (2008). In 2008, he started working at the Higher Institute of Engineering Professions as a lecturer. He started his Ph.D. education program at Karabuk University in Department of Electrical-Electronics Engineering in 2016.